ULTRASMALL, WHITE-LIGHT CDSE NANOCRYSTALS: LIGAND EFFECTS AND INCORPORATION INTO SOLID-STATE LIGHTING

By

Michael Alan Schreuder

Dissertation

Submitted to the Faculty of the

Graduate School of Vanderbilt University

in partial fulfillment of the requirements

for the degree of

DOCTOR OF PHILOSOPHY

in

Chemistry

May, 2010

Nashville, Tennessee

Approved:

Professor Sandra J. Rosenthal

Professor David Cliffel

Professor Eva Harth

Professor Sharon Weiss

Dedicated

to

Mary-Celeste May Schreuder, my wonderful wife

ACKNOWLEDGEMENTS

God, you are the reason I try my best. Jesus, you saved me from a very dark existence. I am sorry for every time that I fail you and put you second; help me to do better for you.

To an excellent advisor and boss, Dr. Sandra J. Rosenthal, I appreciate everything you have done for me. The freedom you gave me to set my hours and work on the interesting stuff, allowed me to flourish and recognize the responsibility that came with that freedom. Your knowledge of how both the academic and real world operate still astounds me.

I must thank my great committee members: Dr. David Cliffel, Dr. Eva Harth, and Dr. Sharon Weiss. Your guidance, questions, effort, and time in this endeavor are much appreciated.

I want to thank Dr. Donald Stec, for his NMR support; Mr. Tommy Howe, for fabricating and repairing several pieces of glassware; Mr. John Fellenstein and Mr. Bob Patchin, for fabricating a multitude of holders and evaporating masks, and easily showing me how to repair what to me was the most complicated machinery; Dr. Anthony Hmelo, for showing me how to use a variety of tools in the VINSE labs; and Mr. Andrzej Balinski, for your help in using the 4^{th} floor analytical lab.

To the people who have been part of many collaborations, I say thank you: Dr. Christopher D. Williams and Dr. Anvar Zakhidov at the University of Texas at Dallas; Dr. Kai Xiao and Dr. Ilia Ivanov at the Center for Nanophase Materials Science at Oak Ridge National Laboratories; Mz. Sarah Sparks and Dr. Kathryn Uhrich at Rutgers; and

Dr. Jack Jin, Dr. Jeff DiMaio, and Dr. Earl Wagner at Tetramer Technologies LLC. In particular I need to acknowledge Jonathan D. Gosnell for working on the white-light devices project for several years. We shared a lot of good and not so good times.

At Vanderbilt, I met a lot of great researchers, scientists, colleagues, and friends. I appreciate the help of those that have left Vanderbilt but helped me along the way: Dr. Nathanael Smith, Dr. Michael Bowers, Tony Watt, Dr. Maria Danielle Garrett, Dr. Becky Orndorff, and Jessica Sammons. Shawn Rosson, you reminded me that my beliefs don't belong on the back burner. Dr. Ian Tomlinson, thank you for the tips you gave me on organic chemistry and for putting out the lab fires. Oleg Kovtun, thanks for being a soccer buddy and explaining some of the bio-side to me. Jerry Chang, your energy was contagious; your literature knowledge helpful and confusing; and your wafer cookies were a great snack. Thanks for sharing a cubby with me, Albert Dukes; knowing that my science had to pass muster before you, made me work harder. I have nothing but admiration for Dr. James McBride, my running partner. You taught me many things about research, but more importantly you showed me how to be a good critic, a fine father, a forgiving friend, that semicolons are not always right, and that it doesn't matter how fast you run, but who you run with.

To my friends, I appreciate your patience and companionship. Dr. Teresa Croce, Mark Dobish, Reese Harry, Jonas Perez, Vanessa Phelan, Steve Townsend, and Brian Turner, you all made this place more fun. To my constant cohort, David Nannemann, thanks for having my back. Someday we will have a night where we are both Lord of Catan and Mary won't win. I am grateful that you always gave me strong competition and made sure I put forth a good witness.

My family made me who I am; if you don't like me, blame them. Steve, Celeste, Matt, and Stewart, when I married into your family, I could never have predicted the results. Every Christmas, it is as treat to be with you. Mom and Dad, you gave up more for your beliefs than most people and I will always respect that. Mom, you taught me how to learn and showed me what compassion means. Dad, your support helped me be a hard worker and made me want to be better at sports. You both showed me the love of God and its importance. Becky, your birthday cards are the best and I wish we all lived closer. Jenni, knowing that you wanted to call me and say "what's up doc," was an inspiration during some lonely hours in the lab. To my other best friend, Angie, thanks for sharing a room with me, keeping me honest, bringing me to Northwestern College, and the scar on my lip.

Mary, you get your own paragraph because you are my best friend in life. You not only make me want to be better, you make me better. I am sorry for all the missed dates, suppers alone, and conflicts this PhD has caused. In the end, I wouldn't have done it unless it makes your life better. I appreciate your insight, conversations, humor, and spirituality. I hope that someday I can have the same faith and trust in God that you show. You deserve eternal happiness because you are an amazing teacher, coach, wife, and friend; most importantly, I love you.

This work would not have been possible without the financial support of Vanderbilt University, a Vanderbilt University Discovery Grant, a Vanderbilt University Dissertation Enhancement Grant, and the US Department of Energy.

TABLE OF CONTENTS

Page

LIST OF TABLES

LIST OF FIGURES

CHAPTER I

INTRODUCTION

1.1 The World's Energy Crisis

When looking at the challenges facing humankind, one of the most critical problems is in the area of energy. Energy creation and usage are vitally important to the environmental, economical, and political stability of not just the United States of America (USA), but the world. Human relationships have been shaped, cultures/civilizations advanced or receded, and wars waged due to the availability and usage of energy resources, making energy not only the universal, but also the timeless currency. Since fire was first discovered and wood was used for fuel, carbon-based resources have been the mainstay of humanity's energy production. Fossil-fuels have driven advances and discoveries in society, clearly seen in the example of coal stimulating the Industrial Revolution. However, the era of fossil fuels is inevitably coming to an end, due to their non-renewability and our ever-increasing thirst for more energy.

It is estimated that half of the available world-wide oil has already been consumed, the majority of that in the last 30 years.[1-3] Driven by an expanding population, the world's energy draw is expected to double from the year 2000's usage (14 terawatts) by the year 2050.[2, 4-6] Should fossil fuels continue to feed this energy requirement, the accompanying air, water, and soil pollution will continue to damage personal and public property, jeopardize public health, and threaten international political and economic

constancy. For example, around 800,000 annual deaths are linked to air pollution from carbon-based fuels.[1, 7] Of particular interest in the USA is the 16 million barrels per day energy deficit; this represents about $700 billion per year in imported energy cost.[2] Considering that 85% of Americans' energy requirements come from fossil fuels (with ever increasing demands and ever decreasing reserves), without significant change the USA will forever be energy-dependent on other countries.[1, 2]

The energy future does indeed look daunting without significant modifications to the way in which energy is obtained and used. However, modern civilization has shown that ingenuity and improvisation can solve even the most intimidating dilemmas. Research and development in the areas of harvesting renewable energy sources, such as solar, water, and wind energies, must be pursued in order to move away from an energy economy based on fossil fuels. Thus far, these energy sources have not proven to be easily integrated into all societies due to their production of energy as electricity which does not have the convenience or flexibility of the more potable coal or gasoline when it comes to on-demand usage. While this predicament is being resolved, the second and equally important half of the energy solution should also be researched: energy efficiency. All areas of energy usage have some percentage of wasted resources; however, if inefficiencies can be minimized, the amount of energy required may decrease below the threshold of what is currently obtainable from renewable sources. Modernization of methods and the use of innovative materials to solve these efficiency problems is not only the right thing morally, but the economy will benefit from job creation in previously unforeseen sectors fabricating, outfitting, and installing more efficient products.

One area where improved energy efficiency is clearly required is lighting. Around 3000 BC, the first candle was invented; since that time humans have made many advances in the types of lighting used.[5, 8] With each new technological advance, more freedom to work, play, and live in places or at times not lit by the sun was achieved; current societies depend on artificial lighting to the point that it is taken for granted. Regardless of the advances during this time, the same flawed thinking was at the center of each technology: production of light as the by-product of a different process, typically heating. This applies even to the most commonly used light sources today, fluorescent and incandescent bulbs. This explains the low conversion efficiency percentages for incandescent (~5%) and fluorescent (~20%) lighting, when compared to other types of building technologies such as electric motors (~85-95%) and heating (~70%).[3-6, 8-11] Presently, approximately 22% of electricity consumption in the USA goes to producing light, representing 8% of total energy usage.[4, 5, 8] The cost of this wasteful energy consumption is close to $50 billion per year to the US consumer, not to mention the 130 million tons of carbon emitted to produce this electricity (approximately 7% of all carbons emissions in the US).[5, 9, 10]

Figure 1.1 Types of lighting through history. Despite the changes in historical lighting technologies, the light has remained a by-product of some type of reaction. These by-product based technologies have inevitably led to low efficiencies. Below each image is the date on which it first was discovered. From left to right the light sources are: a candle, gas lamp, incandescent light bulb, and fluorescent bulbs. (Images from a) Michael Bowden, c) AP/Mike Derer, and b) and d) public domain)

As a consequence of the current lighting situation, the US Department of Energy (DOE) has proposed a roadmap for revolutionizing the lighting industry. This roadmap proposes the replacement of inefficient light sources with the significantly more efficient solid-state lighting (SSL).[10, 11] Solid-state lighting is the direct conversion of electrical energy into visible light through the use of semiconductor materials; SSL is also commonly known as light-emitting diodes (LEDs). The conversion efficiencies for SSL have been predicted to swiftly reach 70% and even approach 100% or 375 lm/watt.[2, 5, 8] Energy consumption could be reduced by 620 billion KWH per year by the year 2025 through extensive use of even a 50% efficient technology, eliminated the need for 50-70 nuclear power plants.[4, 5, 9]

The first report of electroluminescence was in 1907 by H.J. Rounds, when he published "A Note on Carborundum."[8, 12, 13] Although this can be considered the first

LED, due to the lack of follow-up work and publications, the invention of the LED should be attributed to O.V. Losev. Throughout the 1920s, Losev published 16 papers in various journals detailing his broad studies on the LED, explaining the non-thermal emission, the related diode action, the current-voltage characteristics, and temperature dependence of the emission.[12] After Losev's death in World War II, work on LEDs was not continued until a 1951 work describing *p-n* junctions, followed by the fabrication of the LED semiconductor laser in 1962.[14-18] These works all refer to monochromatic LEDs, commonly used for traffic lights or signage already, while the interest in replacing conventional general lighting with SSL requires white light. The replacement of inefficient light sources with white LEDs for general illumination is where the largest energy impact lies.

There are two main ways of achieving white-light with monochromatic emitters (Figure 1.2). The first is to combine a single LED (most often blue) with phosphor(s) that will absorb a portion the higher energy light from the LED and emit a balancing color to produce white. The second is packaging multiple LEDs into a single device, whereby the emission from the LEDs will combine producing white light. Efficiencies from these types of SSL have already reached 35%, with the announcement of a 131 lm/watt white-light device.[5] However, a large gap still lies between current efficiencies, device lifetimes, and cost-of-light compared to future predictions or even existing lighting technologies.

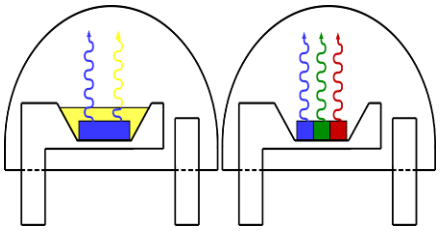

Figure 1.2 Common methods for fabricating white LEDs. In the image on the left an LED chip emits blue light, part of which is absorbed by a phosphor which then emits yellow light. The right image demonstrates the packaging of three LED chips together into one device.

In addition to improving lighting through high luminous efficiencies (luminous flux output divided by electrical input power), the DOE's roadmap calls for the lighting to be of high quality. Human vision is extremely discerning with respect to distinguishing color. The eye is sensitive to electromagnetic radiation with a wavelength of 400 to 750 nm, with approximately a Gaussian distribution centered at 555 nm (Figure 1.3a).[5, 8, 19] What the eye views as white light is a balanced distribution of light over this region, in particular the Commission Internationale de L'Eclairage has determined how the eye will interpret an emission, providing CIE color chromaticity coordinates which can be graphed on the plot shown in Figure 1.3b. Pure white light will have CIE coordinates of (0.333, 0.333). A balanced white spectrum need not be very broad, covering the entire eye sensitivity wavelength range, in order to be defined as white in color; however, the more broad an emission, the better such a light source will render colors. For this ability, the standard of measure is a color rendering index (CRI) which quantifies how well a light source allows a viewer to distinguish between colors compared to an ideal light source with a CRI of 100 (Figure 1.3c and 1.3d). A full discussion of how to calculate CIE coordinates, luminous efficiency, and the CRI of a light source is contained with

Appendix A. In its roadmaps, the DOE has declared that for general illumination SSL must have white CIE coordinates, a CRI greater than 80, and a luminous efficiency of at least 200 lumen/watt.[2-5, 8, 10, 11, 20] It is here that current SSL has found its primary nemesis. The CRI values for the white multi-LED devices described earlier are very low due to the narrow-band emitters on which they are based. In addition to this problem, blue/phosphor-based lights also generally suffer from a halo-effect in which the directional LED light doesn't mix appropriately with the diffuse light from the phosphor.

Thus the promise of SSL to have an efficiency that overshadows conventional efficiencies, with a high CRI, good CIE coordinates, and low cost of ownership has remained unfulfilled. While incremental steps are important and should be pursued, it is to new materials and technologies that we must turn to find the solution.

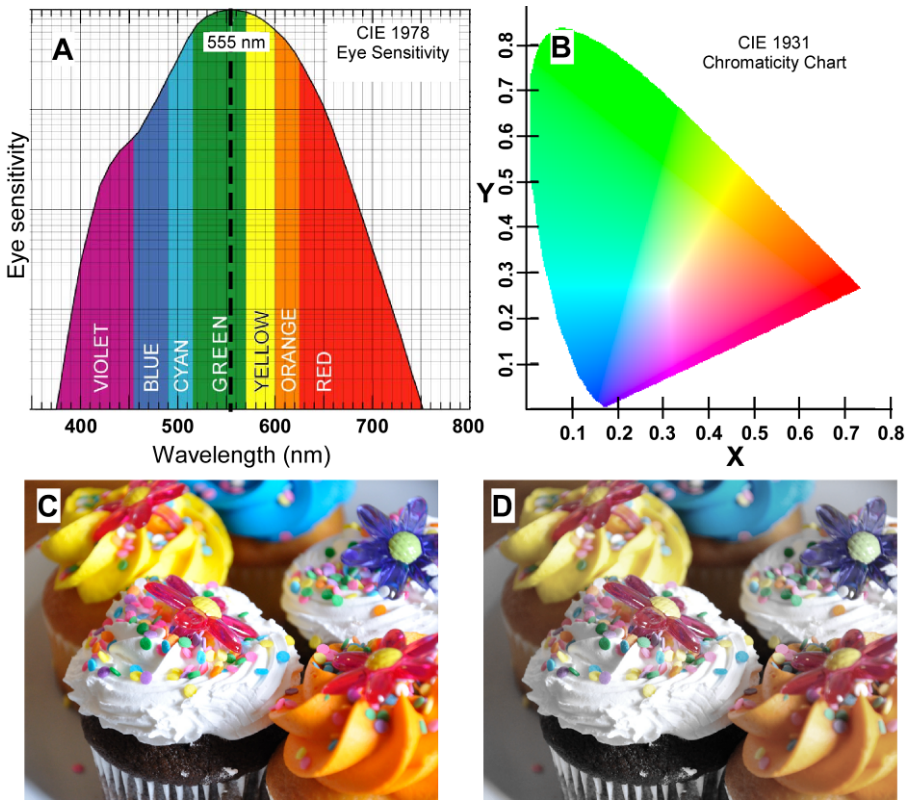

Figure 1.3 A) Spectrum showing the wavelength range for the human eye's sensitivity. B) The 1931 CIE chromaticity plot showing where various color regions fall. C) Photograph of cupcakes taken under lighting with a CRI value of 100 and D) the same image passed through a low CRI filter. In A, the dashed black line denotes 555 nm, the wavelength at which the eye is most sensitive to light.

1.2 Quantum Dots

Nanotechnology and materials based on the knowledge acquired from research into nanotechnology have become of interest in recent history. Distinctive properties have been discovered when the dimensions of various materials are reduced to a level between the bulk material and individual molecules.[21, 22] In particular, semiconductor materials exhibit unique optical and electrical properties when crystals of these materials are made with dimensions in the nanometer (10^{-9} m) range. In a bulk semiconductor, continuous energy bands arise, due to the loss of the well-defined orbitals in molecules that lead to

discrete energy levels. Between these continuous energy bands, there exists a gap or lack of allowable energy states known as the band-gap. Above, in energy, this gap lies the conduction band, while below is called the valence band. When a semiconductor receives enough energy to promote an electron from the valence band to the conduction band, an exciton can be formed. An exciton in a bulk semiconductor is a semi-stable state in which the electron orbits a hole—a hole has the opposite charge and a larger effective mass than an electron—at a specific radius known as the bulk Bohr exciton radius.[23] When crystals of a specific material are made with dimensions approaching the bulk Bohr exciton radius, the electron-hole pair experience weak confinement in physical space.[23] This confinement leads to tuning of the energy band gap with size. When a nanocrystal has a radius smaller than the Bohr exciton, Bohr electron, and Bohr hole radii in all three spatial dimensions, the nanocrystal has now entered into the strong quantum confinement regime and can be referred to as a quantum dot.[24, 25] At this point the nanocrystal's valence and conduction bands are almost exclusively tuned by the size of the nanocrystal. Brus provided the explanation for this phenomenon with his solution to the Schrodinger equation, showing that the energy levels are inversely proportional to the radius of a semiconductor crystal.[21, 22, 26-32]

For the semiconductor cadmium-selenide (CdSe), the bulk Bohr exciton radius is 5.6 nm and the bulk band gap is 1.75 eV (the energy of light with a wavelength of ~710 nm).[32-36] Thus, nanocrystals with a diameter less than ~10 nm will exhibit strong quantum confinement. Since the band gap is inversely proportional to the nanocrystal radius, as the nanocrystal diameter is decreased from 10 nm, the energy required to excite an electron from the valence band to the conduction band will increase (referred to as

exciting a nanocrystal). The wavelength of a photon is inversely proportional to the energy of that photon, consequently as the diameter of a nanocrystal is decreased the wavelength required to excite that nanocrystal will also decrease (blue-shift). Furthermore, since the wavelength required to excite a bulk CdSe crystal is in the deep red, the light required to excite smaller nanocrystals will fall within the visible region. In practical terms, this means that the light which CdSe nanocrystals absorb and nearly monochromatically emit can be tuned over the visible light spectrum *via* size control (Figure 1.4).

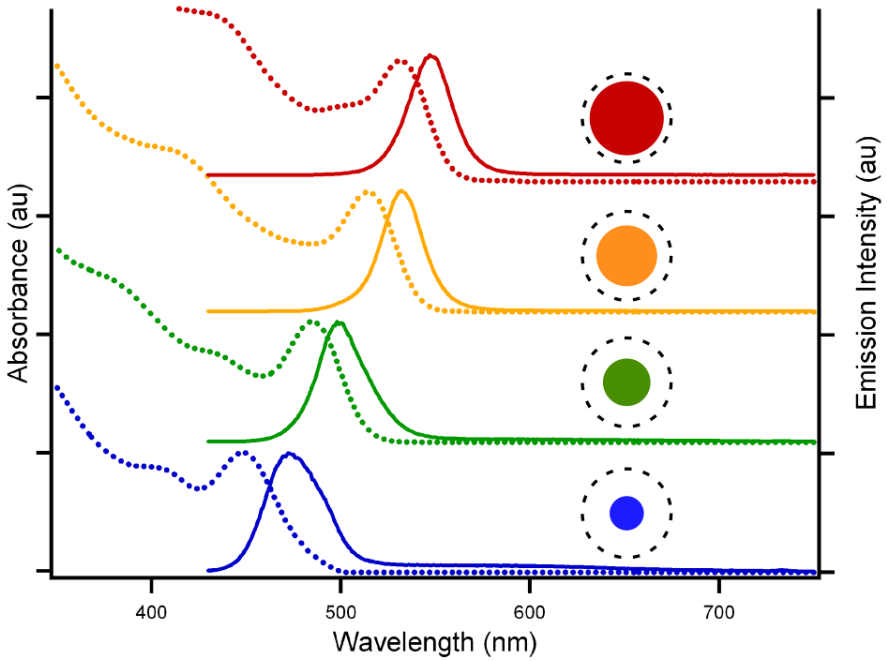

Figure 1.4 Absorption spectra (dashed lines) and emission spectra (solid lines) of 4 different sizes of nanocrystals. Beside each the spectra is a diagram showing how the emission color would change with the nanocrystal size (blue being the smallest and red the largest). The black dashed line surrounding each "nanocrystal" represents the bulk Bohr diameter.

The tunable electronic and optical properties, high extinction coefficients, and high quantum yields of quantum dots have made the study of their synthesis and applications an area of intense research. This research has already exposed nanocrystals' usefulness in biological labeling, photovoltaics, and monochromatic LEDs.[37-51] Multiple colors of nanocrystals have even been used to create white LEDs with the same color quality drawbacks as other narrow-band based white LEDs.[52-55] In all cases where the emission was the useful property for a specific application, it was always near monochromatic emission. It was long believed that a single Gaussian distribution of wavelengths, centered around a specific energy, was possible from a single size of nanocrystals.[21, 26] In 2005, Bowers *et al.* synthesized CdSe nanocrystals with a diameter less than 2 nm, expecting to detect deep blue emission.[56] Instead of a monochromatic emission, however, they detected broad-band emission which covered nearly the entire visible spectrum of light (Figure 1.5). With this discovery came the possibility of combining the positive aspects of nanocrystals (mainly high quantum yield and solution processability) with the broad emission to form high-quality white and efficient SSL.

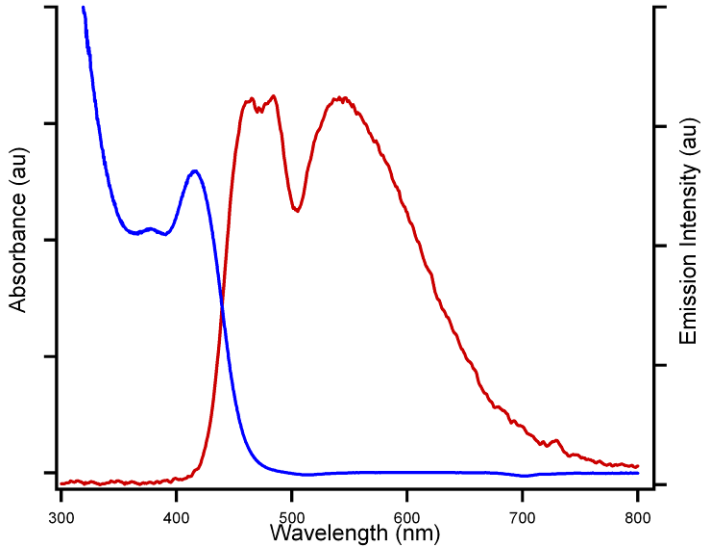

Figure 1.5 Absorbance (blue) and emission (red) spectra of ultrasmall, CdSe while-light emitting nanocrystals. The broad emission provides excellent CIE color coordinates and a very high CRI value.

1.3 Scope of This Work

This dissertation provides information on how white-light, ultrasmall nanocrystals are synthesized and the incorporation of these into electroluminescent and photoluminescent devices. Initially described is the synthesis of nanocrystals, including traditional (diameters > 2 nm) CdSe, ultrasmall CdSe, and growth/shelling procedures for very large and core-shell nanocrystals. This is followed by a description of the synthesis and characterization of various phosphonic acids, along with the modified nanocrystal synthesis for their use. Next, encapsulation of nanocrystals into various polymers and the coating of UV or blue LEDs for the fabrication of photoluminescent devices are detailed. The final experimental section depicts the fabrication techniques and characterization of various layers involved in the production of nanocrystal based electroluminescent devices.

The chapters that follow provide results and conclusions from the three main projects which I worked on during my time at Vanderbilt University. The first (Chapter 3) is the pinning effect seen in ultrasmall nanocrystals and subsequent modulation of the quantum yield and emission wavelength of the pinned emission via phosphonic acid alterations. Subsequently, the results from photoluminescent devices (Chapter 4) and interpretation of the results are presented. This is followed by a proof of concept report on nanocrystal electroluminescence (Chapter 5).

Finally, a chapter is presented which describes the current outlook for ultrasmall CdSe nanocrystals. The appendixes provide some technical information on color characteristics, efficiency comments, and spectra concerning the characterization of phosphonic acids.

CHAPTER II

EXPERIMENTAL

2.1 Introduction

Herein are described the details on the experimental work done during my time at Vanderbilt University. In section 2.2 the synthesis of phosphonic acid ligands and their characterization is described. The synthesis of nanocrystals in described in section 2.3 in the following order: 2.3.1 PbSe, 2.3.2 traditional and ultrasmall CdSe with phosphonic acid, 2.3.3 CdSe/ZnS core-shells, 2.3.4 CdSe with oleic acid, and 2.3.5 Cd-phosphonate studies.

The fabrication of solid-state lighting devices with ultrasmall CdSe nanocrystals falls into two categories: 2.4 encapsulation and photoluminescent studies and 2.5 electroluminescent studies. The encapsulation in various polymers is described in section 2.4.1 through 2.4.3, while the monomer encapsulation is described in 2.4.4. The description of the testing of photoluminescent films and coated LEDs is contained in section 2.4.5. Section 2.5.1 describes the initial thin film fabrication and characterization of the films for EL devices. Section 2.5.2 illustrates the testing setups used for these devices, and the work performed at CNMS-ORNL is detailed in section 2.5.3.

2.2 Phosphonic Acid Synthesis and Characterization

Below is described the synthetic route to a range of phosphonic acids used in the synthesis of nanocrystals. In general, an S_N2 substitution is carried out between a nucleophilic phosphite and an electrophilic alkyl halide, the Michaelis-Arbuzov

reaction.[57-60] Following an acid hydrolysis of this product, the pure phosphonic acid can be obtained via recrystallization. The successful synthesis of each phosphonic acid was verified by the melting point of the collected crystals and analysis of these crystals using proton and carbon nuclear magnetic resonance spectroscopy (NMR), infrared spectroscopy (IR), and electrospray ionization mass spectrometry (ESI-MS).

2.2.1 Reaction Steps

Initially, 2.1 moles of triethyl phosphite (TEP, Sigma-Aldrich, 98% purity) and 2.0 moles of a brominated alkane (Sigma-Aldrich, >95% purity) were placed in a customized 3-liter, 2-neck round bottom flask. The choice of brominated alkane depended on the structure of the phosphonic acid being synthesized; Figure 2.1 shows the structures of the various phosphonic acids synthesized during this work. A glass coated temperature probe, attached to a heating mantle via a temperature controller, was placed into the threaded, smaller neck of the flask. In the center neck a 24/40 to 14/20 converter was used to accommodate a water jacketed, 6-inch condenser. The contents of the flask were stirred and heated at a temperature of ~150 °C for 24 hours; the exact temperature depended on the boiling point of the bromoalkane used. The reaction was considered completed after 24 hours due to a slight yellow color that was noted, along with the slackening of bromoethane venting (38.4 °C boiling point).

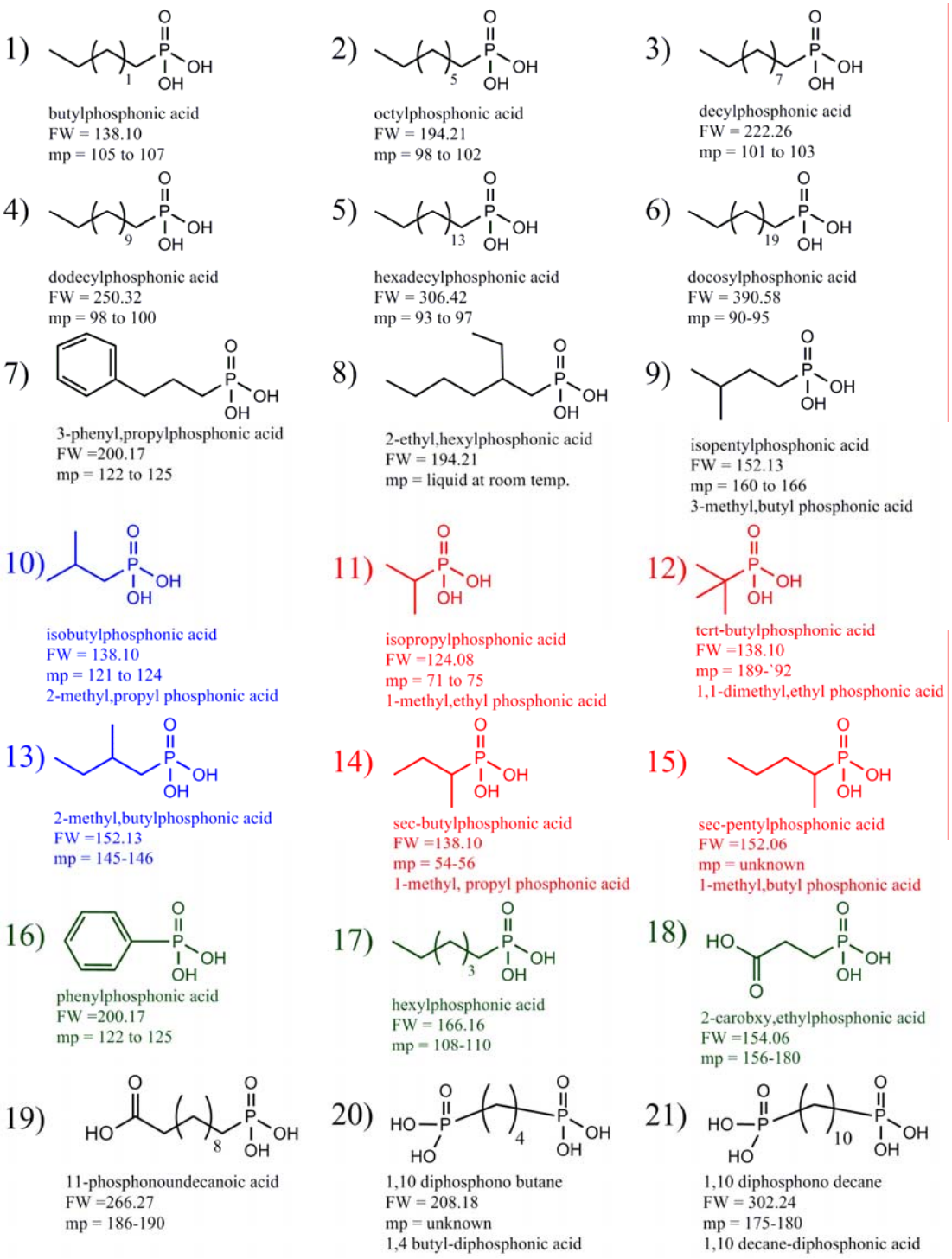

Figure 2.1 Structures of the phosphonic acids utilized during this work. The structures in red were unsuccessfully synthesized, due the steric hindrance or loss of electron deficiency because of their secondary or tertiary nature; the blue structures were successfully synthesized, however, they could not be purified; and the green structures were purchased from Sigma-Aldrich or Alpha Aesar. The literature melting points and formula weights for most of the phosphonic acids are listed.

The desired phosphonate had been created at this point (Figure 2.2) and needed to be hydrolyzed in order to produce the phosphonic acid. Using an acid hydrolysis allows for the reaction mixture described previously to be used without any purification—any unreacted bromoalkane or TEP molecule will act as solvents. The flask and its contents were cooled to 80 °C, to allow for the introduction of 4.25 moles of 12.1 M HCl. When scaling down this reaction, a small amount of deionized water was added to increase the total volume. The reaction was stirred and refluxed at ~105 °C, with water running through the condenser's water jacket for 6 hours and without *running* water for 14 to 18 hours. It was likely that the hydrolysis had already been completed, however, further heating at ~110 °C for 24 hours aided in removing excess water and any solvated ethane.

The reaction mixture was cooled to 60 °C allowing a recrystallization process to be carried out with ethyl acetate. In the cases where the longer chain alkyl phosphonic acids were synthesized, a solid product could be noted falling out of the solution prior to the addition of any recrystallization solvent. Approximately 300 mL of ethyl acetate was added to the reaction flask and stirred. The subsequent solution was then poured into two 1-liter recrystallization dishes and placed on ice for at least 3 hours. The solid phosphonic acid crystals were then collected *via* vacuum filtration (a water-aspirator provides enough vacuum for this process) through a 10½ inch Buchner funnel with custom-cut filter paper and a heavy-walled, 4-L filter flask. The dishes were simultaneously vacuum-filtered and the collected crystals washed twice with ~200 mL of cold ethyl acetate. Post-washing, the crystals were allowed to dry on the vacuum filtering setup for ~20 min. The product crystals were then collected into a clean recrystallization dish and covered with a XL Kimwipe, held in place by a rubber band. This entire setup

placed in a dry box antechamber under >30 inches of Hg vacuum for ~12 hours, removing any excess ethyl acetate.

Unfortunately, when recrystallizing the phosphonic with ethyl acetate from the solution containing excess HCl some acetic acid formed. This acetic acid will contaminate the nanocrystal synthesis, causing the reaction to proceed too quickly, eliminating almost all size control. To remove the acetic acid, a traditional recrystallization was performed using about 1.5 L of acetonitrile for every 100 grams of phosphonic acid recovered from the 1st recrystallization. The acetonitrile was heated almost to boiling in a large beaker on a hot plate (a heat gun was also used to heat the solvent more quickly) and the phosphonic acid stirred into the solvent with continued heating. Once completely dissolved, the solution was poured into a recrystallization dish and left on a countertop to cool overnight. Almost immediately some crystals began to form; however, allowing the solution to cool for more than 12 hours increases the overall yield. The crystals were vacuum filtered and washed with a small amount of cold acetonitrile. Placing the clean phosphonic acid in the dry box antechamber under full vacuum for 24 hours removed any residual solvent.

2.2.2 Mechanism

The mechanism for the Michaelis-Arbuzov reaction is shown in Figure 2.2. At the beginning, the lone pair of electrons on the TEP attacks the electron deficient carbon adjacent to the bromine in the bromoalkane, forming a phosphonium ion and ionized bromine. The bromine anion then becomes the nucleophile in a second S_N2 reaction with the phosphonium ion, producing the phosphonate and bromoethane; the bromoethane is

displaced almost immediately due to its low boiling point. Care should be taken with the bromoalkane chosen for the reaction based on the boiling point and ability of the molecule to participate in an S_N2 reaction. Aryl, vinyl, and tertiary bromoalkanes do not react and only a few secondary bromoalkanes can proceed via an S_N2 mechanism due to the loss of electron deficiency and steric hindrance in these structures (Figure 2.1).[57, 60-62]

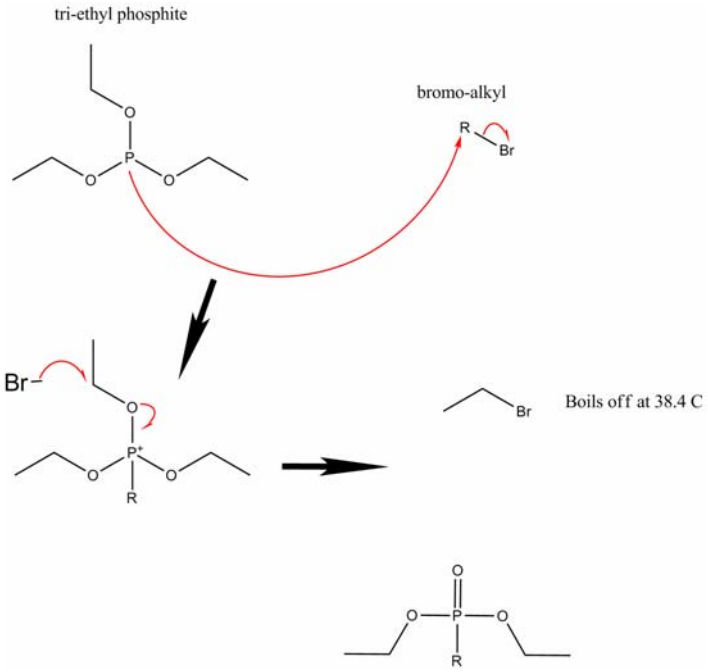

Figure 2.2 Mechanism for the Michaelis-Arbuzov reaction of triethyl phosphite with an alkyl bromide.

As can be seen from the acidic hydrolysis mechanism presented in Figure 2.3, the mechanism is similar to the hydrolysis of an ester. The phosphonate is activated toward nucleophilic attack by the addition of a proton to the carbonyl-like oxygen (in this case the oxygen is doubly bonded to phosphorus, not carbon). Water then becomes the nucleophile in the attack directly onto the phosphorus, yielding an intermediate with

phosphorus bonded to 4 oxygens and 1 carbon. One of the ester-like oxygens is protonated, creating a good leaving group, which is kicked out as an alcohol. Deprotonation regenerates the carbonyl-like oxygen on the phosphorus, producing the phosphonic-acid ester. This cycle is repeated in order to move from the phosphonic acid-ester to the fully acidified phosphonic acid.[57, 60, 62, 63]

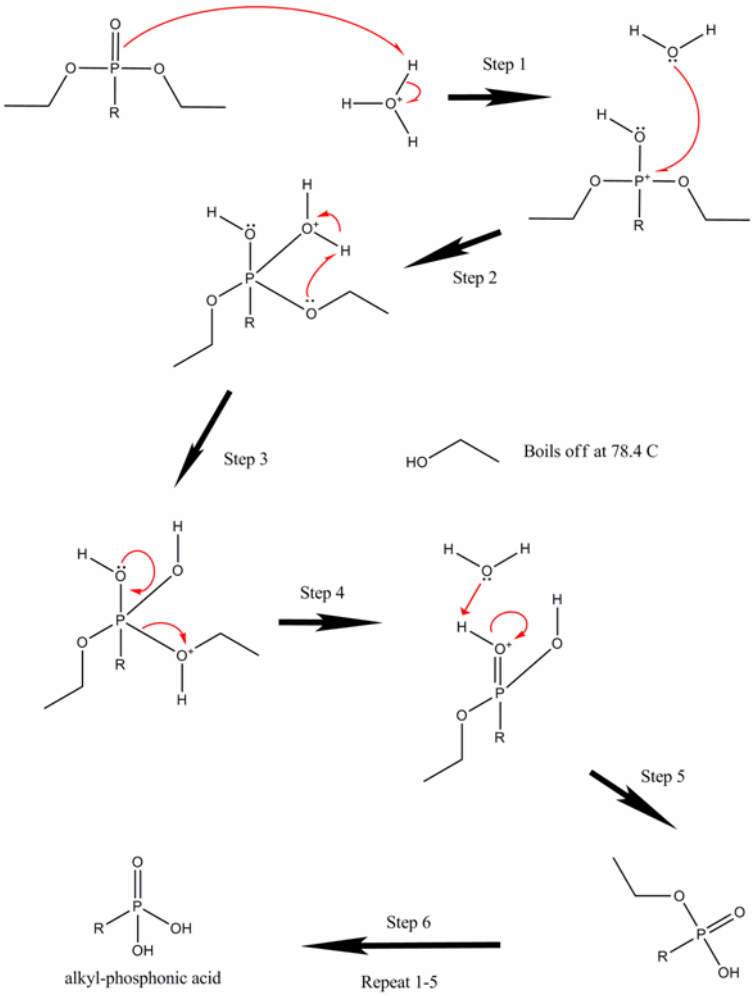

Figure 2.3 Acid-catalyzed hydrolysis of an alkyl phosphonate into the phosphonic acid. This essentially follows the same steps as the hydrolysis of an ester.

2.2.3 Characterization of Phosphonic Acids

Phosphonic acids can be characterized by many analytical techniques to determine the degree of purity. When weighing out specific quantities of the phosphonic acid, any contamination will reduce the molar ratios used in the synthesis described later in this dissertation. Further, some contaminants will adversely affect the reaction and subsequent nanocrystals size or shape. The easiest and least sensitive of the methods is to determine the melting point of the phosphonic acid crystals. Phosphonic acids are hygroscopic and consequently the crystals' melting point is not precise enough by itself to confirm a high degree of purity. However, this should allow for determination that a relatively successful synthesis and purification has been carried out. The literature melting point values are shown in Figure 2.1 for the phosphonic acids which were synthesized.

Infrared spectroscopy was carried out to confirm that the hydrolysis of the phosphonic-ester had actually been successful. In particular, the presence of a strong, sharp P—O—H stretch in the 1040-910 cm^{-1} region and a strong, sharp P==O stretch (1200-1100 cm^{-1}) with the lack of both an intense 1050 cm^{-1} and a weaker 1190 cm^{-1} P—O—C peak confirm that the Michaelis-Arbuzov reaction and hydrolysis were successful (Figure 2.4). The samples were prepared by crushing approximately 200 mg of dried KBr with about ~3 mg of phosphonic acid crystals. This powder was then placed into a die-set and pressed to form a thin, translucent disk. After calibrating with a blank KBr pellet, each sample was analyzed using a Thermo Nicolet IR300 spectrometer with EZ OMNIC version 6.1 software.

All phosphonic acids exhibit stretches in the 2350-2080 (broad, P—O—H bend), 1740-1600 (very weak, P—O—H deformation), and 1440-1490 (sharp, P==O bend) cm^{-1} regions. Additionally, a large broad peak centered slightly below 3000 cm^{-1} will represent any adsorbed water. Unique alkyl stretches dependent on the carbon side-group allow for further determination of the total phosphonic acid structure. Specifically, 2 very sharp absorption peaks should appear from 3000-2800 cm^{-1} due to the methyl and/or ethyl stretches overt top of the "water peak." Should these specific peaks not appear, it is likely due to the hygroscopic nature of the phosphonic acid; drying a small crushed sample of the crystals at 80 °C for 48 hours should reduce the water content.[62, 64-67]

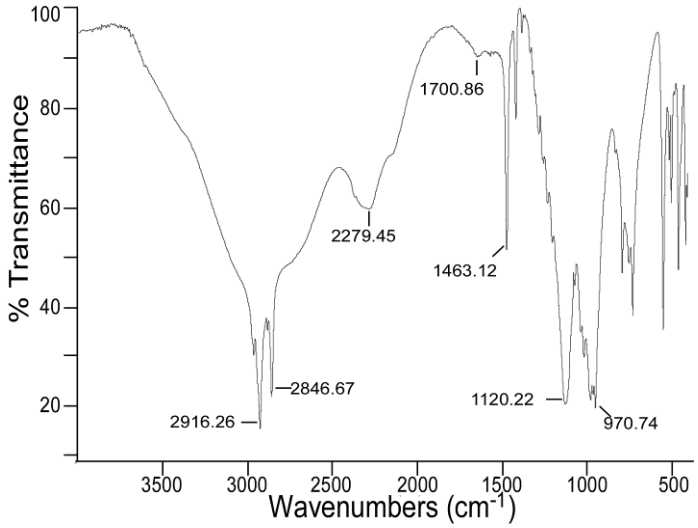

Figure 2.4 Graph of IR transmittance of dodecylphosphonic acid. The analysis of further samples is located in Appendix 2.

Nuclear magnetic resonance spectroscopy is crucial to the determination of any contamination of the phosphonic acid, particularly if the contaminant is acetic acid or excess ethyl acetate. Additionally, NMR allowed for the discrimination of the various

phosphonic acid structures synthesized. Both ^{1}H and ^{13}C NMR were employed extensively, while ^{31}P did not yield results significant for structural characterization. NMR samples were prepared by placing 15-20 mg of the phosphonic acid crystals in an NMR sample tube and dissolving these crystals with deuterated chloroform, methanol, or dimethyl sulfoxide. All the samples were evaluated on a Bruker 300 MHz spectrometer equipped with a 7T Oxford magnet controlled by a Bruker DPX-300 console at ambient temperatures. The spectra were then analyzed using TopSpin 2.0 software.

Both the proton and carbon NMR were most useful in characterizing the carbon side-chain. Aside from noting any contamination due to acetic acid, ethyl acetate, or tri-ethyl phosphite, the ^{1}H NMR structural characterization was straightforward (Figure 2.5A). The acidic protons may or may not appear due to any deuterium exchange; however, should their relatively broad peak be present, it generally fell beyond 10 ppm. For the straight chain alkyl phosphonic acids: the methyl group should be around 0.9 ppm with an integration of 3H, the two ethyl groups closest to the phosphorus produced overlapping doublets that appeared between 2.0 and 1.5 ppm with a total integration of 4H, and the rest of chain created a single peak with the anticipated integration slightly above 1.0 ppm. Any branching, double or triple bonding, and aromaticity was consistent with the expected number, location, and integration of peaks.

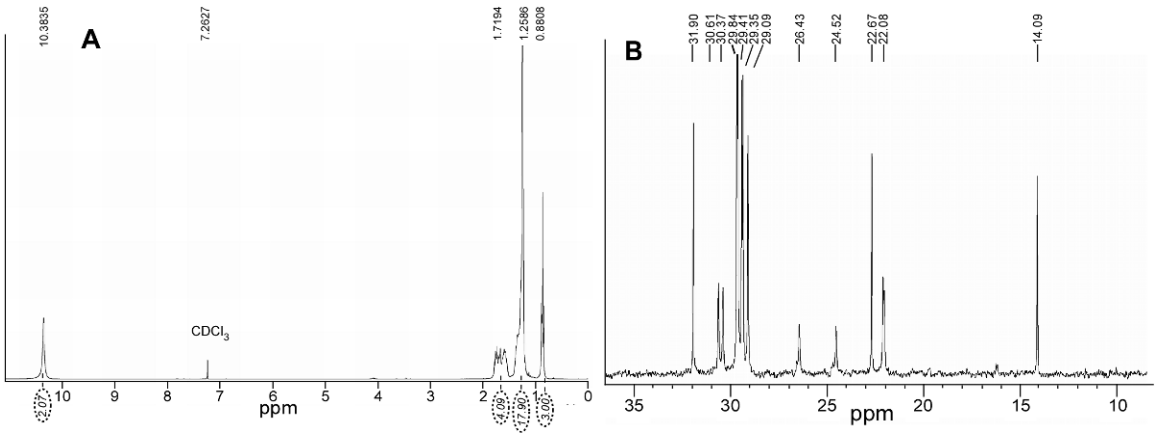

Figure 2.5 NMR spectra for dodecylphosphonic acid in $CDCl_3$ A) ^{1}H spectra and b) ^{13}C spectra. The analysis of further samples is located in Appendix 2.

The analysis of ^{13}C NMR spectra for phosphonic acids was slightly more complicated, due to the purity of the bromoalkanes used. The most common contaminant in the n-bromoalkane starting material is slightly branched bromoalkanes of the same molecular weight. The slight branched chain phosphonic acid contamination could cause a few small peaks to appear, in some cases, almost directly on top of the authentic peaks. Since the integration in ^{13}C NMR does not directly correlate to the number of carbons, it was difficult to discern which peaks represent the majority product and which were contaminates. As far as the actual nanocrystal synthesis reaction is concerned, this slight phosphonic acid impurity is not as significant as other impurities, such as acetic acid. Figure 2.5B demonstrates an impurity free ^{13}C NMR spectra of dodecylphosphonic acid.

Electrospray ionization mass spectrometry was the last analytical technique used to verify the successful phosphonic acid synthesis and purification. For negative mode ESI-MS, the sample preparation involved dissolving a known mass (typically less than 2 mg) into HPLC-grade methanol, followed by dilution of the solution to 5-15 µg/mL. The

phosphonic acid groups tested dissociated easily enough that the addition of any base was not necessary. Positive mode samples can be prepared by the addition of one drop of glacial acetic acid to the pre-diluted sample, although little pertinent information was obtained from positive mode ESI-MS. Once diluted, the solutions were analyzed on a FinniganMat electrospray ionization LCQ mass spectrometer system with TunePlus version 1.3 software. The crucial determination with negative mode ESI-MS was whether both phosphonate esters had been hydrolyzed. Verification of complete hydrolysis was provided by the phosphonic acid minus one, dimer, trimer, tetramer, and sodiated versions (22 m/z greater) of these mass peaks (Figure 2.6). In the cases of only partial hydrolysis, peaks with 28 m/z greater should be noted. Due to the low masses of several of the phosphonic acids tested, butyl phosphonic acid for example, only analysis of the dimer, trimer, etc peaks was possible. Beyond the phosphonic acid tetramers, the spectra could become convoluted to due to multiple sodium ions adding to the mass and multiple dissociations within a coordinated group of phosphonic acids, thus the analysis should be confined to the lower mass groupings.

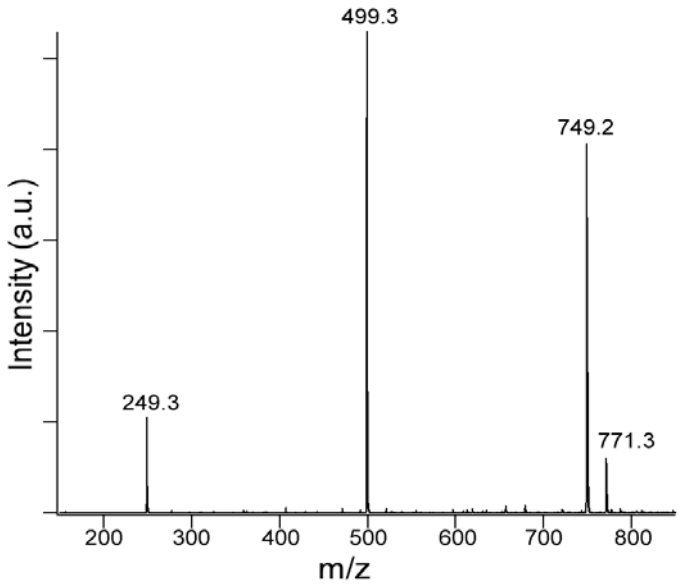

Figure 2.6 Negative mode ESI-MS spectra for dodecylphosphonic acid in methanol. The phosphonic acid minus one, dimer minus one, trimer minus one, and sodiated trimer minus one can be clearly seen. The analysis of further samples is located in Appendix 2.

2.3 Nanocrystal Synthesis

The following details the assorted synthetic techniques used for the fabrication of PbSe, "traditional" CdSe, ultrasmall CdSe, and CdSe/ZnS core-shell nanocrystals. For each semiconductor nanocrystal batch synthesized, the type of solvent used as well as the ratio of reactants and solvents could be tuned for specific purposes.

2.3.1 PbSe Synthesis

In order to fabricate photovoltaics using nanocrystals which absorb the solar spectrum, IR absorbers are required. The PbSe synthesis that follows was slightly modified from the reactions used by Murray, *et al.* and Guyot-Sionnest, *et al.*[68-70]

To synthesize a stock Pb-precursor, 5 mmol of Pb (II) acetate trihydrate were dissolved in 24 mL of trioctylphosphine (TOP), 6 mL of phenyl ether (PE), and 5 mL of

oleic acid (OA) in a 2-neck, 50 mL flask fitted with a temperature probe and gas adaptor fit with a stopcock. The flask was placed under full vacuum (<100 mTorr) on a Schlenk line (complete with a dry ice/acetone cold trap) and heated at 85 °C for 60 min. During this time the solution turned colorless and clear, indicating the creation of lead oleate. The flask was then charged with N_2 and cooled to 40 °C under N_2 pressure. After sealing the flask, the solution was allowed to cool to ambient temperature. Depending on the seal, this solution remained oxygen free for about 2 weeks. In a glove box, 10 mmol of selenium powder was mixed into 10 mL of TOP in a glass vial with a Teflon coated rubber septum top. After the vial was sealed, the contents were heated and stirred until no selenium powder was visible; this stock solution was used as the selenium precursor.

In a 50 mL, 3-neck flask, 10 mL of phenyl ether were heated at 80 °C for 60 min under full Schlenk line vacuum. The solution was then heated to 200 °C under N_2 atmosphere. In a 12 mL syringe, 1.3 mL of the Se:TOP and 9.5 mL of the Pb-OA solutions were mixed, before injecting the contents of the entire syringe into the hot phenyl ether. The flask was cooled to 120 °C with compressed air applied to outside of the flask and allowed to react. The time that the solution was maintained at 120 °C determined the size of the PbSe nanocrystals formed. Once the desired size was obtained, the flask was cooled to less than 80 °C and the entire solution poured into three plastic vials (~11 dram). Filling these vials with methanol and centrifuging for 5 minutes at 6000 rpm caused the nanocrystals to form a pellet. After decanting the liquid, each dried pellet was solvated in a small amount (~3 mL) of hexanes. Spinning the tubes again for 10 minutes at 6000 rpm removed any large aggregates that had formed; the cubic PbSe nanocrystals remained in solution and were analyzed *via* near-IR absorption

and transmission electron microscopy (Figure 2.7) prior to use in photovoltaic fabrication.

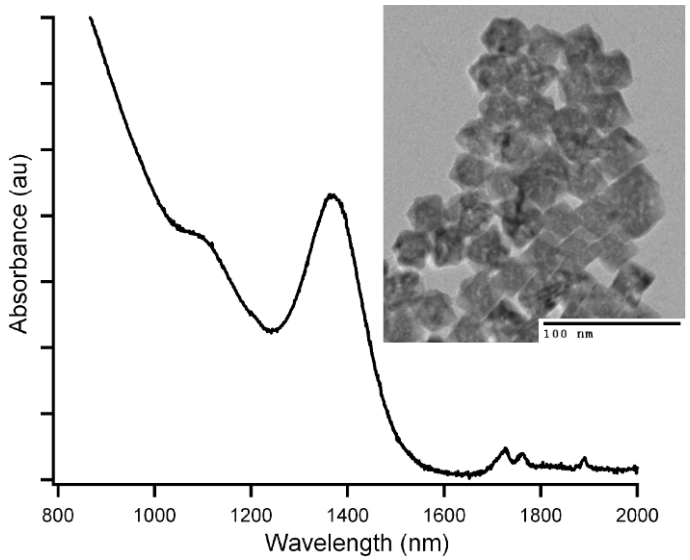

Figure 2.7 Absorption spectra and transmission electron micrograph (inset) of PbSe cubic nanocrystals. The TEM image is from a larger size of PbSe than the absorption spectra, but was chosen in order to show the cubic nature of the crystals.

2.3.2 Traditional and Ultrasmall CdSe Synthesis

CdSe nanocrystals have been fabricated with many solvents and precursors for several years.[71-73] The method employed for the synthesis of traditionally sized nanocrystals in this work has been modified from that used by Peng, et al.[74-76] The synthesis can be scaled to produce more or less nanocrystals, as desired.

These syntheses were carried out in the setup shown in Figure 2.8. To a 50 mL, 3-neck, round bottom flask, 1 mmol of cadmium oxide (CdO) and ~2 mmol of dodecylphosphonic acid (DDPA) were added with 6 g of tri-n-octyl phosphine oxide (TOPO) and 4 g of hexadecylamine (HDA) as high boiling point solvents. The flask was

heated to 150 °C under an argon purge, at which point the "purge needle" is removed and the flask heated at 325 °C. At this temperature, the CdO and DDPA form a Cd-phosphonate complex, acting as the cadmium precursor, indicated by the solution turning clear and colorless.

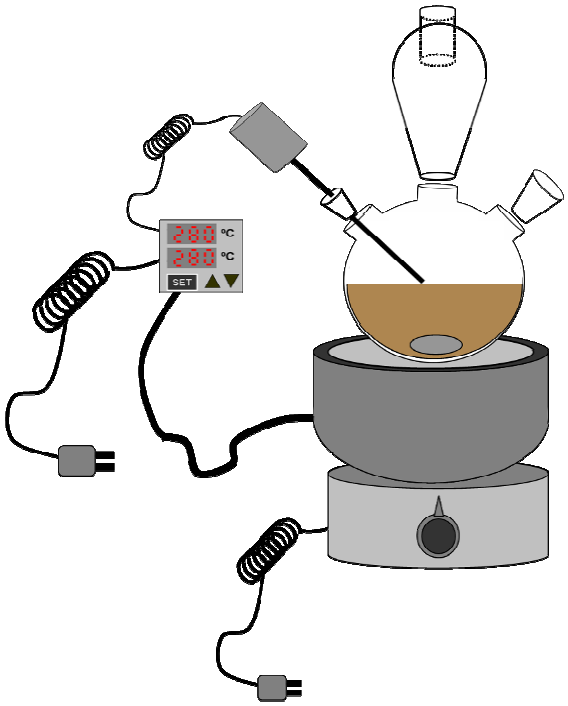

Figure 2.8 Setup for synthesis of CdSe nanocrystals. The reaction mixture is placed inside a 3-neck, round bottom flask with a stir-bar. The flask is placed in a heating mantle, powered by a pre-set external temperature controller connected to a customized thermocouple temperature probe. The 3 necks of the flask are filled with the temperature probe, a self-washing bump trap, and a rubber septum. The entire setup is loaded onto a stir plate and held in place *via* several clamps attached to a hood manifold. Argon is connected to the bump trap with a 24/40 gas adapter; while a 12 gauge needle punctured through the septum is used as an outlet during the purge phase of the synthesis.

A 1 M stock solution of selenium in tri-n-butyl phosphine (TBP) was diluted to a 0.2 M reaction solution, 4 mL of which were swiftly injected into the reaction vessel at ~310

°C. The temperature was allowed to cool to 260 °C, and the nanocrystals were grown to the desired size by monitoring the absorption spectra (Figure 2.9). Absorption spectra were collected on a Varian-Cary 50 Bio ultraviolet-visible (UV-VIS) spectrophotometer with accompanying software. When the desired size was reached, the flask was air-cooled to less than 100 °C.

The reaction vessel's contents were emptied into three plastic vials (~11 dram). These vials were filled with methanol and centrifuged for 5 min. at 6000 rpm causing the nanocrystals to form a pellet. After decanting the liquid, each dried pellet was resolvated in a small amount (~8 mL) of octanol, followed by 20 min. of centrifugation at 6000 rpm. The nanocrystals in octanol were decanted into three clean vials, which were then filled with methanol and centrifuged for another 20 min. at 6000 rpm. The nanocrystal pellet was then dried and resolvated in a non-polar solvent such as toluene or hexanes for characterization. This synthesis yields nanocrystals with quantum yields around 10%.

Ultrasmall nanocrystals (diameter < 2.0 nm) followed a similar synthesis to that of the traditionally sized CdSe nanocrystals with a few crucial modifications.[56, 77] After the Se:TBP injection described above, a 2nd syringe filled with butanol was quickly injected into the flask as soon as a slight yellow color was noted. This injection immediately lowered the temperature to 130 °C, followed by air-cooling to less than 100 °C. The cleanup process followed the same steps used for the larger sizes, with the substitution of hexanol for the octanol. In order to verify the successful synthesis of ultrasmall nanocrystals, the band-edge absorption peak should be centered at less than 420 nm and a broad-band emission should be noted (Figure 2.9). The emission of nanocrystals was

recorded using and ISS PC1 photon counting spectrofluorimeter with Vinci version 1.6.SP5 software.

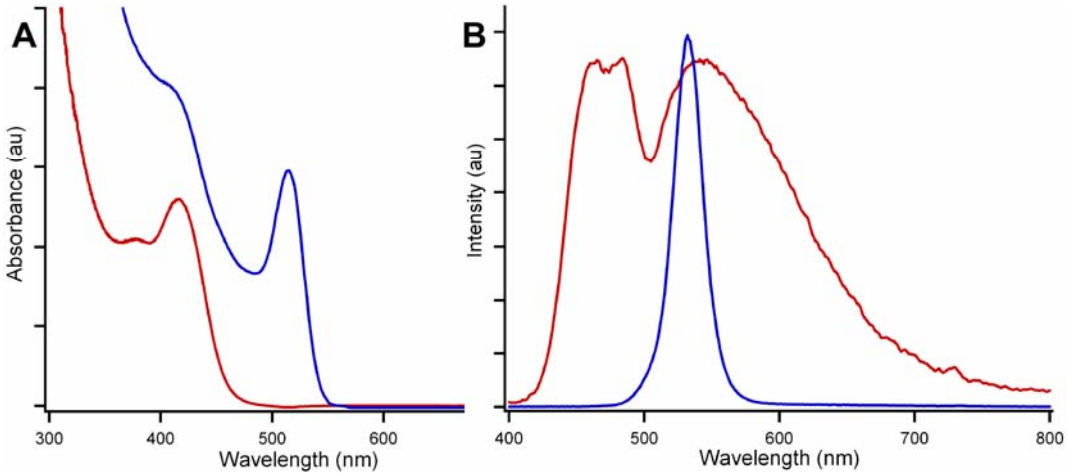

Figure 2.9 A) Absorption spectra of ~2.5 nm (blue) and ultrasmall (red) CdSe nanocrystals. B) Emission spectra of the same ~2.5 nm (blue) and ultrasmall (red) nanocrystals.

2.3.3 CdSe/ZnS Core-Shell Synthesis

For several applications including biological labeling and the fabrication of LEDs higher photoluminescent quantum yields than 10% are desired. Shelling the traditionally sized CdSe with a higher band gap material such as ZnS forces a higher percentage of the generated excitons to radiatively recombine, due to surface passivation, emitting more photons.[74, 78-80] The synthesis for CdSe/ZnS nanocrystals begins with the same synthesis already described, with the nanocrystal "cores" solvated in hexanes. A similar setup as the standard synthesis (Figure 2.8) is used with the main changes being the replacement of the 50 mL reaction flask for one with a 100 mL volume and the self-washing bump trap exchanged for a short-path distillation column filled with acetone.

Into the 100 mL flask, 18 g of TOPO and 12 g HDA were placed and the temperature was raised to 210 °C. After a few minutes, during which the temperatures settles, an entire batch of CdSe nanocrystal "cores" solvated in hexanes was injected into the reaction flask. While the temperature was rising to 200 °C, a shelling solution of 10 mL of 1.0 M Zn-naphthenate in toluene, 10 mL of 1.0 M S in dibutyl ether, and 10 mL of toluene was mixed in a 30 mL syringe. Once the desired temperature was been reached, the solution was added dropwise (~40 drops per minute) using a syringe pump and a piece of small diameter plastic tubing. Throughout the course of the shelling process the absorbance and emission were monitored to determine when the maximum quantum yield had been reached. In most cases, less than 25 mL were required to see significant brightening of the nanocrystals, at which point the addition of the shelling solution was halted and the reaction allowed to stir for 5 minutes. As the shelling proceeded, the toluene and dibutyl ether were distilled from the reaction flask leaving only the core-shells, TOPO, and HDA. The isolation of the core-shells follows the same procedure as the synthesis of traditionally sized CdSe.

2.3.4 CdSe with Oleic Acid Synthesis

As described earlier, the ligands of the nanocrystal are dependent on the reaction solvents and precursor materials. In some cases, a phosphorus based cadmium precursor was not desired, at which point the following synthesis based on the work of Peng, *et al.* and van Embden, *et al.* was followed.[75, 81] In the setup shown in Figure 2.8, Cd-oleate was generated as the cadmium precursor; to the 50 mL flask the following were added: 10 mL of octadecene (ODE), 1 mmol of Cd, and 4.5 mmol oleic acid (OA). The solution

was purged with argon while raising the temperature to 150 °C, followed by heating at 320 °C under an argon atmosphere until the solution turned colorless. A 4 M stock solution of Se:TBP was diluted with ODE to a 0.1 M solution of Se in TBP/ODE. Into the reaction flask, 10 mL of the Se:TBP/ODE were injected and the solution allowed to cool to 230 °C. When the desired size was obtained, as determined by monitoring the absorption, the entire vessel was air cooled to less than 100 °C. The isolation procedure for these nanocrystals was to split the entire reaction mixture into two glass vials along with 8 mL of butanol and 8 mL of ethanol in each vial, followed by vigorous shaking. The vials were filled with methanol and spun for 15 minutes at 2500 rpm. The liquid above the precipitated nanocrystals was decanted and the pellet was allowed to dry. The nanocrystals were then dissolved in 8 mL of hexanes through vigorous shaking and then precipitated with methanol and 15 min of centrifugation at 2500 rpm; this step was repeated 4 times at which point the nanocrystals were considered fully cleaned.

Ultrasmall nanocrystals synthesized *via* the oleic acid method followed almost the same procedure. In these cases, a 20 mL butanol injection was used to cool the reaction almost instantaneously due to the accelerated speed of this reaction, with respect to the Cd-phosphonate synthesis. This 2nd injection required that during the cleanup procedure no more butanol was added to the vials, as a significant portion of the cooling butanol remained.

2.3.5 Cd-phosphonate Studies

The ultrasmall nanocrystals' broad emission is due to trap states on their surface. These traps states were believed to be controlled in a small part by the nanocrystal's

ligands. In order to study nanocrystal ligands, involving thermogravimetric analysis (TGA) and IR absorption spectroscopy, Cd-phosphonate precursors of each of the phosphonic acids previously mentioned were synthesized. In order to differentiate between HDA, TOPO, and the phosphonic acid ligands, the precursors were synthesized in hexanol (in the case of docosyl phosphonic acid, octanol was used). A stir bar, 2 mmol CdO, 18 mL of hexanol, and 5 mmol of the phosphonic acid of choice were placed in an 11 dram glass vial, which was sealed with a thin Teflon-coated rubber septum inside the standard vial top. In order to maximize productivity, 4 reaction vials were placed in a metal heating block simultaneously. A thermocouple temperature probe was put in the center hole of the heating block and the entire setup placed on a VWR 220 mini hotplate/stirrer. The temperature was monitored by the probe, while the heating and stirring were controlled *via* the hotplate/stirrer. The samples were heated at refluxing temperature (~155-160 °C) until no brown color (CdO) was visually detected, generally ~60 hours (Figure 2.10). At this point, only a white semi-solid and hexanol remained in the vials. The entire metal block was placed on cardboard to cool below 100°C, at which point the temperature probe was removed. The vials were opened, filled with methanol, vigorously shaken, and centrifuged for 10 min. at 2500 rpm. The liquid was decanted and the Cd-phosphonate solid mixed with 20 mL of methanol. The solution was shaken and the solid collected *via* vacuum filtration; any remaining phosphonic acid should be removed by repetition of this simple cleaning process (for a total of 2 times). The solid was dried at 100 °C for 2 hours.

Figure 2.10 Image of Cd-phosphonate reactions. From left to right the reaction times for the vials are: 15, 34, 49, and 62 hours.

The Cd-phosphonate was then analyzed using the same IR absorption procedure used with the phosphonic acids. Using an Instrument Specialists Inc. TGA1000, each Cd-phosphonate, phosphonic acid, HDA, TOPO, and several nanocrystal batches were evaluated. For each TGA run, ~10 mg of solid was placed in a platinum weigh boat and loaded into the TGA1000. Each scan was run under air, while generally following this protocol: 1) ramping the temp. to 80 °C at 20 °C/min, 2) hold for 5 minutes, 3) ramping the temp. to 600 °C at 5 °C/min, 4) ramping the temp. to 820 °C at 1 °C/min, and 5) the furnace was allowed to cool to room temperature.

2.4 Nanocrystal Encapsulation and Photoluminescent Studies

After the discovery of white-light nanocrystals, their application in solid-state lighting immediately came to mind. As the broad fluorescence of these ultrasmall nanocrystals had first been seen when pumping them with ultraviolet light in a spectrofluorimeter, it is no surprise that the first example of their use was based on photoluminescence. Initially Bowers, *et al.* mixed the white-light nanocrystals into commercially available

polyurethane Minwax and excited a thin film of this dried mixture with a 400 nm laser line.[56] Next, a thin film of this CdSe:polyurethane mixture was coated on a standard 5 mm UV LED, yielding a primitive solid-state white device based on ultrasmall nanocrystals. Detailed next are the subsequent steps in creating and characterizing more sophisticated iterations of this light source. All the nanocrystals used are ultrasmall, white-light CdSe nanocrystals unless otherwise noted.

2.4.1 Encapsulation in Epoxies and Silicones

Polyurethane encapsulation of ultrasmall nanocrystals proved problematic for several reasons. The primary reason that polyurethane proved unsuccessful was that when mixed with any significant amount of toluene or hexanes, it proved extremely hard to cast and harden without extensive heating. The consequential bubbling reduced the light extraction from these films and impeded any shaping or molding of the mixture. An organized study was conducted into finding a commercially available polymer to encapsulate the nanocrystals.

Epoxies and silicones are the most common resins available for the encapsulation of materials and objects (Figure 2.11 A and C). Several companies were contacted and samples of their products were requested (Table 2.1). The accompanying instructions for each type of polymer were followed, to create samples of the epoxies and silicones,. In general, this involved mixing specific volumes or masses of two components (a hardener and a resin) followed by deposition within a 2 dram vial (used as a breakable mold) or drop casting a thin film onto a glass slide. The mixtures were then degassed for ~5 minutes in a small antechamber of a dry box at full vacuum and then heated at the

specified temperatures in an oven for several hours until the polymer had fully hardened. The polymers chosen were advertised as being glass-like when cured, and for the pure polymer samples this proved true.

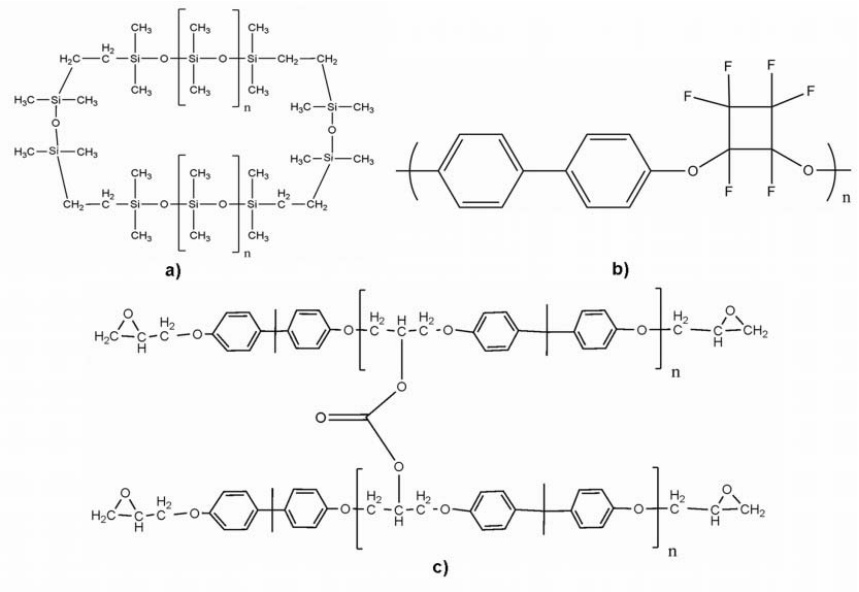

Figure 2.11 General structures of the a) silicones, b) BP-PFCB, and c) epoxies.

Encapsulation of nanocrystals within these polymers proved problematic. Initially a small amount of nanocrystals (<2% by weight compared to the encapsulant) in toluene (~25% by weight compared to the encapsulant) was added to a small portion of each mixture and a film cast. Upon mixing, the solution became turbid and often bubbles or cracks within the films were noted when cured. Most of the curing schedules were slowed significantly, most likely due to the addition of toluene as an extra solvent. In the cases of EP965LVLX clear and EasyCast, the films and molds did not cure into solids after 72 hours at 115 °C. This was more than 4x the expected curing time at much lower

temperatures; the chemical explanation will be discussed in a separate section. Concentration studies were carried out by changing the concentration of the nanocrystals in solution as well as the mass of nanocrystal solution added to the polymer mixtures.

Table 2.1. Polymer encapsulants used for studying the effects of ultrasmall nanocrystals encapsulation.

Corporation or Supplier	Trade name	Type of encapsulant
Environmental Technologies Inc.	Easy Cast Castin' Craft	Epoxy Polyester
Epoxy Technologies	EpoTek 301-2	Epoxy
Insulcast	510PTA-B RTVS61	Silicone Silicone
Aptek Labs	6100-1AB	Epoxy
Resinlab/Ellsworth Adhesives	EP965LVLX clear EP961 clear	Epoxy Epoxy
Halocarbon Production Corporation	Series 40 Series 2300	Halowax Halowax
Artmolds	Aqua Clear	Epoxy
GE Silicones	TSE3033	Silicone
Tetramer Technologies, L.L.C.	Biphenyl-perflurocyclobutyl polymer (BP-PFCB)	Thermoplastic fluoro-carbon chain polymer

2.4.2 Other Polymers

One polyester polymer, Castin' Craft, was also analyzed for its ability to effectively encapsulate nanocrystals. The same protocol used with the silicones and epoxies was used for this polyester polymer. A hardener was mixed with the resin, nanocrystals in toluene were added and stirred, followed by degassing of the sample, and finally curing under the manufacturer's specified temperature schedule.

Two halowaxes (Table 2.1) were studied for the same purpose. These halowaxes did not need to be polymerized, but merely solidified or melted depending on temperature. Series 40 was a liquid at room temperature, while Series 2300 had a boiling point of ~130

°C. Series 40 was mixed with a sample of the nanocrystals and while in liquid form appeared to have no affect on the emission properties. When placed within a fridge, the QD:wax combination solidified into a cloudy and cracked mass. A known mass of the Series 2300 was placed in a vial and melted in the oven at 150 °C. The addition of a small amount of 2% nanocrystals in toluene caused the temperature to drop below the melting point, prior to any significant mixing of the nanocrystals. The mixture was reheated until it was completely liquid, at which point it was stirred with a pipette and then allowed to cool. This process destroyed the nanocrystals such that they no longer emitted white-light; instead of the standard yellow colored solution, a sickly brown color was noted.

2.4.3 Encapsulation with BP-PFCB

Several months into this project Tetramer Technologies, LLC contacted the Rosenthal group and proposed providing several polymer materials for encapsulating nanocrystals. The polymer provided was biphenyl-perfluorocyclobutyl polymer (Figure 2.11B, BP-PFCB), which was later sold under the name TetramerNDM (Nanoparticle Dispersion Matrix) in part due to this work.

In contrast to the epoxies and silicones used previously, this is a one part thermosetting polymer. The pre-set solid for BP-PFCB has a fluffy, white textile-like appearance and is extremely electrostatic, clinging to clothes, gloves, glass, and even metal tweezers. In order to cast a film of BP-PFCB, it was suspended in mesitylene at various w/w ratios, the most successful of which was 20%. Since the nanocrystals were dispersed within toluene at a specific weight ratio (generally around 2% to avoid

aggregation), mathematical analysis allowed for many QD:polymer ratios to be fabricated (from ~3 to ~20%). Using vials as molds and the addition of different volumes of the same mixture enabled the study of how film thickness affected the nanocrystal absorbance and emission properties.

Once a film had been drop cast on a glass film or a mold filled with a specific QD:BP-PFCB mixture, it was degassed for 15 min. in a dry box's small antechamber at >30 in. Hg vacuum. The films were then placed in an oven under ambient atmosphere for curing along a scale of 60 °C for ~20 hours or 80 °C for ~4 hours. The curing schedule was mostly determined by the evaporation of the mesitylene and toluene. Once cured the BP-PFCB films could be removed from the slides through gentle sonication in DI-water or gentle lifting with tweezers. The same procedure was used when studying films of the functionalized BP-PFCB polymers.

To study the effect of curing these QD:BP-PFCB films under Ar, O_2-rich, or ambient conditions a specific holder was fabricated in the Vanderbilt glass shop (Figure 2.12). It consisted of a recrystallization dish with the top ¼ inch of the outer surface converted to ground glass. The top of this apparatus was a large Petri dish with a 24/40 flask neck molded directly in the center, with the inner surface of the Petri dish walls converted to ground glass. The bottom was half filled with sand to allow uniform heating and prevent tipping of the samples when placed with the apparatus. Once the degassed QD:BP-PFCB films or vials containing the mixture had been placed on the sand, Dow Corning 44 high temperature grease was placed on the ground glass joint and the top sealed in place. A hollowed out 24/40 Teflon plug was placed within the top neck to narrow the opening. A pipette was connected to rubber hosing, through which the chosen gas was run, and

placed within the opening. This pipette filled only about ½ of the opening allowing any unwanted gas to escape. The selected gas was run through the apparatus for 10 minutes prior to placing the entire setup within the oven at 60 °C for ~20 hours and continued to flow in order to prevent any diffusion of unwanted gas into the setup.

Figure 2.12 Image of the custom-made curing apparatus used when curing films under an inert atmosphere.

2.4.4 Monomer Encapsulation

In addition to the BP-PFCB, Tetramer Technologies provided the Rosenthal group with several monomers. One sample was the monomer for BP-PFCB (BPVE) and the other was trifluorovinyl ether (TVE); the structures are shown in Figure 2.13. The plan was to mix the nanocrystals with the monomers, prior to polymerization. To study these monomers the following procedure was followed.

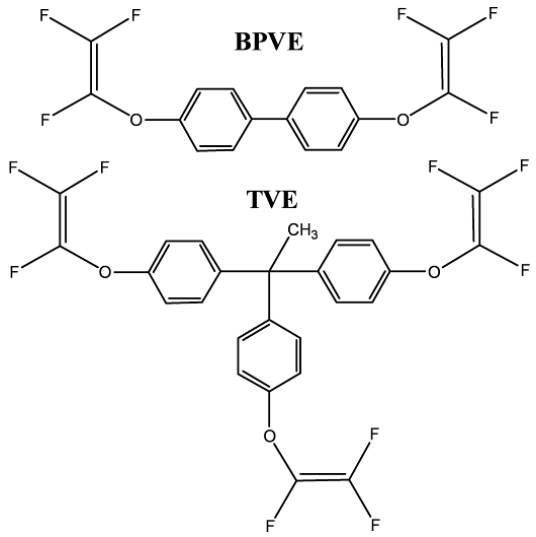

Figure 2.13 Structures of BPVE and TVE monomers provided by Tetramer Technologies, LLC.

Approximately 100 mg of the monomer was weighed out and placed inside a mold (an 11 dram vial which had been cut down to a height of ~5 cm). The molds were placed in the tube-furnace-like apparatus described previously and heated in an oven at 100 °C for ~30 minutes to melt the monomers. The samples were allowed to cool below 60 °C and a known volume of nanocrystals of a known concentration in hexanes was added. For most tests, the final nanocrystal to monomer ratio was maintained at less than 5%. The setup was then heated in the oven at 60 °C for 20 minutes, to remove the hexanes, followed by mixing the nanocrystal:monomer mixture with a pipette tip. The entire setup was purged with Ar for 15 min. and an Ar atmosphere was maintained thereafter. The samples were then heated at 100 °C for 1 hour, and then heated at 185 °C for 16 hours. The samples were allowed to cool slowly within the apparatus for 45 min. Next, the setup was opened and the samples were allowed to cool to room temperature on cardboard to prevent cracking of the films or the molds.

2.4.5 Testing Thin Films and Coated LEDs

Several techniques were used to test the various encapsulations' effects on the nanocrystals. The thin films were positioned in the UV-VIS spectrometer by taping the glass to the side of the sample compartment, such that the sample of interest covered the hole leading to the detector but the tape did not. Film thicknesses were measured using an Aerospace IP54 electronic micrometer and a Veeco DekTak 150 profilometer.

To measure the photoluminescence of the thin films, 2 systems were used. The primary and most useful setup was to front illuminate the thin film on glass with a 365 nm LED (Figure 2.14 A). A 365 nm LED was chosen to spectrally discriminate the excitation light from any emission, while the front side illumination allowed for any LED light in the visible region to be further eliminated due to spatial discrimination. The UV LEDs were powered using a Keithley 2400 sourcemeter at 20 mA and 4 V, connected to the LED *via* alligator clips. To assure that the samples were placed in the same position for each measurement, a Teflon holder was fabricated in the Vanderbilt machine shop (Figure 2.14 B). The sample holder and LED were placed in the sample compartment of the PC1 spectrofluorimeter, in order to use the photomultiplier tube as the detector. The excitation beam of the fluorometer was blocked using a piece of black plastic covering the lens the beam passes through; additionally, the excitation wavelength was set to 800 nm to assure that any stray light would be irrelevant to the spectra collected. This setup was used specifically to monitor the emission intensities and emission spectral characteristics of the thin films.

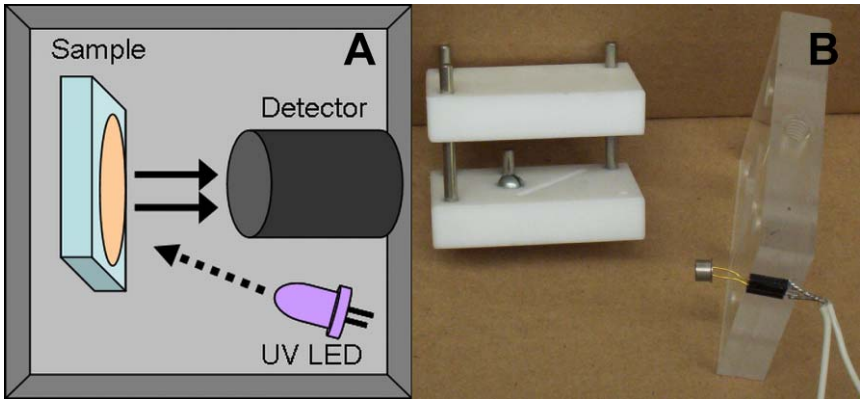

Figure 2.14 Configurations for testing the nanocrystal:polymer films. A) Testing films in a spectrophotometer: the dashed line is UV excitation light, while the solid line is white emission going to the detector. B) Image of the sample and LED holders used.

The second setup used, excited the sample films with a 365 nm LED within a Labsphere SLMS-LED-1050 integrating sphere system, fiber coupled to a CDS 500 CCD-based spectrometer with accompanying software. The luminous efficiency, CIE chromaticity coordinates, and the CRI of each thin film or coated LED was determined using this system.

The last analysis was to monitor aggregation on the micron scale. Although it was apparent, due to their turbidity, which of the samples had extensive aggregation, further characterization of this aggregation was desired. To this end, thin films of the encapsulated nanocrystals were drop cast onto cover slips which could be used for fluorescence microscopy. The imaging was done on a Zeiss Axiovert metrics Coolsnap HQ2 CCD camera with Metamorph image acquisition software.

2.5 Electroluminescent Studies

After beginning work on the study of PL-based light sources, it became apparent that the low efficiency of the pump sources was a hindrance to creating a high efficiency device. The idea of electrically pumping these nanocrystals with charge carriers directly, was suggested as a way of avoiding pump source losses. Previous work using traditionally sized and core-shell nanocrystals has already proven that electroluminescence was viable.[40, 47, 48, 51-53, 55, 82-85] The fabrication and characterization of electroluminescent devices, as well as the preceding steps to the actual fabrication, are described below.

2.5.1 Thin Film Fabrication and Characterization

Initially, the goal was to test the film thicknesses and surface characteristics of the various layers used in a nanocrystal-based electroluminescent device (Figure 2.15). This information will prove valuable in improving future device structures. Indium tin oxide (ITO) coated, polished float glass (R_s = 15-25 ohms) purchased from Delta Technologies, Ltd. was cut into dime-sized pieces in order to test the surface roughness using atomic force microscopy (AFM). Once the samples had been cut, they were sonicated for 10 min. in toluene and blown dry with N_2. This process was repeated with acetone and isopropanol (IPA). The samples were then placed in a Jelight Company Inc. UVO cleaner Model 42 for UV-ozoneolysis for 10 min, to remove any remaining organic material. At this point, standard techniques were used to analyze the surface of several samples using a Digital Instruments Nanoscan III AFM with a 300 KHz, 40 N/m silicon with Al coating AFM tip.

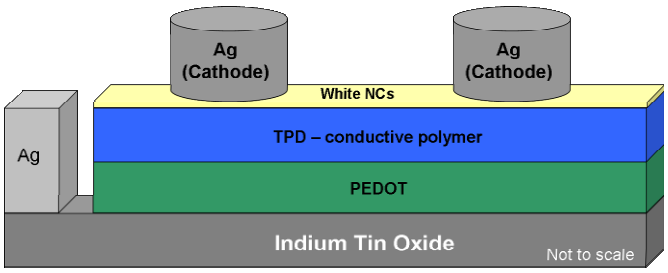

Figure 2.15 Structure of electroluminescent devices fabricated. The Ag anode was not needed when using the custom-made plastic holder described in a future section.

Onto the remaining samples, a layer of poly(3,4-ethylenedioxythiophene) poly(styrenesulfonate), or PEDOT:PSS, was spun-cast using varying spin rates, times, and concentrations of PEDOT:PSS in water. The samples were then annealed at 100 °C for about 60 min. The surface of several of these samples was analyzed, to determine the change in surface roughness due to the deposition of this layer. To determine the thickness changes due to the varied spin parameters, slightly larger (25x25 mm) square ITO coated glass pieces were also cleaned, spun coated with PEDOT:PSS, and annealed in the same manner as the smaller samples. Using a razor blade, narrow lines of the PEDOT:PSS layer were carefully scratched away in triplicate on each sample. The height of the PEDOT:PSS layer was then determined using a Veeco DekTak 150 profilometer.

The remaining dime-sized samples were coated with a layer of nanocrystals and/or N,N'-diphenyl-N'N'bis(3-methylphenyl)-(1,1'-biphenyl)-4,4'diamine, a hole transport polymer (TPD). This layer was spun-cast from a 5 or 10 mg/mL TPD in chloroform solution mixed in a 50:50 volume ratio with pure chloroform or nanocrystals solvated in

chloroform at varying concentrations. The surface of the samples was analyzed, as was the thickness of this layer using the same techniques used with the PEDOT:PSS layer.

In order to produce the electroluminescent devices for electrical and optical testing, the procedures above were followed using the 25x25 mm slides. Onto these were thermally evaporated Ag cathodes using an Edwards thermal evaporator. In order to pattern specific cathode areas, the Vanderbilt machine shop fabricated 3 types of stainless steel masks (Figure 2.16). The 1st type of mask is capable of holding 4 devices (25x25 mm slides) and patterning four, 3 mm circular cathodes (pixels) onto each sample. The 2nd mask patterns eight, 7x2 mm oval pixels onto 4 devices. The last and largest mask can hold 15 devices and pattern twelve, 4x2 mm oval cathodes onto each device. A known mass, typically > 250 mg, of Ag wire (Sigma-Aldrich, 1 mm diameter, 99.99% pure) was added to a tungsten evaporating boat. The evaporation chamber was then sealed and roughed to a pressure of less than 10^{-3} Torr, followed by diffusion pumping to 10^{-5} Torr, generally overnight. When the specified pressure was reached, liquid nitrogen was poured into the diffusion pump cooling compartment to allow the pressure to fall below 10^{-6} Torr. At this point the current over the tungsten boat was ramped slowly until the Ag wire had completely melted. All valves to the evaporation chamber were then closed and the voltage ramped slowly until the Ag began to evaporate onto the samples and surrounding bell jar. Once the entire mass of silver had been evaporated, the voltage was turned off and the sample chamber allowed to cool for 15 min. The bell jar was then slowly vented, all the pumps turned off, and the completed samples removed from the evaporation masks.

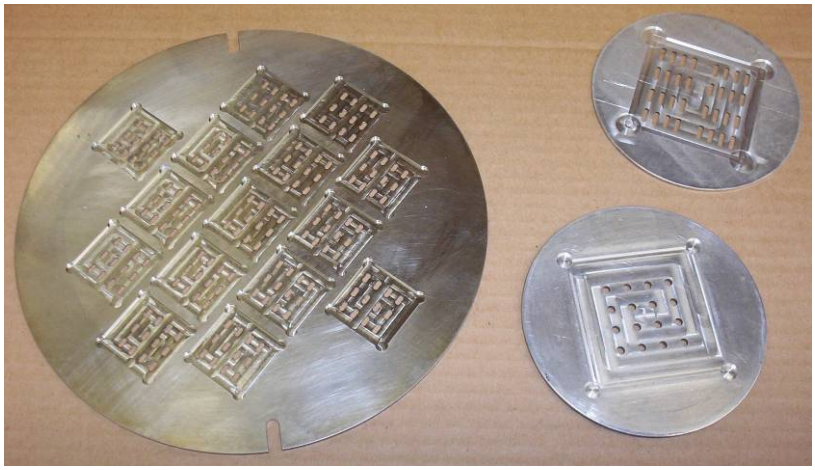

Figure 2.16 Image of evaporator masks fabricated by the Vanderbilt machine shop for use with the Edwards thermal evaporator located in the Rosenthal lab. The largest mask was fabricated with the capacity to be used at the Center for Nanophase Materials Sciences at Oak Ridge National Laboratories.

2.5.2 Testing Setups for Electroluminescence

Two unique systems were used to test the electroluminescence from the devices (QD-LEDs) differing mainly in the way in which the samples were held and connected to a Keithley source-meter. The first system (Figure 2.17) was based on the device testing setup used by Dr. Anvar Zakhidov and Dr. Christopher D. Williams at the University of Texas at Dallas, for testing their organic LEDs.[86] The polymer and QD layers were removed from the ITO surface on one corner of the QD-LEDs and a strip of Ag paint coated onto the ITO surface, to be used as the anode. The QD-LEDs were held vertically in place using a push holder mount and an alligator clip, on the Ag paint strip, connected to a Keithley 2400 sourcemeter. To serve as a the cathode connection, a 2 inch piece of Ag wire (2 mm diameter) was held in place on a micromanipulator and connected to the sourcemeter. An alligator clip was attached to the anodic Ag strip, previously coated on the ITO surface. In order to test the contact of the Ag cathode and the Ag wire, a small

voltage (1 μV) was sourced across the two leads, a small drop of colloidal Ag paint was placed on the tip of the Ag wire, and the wire positioned over the cathode and brought close to the QD-LEDs until a small current was detected on the sourcemeter. This setup was used inside of the PC1 spectrophotometer sample cavity (see prior mention) or with the fiber-optic from the SLMS-LED system (previously discussed) removed from the integrating sphere, held in place with a push holder mount on a micromanipulator, and positioned over the pixel to be tested (through the ITO and glass substrate).

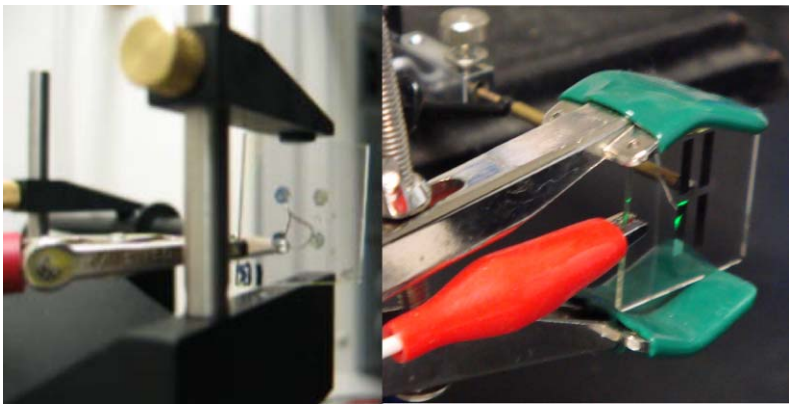

Figure 2.17 Initial arrangements for the electroluminescent studies performed on QD-LEDs. The optical fiber has been removed to clarify the setups.

The second setup was much simpler and more reliable in maintaining electrical contact between the cathode, anode, and QD-LED. The Vanderbilt machine shop fabricated a QD-LED holder assembly, to be used with the large evaporator mask, out of ultra-high purity plastic which consisted of two pieces connected by 4 plastic screws (Figure 2.18). A 25.1x25.1x1.1 mm void was milled out of 35x35x15 mm plastic piece to serve as the sample cavity. Twelve, spring-loaded, 1 mm, round-head, brass pins were pressure sunk into the plastic; these pins were positioned so that the spring head would

protrude ~2/10 mm into the cavity directly where the evaporated cathodes are located on the sample slides. An additional 13th pin was positioned in the same manner, but located in a lower corner of the device to act as the anode. Each device was loaded into the cavity and the top portion screwed into place. In this top piece, a ~23x23mm view hole was centered to allow the LED light to escape the holder for detection. A small plastic coated wire was soldered to the back of each pin, allowing an alligator clip to be easily attached to each pin individually. Sample testing efficiency was significantly enhanced using this sample holder, as the testing for each pixel did not require repositioning of the device. This holder could easily be positioned in the PC1 spectrophotometer or a fiber optic could be positioned over each pixel individually through the use of a micromanipulator.

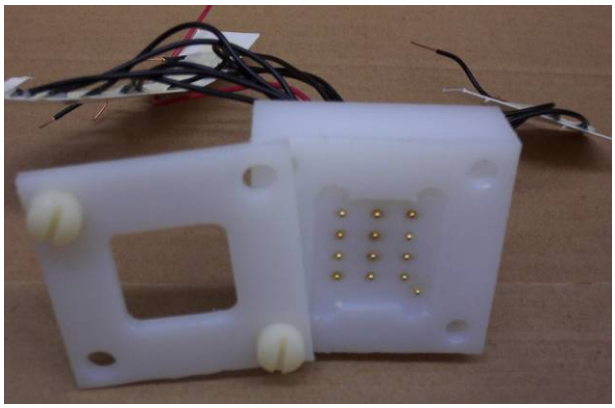

Figure 2.18 Sophisticated plastic holder for the electro-optical analysis of QD-LEDs.

2.5.3 Work Performed at CNMS-ORNL

Shortly prior to the spring of 2009, the Center for Nanophase Materials Sciences at Oak Ridge National Laboratories (CNMS-ORNL) acquired a controlled atmosphere

glove box evaporation system. White-light and core-shell nanocrystal samples were synthesized, isolated, and dried in 2 dram, plastic snap top vials at Vanderbilt (the mass of sample in each vial was recorded). The nanocrystal samples, PEDOT:PSS, ITO coated slides, the largest evaporator mask, and TPD were all transported to CNMS-ORNL for device fabrication and characterization. Knowledge of device fabrication acquired at Vanderbilt concerning film thicknesses and proper handling techniques were used to develop a process, such that with the upgrade in facilities, the device fabrication time was lowered to ~ 5 hours with many calibration steps eliminated.

For each set of devices, 15 slides were sequentially sonicated in toluene, acetone, and IPA for 10 min. with a blow drying step between each solvent, followed by 10 min. of UV-ozoneolysis and 5 min. of cooling. Onto each slide, 0.8 mL of a 50:50 mixture of PEDOT:PSS and deionized water was layered and the slide spun at 3000 rpm for 60 sec. The samples were loaded into a N_2 filled oven and annealed at 650 Torr and 101 °C for 20 min. The oven pressure was reduced to 50 mTorr, raised to 650 Torr, reduced to 50 mTorr, and then vented with N_2. The samples were removed and allowed to cool under nitrogen atmosphere to room temperature, leaving a 20 nm (approximately) PEDOT:PSS solid film on each slide.

Many ratios of nanocrystals to TPD to chloroform were tested. A known volume of chloroform was added to each nanocrystal sample in order to create an array of nanocrystal mass/mL concentrations. Several TPD in chloroform solutions of different mass/mL concentrations were also prepared. These samples were combined with pure chloroform to give 0.4 mL of the desired solutions. Each slide was coated with the entire unique solution, prior to spinning at 3000 rpm for 60 sec. The most successful solution

contained equal volumes of 5 mg/mL TPD in chloroform and 10 mg/mL ultrasmall nanocrystals in chloroform or the same TPD solution with 5 mg/mL of CdSe/ZnS core-shell nanocrystals. Each solution was used on the day it was formulated, as the nanocrystals appeared to aggregate and fall out of solution within 24 hours. The nanocrystals were assumed to mostly phase-segregate into a layer on top of the TPD due to previous AFM studies and similar work done by Coe, et al.[47, 87]

The samples were then pumped into the dual glove box, loaded onto the evaporation mask, placed in the evaporation chamber, and the pressure reduced to $< 2x10^{-7}$ Torr. A 100 nm Ag cathode was then evaporated onto the samples, after which they were removed from the evaporation chamber and glove box for testing.

Each sample was placed in the custom-built plastic holder, previously described, and each pixel tested for the electro-optical properties using a Keithley 2400 sourcemeter while monitoring the emission using a fiber optic cable connected to a Hamamatsu Photonic Multichannel Analyzer C10027 with accompanying Keithley2400 and analyzer controlling software. Initially, the voltage was sourced with either 0.05 or 0.1 V steps from 0 to 15 V, holding each step long enough to obtain the average of two, 250 millisecond integrations of the emission. Often after the initial run, the same sample could be studied using higher voltages with faster ramp times. The second type of experiment run was to monitor the emission of a pixel at a specific voltage over the course of several minutes. The voltage was ramped at 1 volt per second using 0.1 V steps, until the brightest voltage—as determined from the initial sampling—was reached. The voltage was then held constant, and the emission collected every 5 seconds for several minutes (2 avg, 250 ms integrations). Lastly, the same I-V measurements were

performed; however, the detector was replaced with a digital video camera to collect images of the pixels being tested. Several pixels on each device were analyzed with each type of experimental parameters.

CHAPTER III

PHOSPHONIC ACID MODULATION OF CDSE NANOCRYSTAL TRAP STATE EMISSION

3.1 Introduction

The synthesis, and subsequent functionality, of semiconductor nanocrystals for a variety of applications has become a topic of broad scientific interest.[71, 73-75, 88, 89] Initial synthetic investigations of colloidal nanocrystals focused on the crystal structure and size as the sole sources of the unique optoelectronic properties observed. However, it has been determined that the surface ligands on the nanocrystal are not only useful for their tethering and solubility properties, but are also a factor in the photoluminescent (PL) properties.[71, 88-104]

At the outset, dimethylcadmium was used as the cadmium precursor in CdSe nanocrystal synthesis.[71] However, due to the cost and hazards associated with the use of dimethylcadmium, other precursors have been developed.[74, 75, 105, 106] Specifically, CdO combined with a phosphonic acid to form a Cd-phosphonate precursor complex was suggested as a more cost effective and green alternative.[75] As a result of this synthetic innovation, the effects of the phosphonic acid as a component of the Cd precursor and as a surface ligand have been explored—primarily the growth kinetics and shape effects.[103, 107-111] *Ab-initio* and first principles calculations determined that phosphonic acid is the most strongly bound ligand, leading to a nanocrystal surface almost exclusively coated with them.[76, 112-114]

For CdSe nanocrystals, the pattern has been that as the nanocrystal diameter decreased, the band-edge absorption and band-edge emission shifted to higher energies due to quantum confinement.[26] For ultrasmall (<2 nm diameter) CdSe nanocrystals, as shown in Figure 3.1, the emission is no longer dominated by the band-edge emission.[56] It has been shown that, although the absorption continues to blue-shift—indicating smaller diameters—the bluest emission feature appears to be pinned at a specific energy/wavelength (Figure 3.1).[115] This pinned emission is believed to be due to trap states on the surface of the nanocrystal, influenced by the surface ligands.[56, 115]

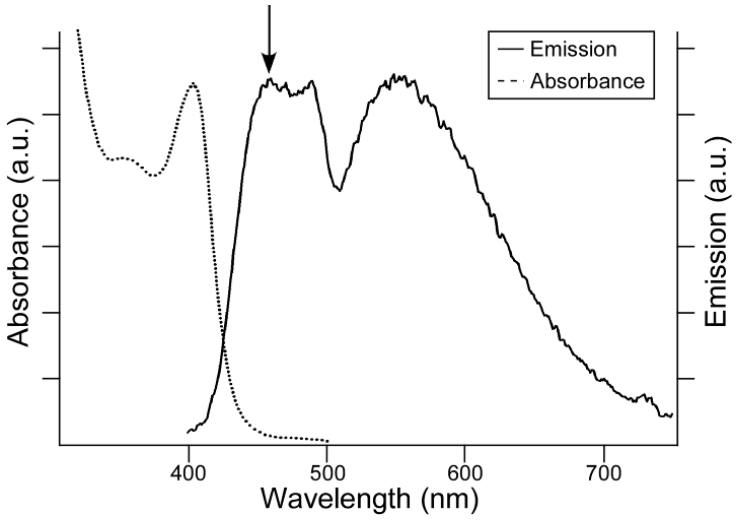

Figure 3.1 Absorbance and emission of ultrasmall nanocrystals. The arrow indicates the pinned emission feature of interest.

Previous reports have differed over whether the emission of these ultrasmall nanocrystals can be altered through ligand modification.[116, 117] These discussions have generally centered on a difference of opinion as to the source of this broad emission. Defect emission coming from either interstitial atoms or vacancies in the core of the

nanocrystals should not be altered by varying the surface ligands. CdSe nanocrystals with these types of defects would also be more amorphous than crystalline due to the small number of inner atoms. Chen *et al.* have previously studied the absorption and emission of nanocrystals of amorphous character.[91] This work showed that amorphous nanocrystal defect emission should be accompanied by absorption of mid-gap states, as well as a blue-shift in the absorption peak maxima due to crystallization over time.[91] However, it has been shown that with the synthesis used in this case (Chapter 2), the ultrasmall nanocrystal's absorption maxima red-shifts due to crystal growth and not a crystallization of a preliminary amorphous phase.[115] This earlier work, along with the large Stokes shift seen in this ultra-small size regime, has led to the hypothesis that the broad-emission comes from surface states suggesting that this emission could be tuned by changing the ligand environment around those states.

The effects that different phosphonic acid ligands have on the PL properties of white-light emitting nanocrystals were observed. Changing the phosphonic acid ligand on the surface of these ultrasmall nanocrystals was found to allow tuning of the highest energy peak in the emission and increase the quantum yield (QY). In addition to the fundamental interest in controlling trap-state emission, tuning this emission will allow for color control over white solid-state light sources that employ nanocrystals as the emissive source. Furthermore, 4 phosphonic acid structures with acid groups on the terminal end of the alkyl chain were used in an attempt to synthesize functionalized nanocrystals.

The various phosphonic acid structures shown in Figure 3.1 of Chapter 2 were synthesized, purified, and characterized. Both traditionally sized and ultrasmall nanocrystals were synthesized using these phosphonic acids in order to determine any

modifications to the quantum yield and pinned emission of ultrasmall nanocrystals. Since phosphonic acids have been shown to be an impurity in TOPO,[73] the synthesis described in Chapter 2 was modified to use only HDA as the high-boiling solvent. In order to monitor emission pinning and avoid slight batch-to-batch variations, an average of 21 batches per phosphonic acid were synthesized that had band-edge absorption features below the ultrasmall threshold of 420 nm. For the ultrasmall size, absorption and PL spectra were acquired for each batch and the data fit with a Gaussian curve to determine the center wavelength for the band-edge absorption and the highest energy emission feature. For the traditional sizes, the absorption and emission were also monitored along the nanocrystal growth process. The average QY was determined for 6 batches each of nanocrystals with band-edge absorption from 400-420 nm and 540-570 nm.

3.2 Results and Discussion

3.2.1 Pinned Emission and Growth Kinetics

Initially, 7 phosphonic acids with unbranched alkyl chains were used to synthesize broad band-emitting nanocrystals (numbers 1-6, and 17 in Figure 2.1 of Chapter 2). These early experiments were intended to show pinned emission, using different phosphonic acids compared to the pinning previously seen with dodecyl phosphonic acid.[115] Plotting the wavelength of the first emission feature vs. the wavelength of the band-edge absorption clearly showed a region of pinned emission (Figure 3.2). It is important to note the slope change from the traditional size regime of nanocrystals (> 2

nm) to the ultrasmall nanocrystals. In the traditional nanocrystal sizes the emission red-shifts with red-shifting band-edge absorption and increasing diameter. For the ultrasmall nanocrystals, the different sizes do not show a change in the wavelength of the emission from the highest energy trap state, despite changes in the wavelength of the band-edge absorption feature.[115] The average and standard deviation for the wavelength at which the first emission feature was located were obtained for each set of nanocrystal batches made with different phosphonic acids.

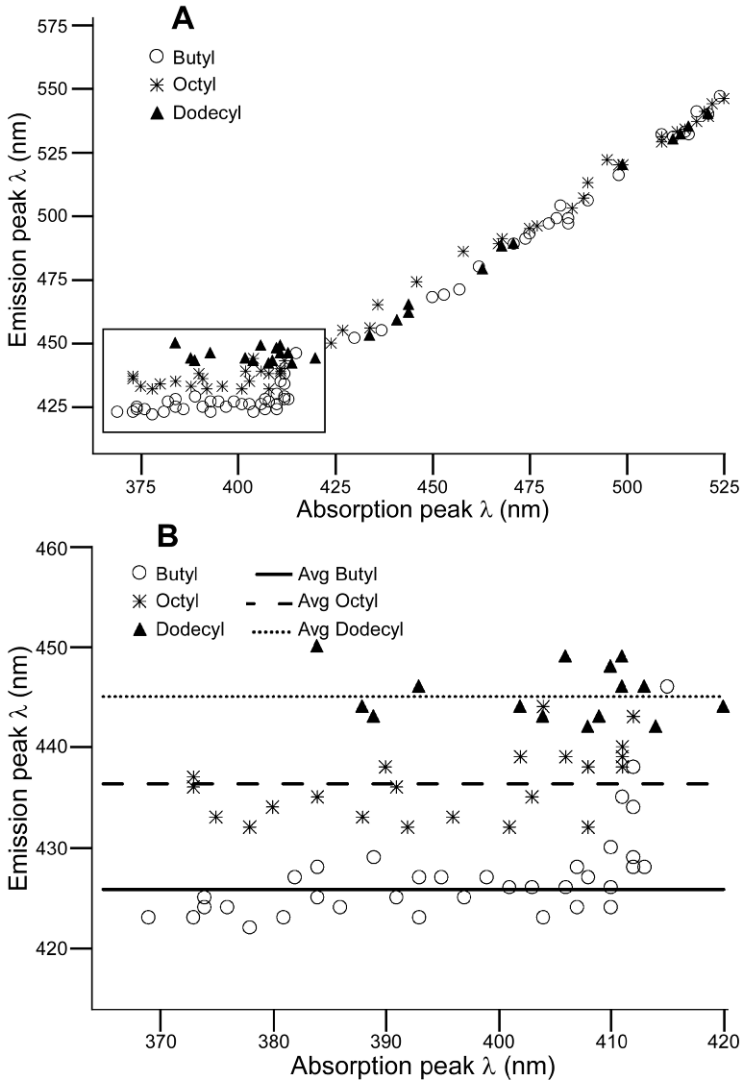

Figure 3.2 First emission feature λ vs. band-edge absorption feature λ. A) Traditional and ultrasmall nanocrystal sizes. The boxed portion is the pinned emission region. B) Enlarged area from graph A, showing only the pinned emission data. Note the slope change from the traditional to ultrasmall nanocrystal regions.

During the synthesis it was noted that it was possible to make the smallest overall size of nanocrystals, as determined using Yu *et al.*'s nanocrystal sizing equations,[118] with the shortest chain phosphonic acid. Table 3.1 lists the shortest wavelength absorption feature achieved with each phosphonic acid. These smallest sizes for each phosphonic acid were achieved by reducing the time between the Se:TBP injection and the "kill-shot" described

previously. The time between the injections was approximately the same (~1 second) for all the smallest sizes, yet different sizes of nanocrystals were achieved. This trend indicated that the shorter the alkyl chain on the phosphonic acid, the slower the reaction would proceed. The slower reaction kinetics allowed for smaller sizes to be obtained using the short chain phosphonic acids than were achievable with the longer alkyl chains.

Table 3.1 Shortest wavelength band-edge absorption obtained for each phosphonic acid

Phosphonic acid	Bluest λ band-edge absorption obtained (nm)
Butyl PA	359
Hexyl PA	371
Octyl PA	373
Decyl PA	376
Dodecyl PA	384
Hexadecyl PA	395
Docosyl PA	392
2-ethyl,hexyl PA (2-EHPA)	378
3-methyl,butyl PA (3-MBPA)	371
Phenyl PA	374
3-phenyl,propyl PA (3-PPPA)	376

The growth kinetics of the CdSe nanocrystals depend on the reactivity of the Cd and Se precursors.[76, 119] Intuitively, the rate at which Cd atoms are added to the initial nanocrystal seeds is dependent on the rate the Cd-phosphonate can be dissociated, generating a reactive Cd species; in turn, this rate should depend on the strength of the Cd-O-P bond. Accordingly, it was hypothesized that the shorter ligands must bind the strongest to Cd in the Cd-phosphonate precursor and to eventually to the nanocrystal surface.

In addition to influencing the nanocrystal growth kinetics, one would expect the Cd-O-P bond would affect the energy of a Cd surface trap state. In a previous study, Hill *et al.* calculated that the density of states for the Cd rich surface of a nanocrystal would be affected by the bonding of the Cd atoms on that surface, including any dangling orbitals (Cd surface trap sites).[120] The trend that was observed in the current experiments was that the shorter alkyl phosphonic acids blue-shift one of the emission features. This trend was seen after locating the shortest wavelength (highest energy) emission feature of the white-light emitting nanocrystals for each of the phosphonic acids (Figure 3.3). Each of these ligands gives a statistically (99% confidence level) different emission wavelength, except dodecyl, hexadecyl, and docosyl phosphonic acid. These three phosphonic acid ligands give the nanocrystals' a statistically similar emission feature, and by association, the same emission energy level. This is not surprising since an energetic difference seen between chain lengths of 12, 16, or 22 carbons would indicate the trap-states interact with atoms through more than 14 bonds. Although, any trend past 3 bonds is surprising in and of itself.

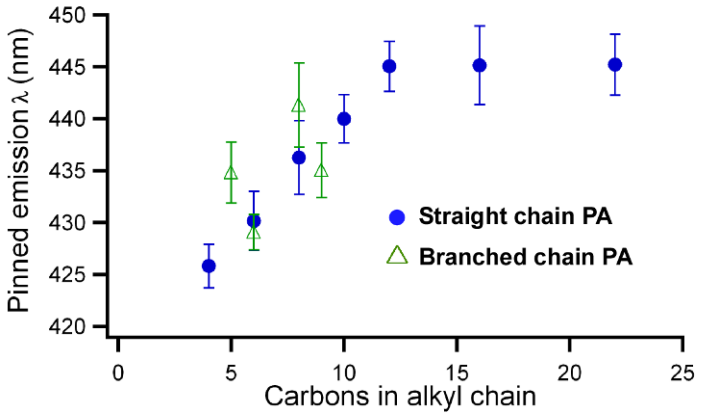

Figure 3.3 Wavelength of the pinned first emission feature vs. the number of carbon atoms in the alkyl chain of the phosphonic acid used during the synthesis.

Four branched chain phosphonic acids were also studied (numbers 7-9, and 16 in Figure 2.1 of Chapter 2). The pinning results from these phosphonic acids indicated that it is not only the number of carbon atoms in the alkyl chain that is important; the arrangement of these carbons also has an influence on the wavelength of the light emitted from the nanocrystals. Table 3.2 lists the pinned wavelengths for all the phosphonic acids tested. Although 3-methyl,butyl PA; octyl PA; and 3-phenyl,propyl PA all have different numbers of carbon atoms in their alkyl chain, the wavelengths of pinned emission they cause are nearly indistinguishable.

Table 3.2 Pinned emission λ of nanocrystals made with different phosphonic acid structures.

Phosphonic acid	Emission λ (nm)
Butyl PA	425.8 ± 2.1
Hexyl PA	430.2 ± 2.8
Octyl PA	436.3 ± 3.5
Decyl PA	440.0 ± 2.3
Dodecyl PA	445.1 ± 2.4
Hexadecyl PA	445.1 ± 3.8
Docosyl PA	445.2 ± 2.9
2-EHPA	441.3 ± 4.0
3-MBPA	434.8 ± 2.9
Phenyl PA	429.1 ± 1.7
3-PPPA	435.1 ± 2.6

3.2.2 Electronegativity Theory

The effect seen in the optical properties of ultrasmall nanocrystals can be considered a consequence of electronegativity. The electronegativity of individual atoms affects the strength of bonds between atoms. As a result, the electronegativity of individual atoms is influenced by the atoms that surround them. This theory of electronegativity

modification is known as inductive electronegativity and is a large factor in many analytical measurements, such as shielding and de-shielding in NMR spectroscopy.[121, 122] Using Bratsch's "Group Electronegativity Method,"[123] the electronegativity of each phosphonic acid with an attached Cd was determined. First, the ligands were broken into groups of ethyl carbons, methyl carbons, branched carbons, hydroxyl groups, phosphorous atoms, and single oxygens (Figure 3.4).

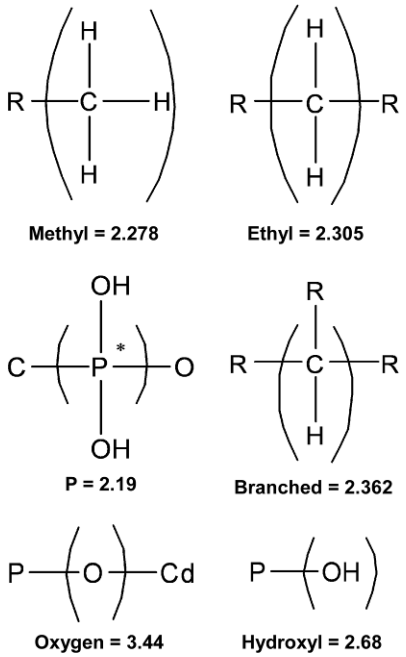

Figure 3.4 Chemical structures and the corresponding calculated group electronegativies for each structure.

The electronegativity (X_G) for each of these groups was calculated using Equation 1, where N_G is the number of atoms in the group, υ is the number of a specific type of atom, and χ is the electronegativity of each atom in Pauling units. The individual group electronegativities were then combined using Equation 2 to determine the ligand's overall

equalized electronegativity (X_{eq}), where N is the total number of atoms, N_G is the number of atoms in each group, and X_G is the electronegativity of each individual group.

$$X_G = \frac{N_G}{\sum \frac{\nu}{\chi}} \qquad (3.1)$$

$$X_{eq} = \frac{N}{\sum \frac{N_G}{\chi_G}} \qquad (3.2)$$

Inductive electronegativity generally is not thought to have an effect on atoms more than a few bonds away. However, for electron traps on surface Cd atoms affected by the phosphonic acid ligand, this does seem to be the case. When the experimental and theoretical data sets were normalized with respect to the each set's butyl PA ligand energy (setting this value to one), the theoretical data matched up well with the experimental emission data for the straight chain ligands and two of the branched chain ligands (Figure 3.5). For the two ligands tested that included phenyl groups, this theoretical treatment did not yield consistent results, in all likelihood due to the conjugation in the ligand's alkyl chain.

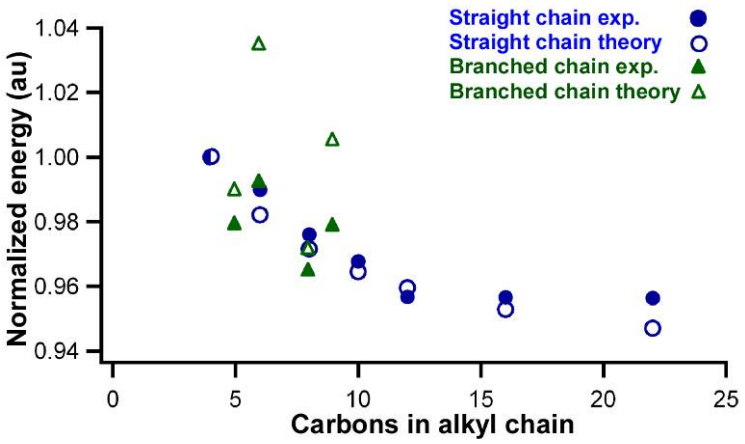

Figure 3.5 Normalized energy of the pinned emission feature and electronegativity of the corresponding phosphonic acid vs. the number of carbons in each carbon side-chain. The experimental and theoretical values are normalized to each data sets butyl phosphonic acid value, hence the half-circle representing the overlapping data for the butyl phosphonic acid.

The pinned emission peak in these broad band-emitting nanocrystals is believed to be due to trap state emission.[56, 115] Previously, surface cadmiums have been suggested as electron traps in nanocrystals.[27, 124] Additionally, it has been shown that the trapping of charge carriers can cause emission from discrete energy states.[27, 124-126] The trapping energy of an electron on a surface Cd will be affected by the available orbitals and the electron density around the nucleus.[120, 127] The electron density around a surface Cd will vary depending on the electron-donating or electron-withdrawing nature of any molecules bound to it. Accordingly, the difference in electronegativity of the phosphonic acids would explain the change in emission wavelength seen in these ultrasmall nanocrystals (Figure 3.5). Experimentally, it appears that shorter alkane chain lengths cause higher energy emissions, due to the increased electron withdrawing nature of these ligands exerted on the Cd's adjacent dangling bond, an electron trap.[120, 124, 128, 129]

Solvation dynamics and ligand sterics were discarded as sources of the emission changes. If the emission changes were due to the solvation dynamics of the various ligands, then solvating the nanocrystals in an assortment of solvents would change the wavelength at which the ultrasmall nanocrystals were pinned. When the nanocrystal emission was analyzed in hexanes, toluene, mesitylene, and chloroform, the emission peak wavelengths were unchanged. The data presented in Table 3.2 and Figure 3.4, allowed for the elimination of steric considerations due to the following deductive logic. Assuming that the steric size of the ligand is the most important factor in determining the location of the first peak, the most bulky ligand is phenyl phosphonic acid and butyl phosphonic acid is the smallest ligand. This should place the phenyl phosphonic acid nanocrystals on one edge of the pinning data, with lessening steric size down to butyl phosphonic acid nanocrystals at the other extreme. However, the phenyl nanocrystals had a pinned wavelength at ~ 430 nm, almost the exact middle of the data.

At this small size—ultrasmall nanocrystals likely consist of less than 25 Cd-Se pairs—it is possible that the phosphonic acids not only affect the kinetics of the growth reaction, but also influences the crystal structure. A change in the crystal structure could be the cause for the modulated emission shown here; although, this does not seem likely due to the ligand exchange data from a previous work.[115] Another alternative is that the ligands are interdigitated, affecting the electron density of a trap state, not through bonds, but instead by direct connection to a separate trap state. This may be similar to the way that thiol-gold self-assembled monolayers act *en masse*. However, CdSe nanocrystals have been reported to have only about 40% to 70% ligand coverage,[130, 131] decreasing the likelihood that the ligands would "cross-talk."

3.2.3 Quantum Yield Effects

In addition to altering the emission wavelength of the ultrasmall nanocrystals, the phosphonic acid ligand on the surface affected the quantum yield of both the ultrasmall and traditionally sized nanocrystals (Figure 3.6, Table 3.3). Initially, the QY changes with phosphonic acid were believed to be an artifact due to the cleaning process, used to separate the nanocrystals from the coordinating solvent and precursors. However, it was noted that a similar trend was seen in "dirty" and "clean" nanocrystals when using the straight alkyl chain ligands. The branched and phenyl ring containing ligands did not fit into this trend once cleaned (Table 3.3). This could be explained by the conjugation in the chain, the cleaning process removing these ligands, or the steric size of these phosphonic acids reducing the surface coverage as compared with the straight chain ligands. It should be noted that the ligand's steric size is a possible cause for the QY effects, but is not likely to be the cause of the energetic differences, as discussed later.

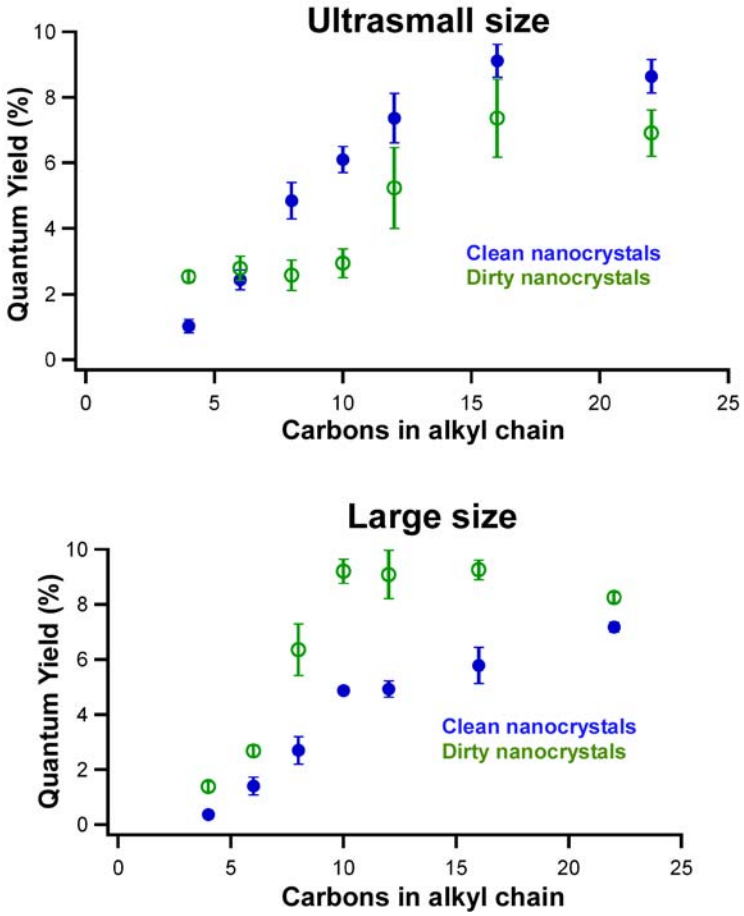

Figure 3.6 Quantum yield of dirty and clean nanocrystals: (top) ultrasmall size and (bottom) traditional size regime. Clean and dirty refer to the nanocrystal before and after the isolation/cleaning process. The branched and phenyl ring containing phosphonic acid values are not presented, see Table 3.3.

Nanocrystals in the traditional size regime (>2nm) made with each phosphonic acid demonstrated the known trend of longer emission wavelength with increased diameter. However, for these nanocrystals, a similar trend in the QY was seen with the straight chain phosphonic acids as in the small nanocrystals (Figure 3.6, Table 3.3). Once again, the branched and phenyl containing ligands did not fit with the rest of the data.

Table 3.3 QY of nanocrystal's synthesized with the different phosphonic acids.

Phosphonic acid	QY of small, dirty QDs (%)	QY of small, clean QDs (%)	QY of large, dirty QDs (%)	QY of large, clean QDs (%)
Butyl PA	2.54 ± 0.17	1.03 ± 0.21	1.37 ± 0.18	0.37 ± 0.15
Hexyl PA	2.80 ± 0.37	2.44 ± 0.31	2.68 ± 0.19	1.40 ± 0.32
Octyl PA	2.59 ± 0.47	4.84 ± 0.56	6.35 ± 0.94	2.70 ± 0.50
Decyl PA	2.96 ± 0.45	6.10 ± 0.40	9.20 ± 0.45	4.88 ± 0.14
Dodecyl PA	5.24 ± 1.24	7.37 ± 0.76	9.08 ± 0.88	4.93 ± 0.29
Hexadecyl PA	7.37 ± 1.19	9.12 ± 0.50	9.26 ± 0.35	5.79 ± 0.66
Docosyl PA	6.91 ± 0.71	8.64 ± 0.51	8.25 ± 0.18	7.18 ± 0.18
2-EHPA	3.18 ± 0.83	3.98 ± 0.99	10.17 ± 1.09	9.14 ± 1.74
3-MBPA	5.00 ± 1.18	0.75 ± 0.59	3.91 ± 0.69	2.55 ± 0.39
Phenyl PA	2.95 ± 0.34	0.50 ± 0.29	2.21 ± 0.44	1.32 ± 0.35
3-PPPA	2.45 ± 0.77	0.22 ± 0.05	5.47 ± 0.94	0.38 ± 0.17

The quantum yield is most likely impacted by the physical nature of the ligands rather than the electronic properties. For the traditional size regime, the nanocrystals have a lower QY when cleaned because some of the ligands are removed, decreasing the surface passivation and increasing the dangling bonds that trap charges. Since the emission in this size regime is mainly from band-edge radiative recombination, this leads to a decrease in the QY. The increased QY caused by longer chain phosphonic acids could be due to these longer chains passivating of any surface states with portions of the alkyl ligand chain.[132, 133] For the ultrasmall sizes, the cleaned nanocrystals exhibit a higher quantum yield due to the removal of ligands during the cleaning process, creating more emitting trap states. The low QY caused by the shorter chain phosphonic acids may be due to the stronger bond that shorter chains have with Cd, consequently they are less likely to be removed, which prevents new trap states from being created. Additionally, the shorter chain length may allow easier access to quenching molecules.

3.2.4 Functionalized Phosphonic Acids

The use of ultrasmall nanocrystals' unique broad-band emission was considered for biological labeling applications. However, they are not water soluble due to the alkyl chain structures of the phosphonic acid ligands used up to this point. It was thought that water soluble ultrasmall nanocrystals might be obtained through the use of phosphonic acid ligands with either another phosphonic acid group or a carboxylic acid group on the ligands terminal end (structures 18-21 in Figure 2.1 of Chapter 2).

During the attempted nanocrystal syntheses with these 4 structures no nanocrystals could be isolated. With 1,10-diphosphonodecane (1,10D-DPA), the Cd-precursor reaction mixture would turn clear and colorless, indicating Cd-phosphonate formation, prior to 280 °C. Heating the solution to higher temperatures resulted in a gray sludge, which began to coat the inside of the flask. Injection of Se:TBP, at this point, produced no results. Nanocrystals could be synthesized using 1,10D-DPA only by maintaining the temperature below 280 °C. Once the Cd-phosphonate had been formed, injection of Se:TBP produced an extremely quick nanocrystal-like color change, despite the temperature dropping below 240 °C, with a total reaction time from injection to dark red/black color of around 10 seconds. Verification that nanocrystals had been successfully synthesized was not possible, as these "nanocrystals" could not be isolated from the HDA solvent mixture; a colored gelatinous substance would form upon cooling any volume of the reaction mixture below ~150 °C, possibly due to polymerization of the nanocrystals and excess 1,10D-DPA.[108, 134] When using 1,4-diphosphonobutane (1,4D-BPA), the Cd-phosphonate was formed prior to 220 °C; however, this did not decompose upon further heating to 320 °C. Injection of Se:TBP, with heating at 260 °C, produced a

very slow color change similar to that seen at sub 230°C for a standard phosphonic acid synthesis. In the same manner as the 1,10D-DPA reaction mixture, a gelatinous substance would form should the reaction temperature fall below ~ 150°C. In both cases this substance was insoluble in methanol, chloroform, toluene, hexanes, octanol, or hexanol (standard nanocrystal solvents). Synthesizing nanocrystals with the carboxylic acid-terminated phosphonic acids proved equally as difficult. The 2-carboxy,ethylphosphonic acid did not the convert CdO, and 11-phosphonoundecanoic acid formed a Cd-phosphonate that was insoluble in HDA, TOPO, or a mixture of both solvents. In DI-water, both reacted with CdO to form a gray solid which melded to the inner wall of the reaction flask.

3.2.5 Thermogravimetric Analysis

TGA was attempted in order to monitor exactly what ligands were on the surface of the nanocrystals. Samples of HDA, TOPO, various Cd-phosphonates, and several nanocrystal batches were analyzed (Figure 3.7). Unfortunately the Cd-phosphonate and nanocrystal decomposition did not provide a clear idea of which ligands were on the surface due to several plateaus in the scans. Further work in this area will require more refined samples of both the precursors and nanocrystals.

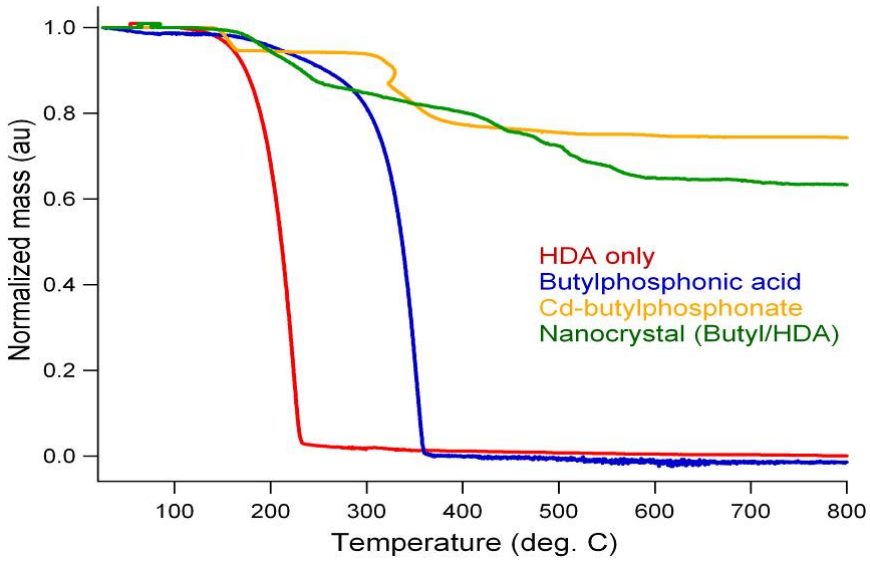

Figure 3.7 TGA data for HDA, butylphosphonic acid, cd-butylphosphonate, and butylphosphonic acid with HDA synthesized nanocrystals.

3.3 Conclusions

The emission of ultrasmall CdSe nanocrystals was shown to be pinned at different wavelengths depending on the phosphonic acid used during synthesis. For straight chain phosphonic acids, longer alkyl chains pinned the bluest emission feature at longer wavelengths than shorter chains. Surprisingly, these energy changes are shown to correlate with the electronegativity of the phosphonic acid ligands. In addition to shifting the wavelength of the pinned emission, these ligands are shown to influence the quantum yield of nanocrystals in both the ultrasmall and traditional size regime. The quantum yield for the white-light emitting nanocrystals has now been increased to nearly 10%.

The nanocrystal growth kinetics were also shown to be influenced by the phosphonic acid chosen to form the Cd-phosphonate precursor. The strength of the bond between the phosphonic acid and the Cd atom, in the Cd-phosphonate, is presumed to control the rate at which Cd atoms become available to for nanocrystal growth. The shortest straight-

chain phosphonic acid produced the slowest reaction, due to the electronegativity of the carbon chain compared to that of the longer chains. Synthesis and purification of CdSe nanocrystals with several carboxylic and phosphonic acid terminated phosphonic acids was unfruitful. However, comparing the reaction color changes for the di-phosphonic acids, it appeared that the same growth rate trend was seen as with the alkyl chains. The longer chain produced a quick reaction, which was slowed in the case of the shorter carbon chain length.

This new size regime, consisting of ultrasmall nanocrystals has stimulated the idea that the nanocrystal and ligands may no longer be considered separately. At the sizes studied here, the ligand has become essential to the crystal's optical properties. This recognition requires a shift in thinking and experimentation. In the ultrasmall size regime, each atom becomes increasingly important regardless of whether it is part of the inner crystal, the nanocrystal surface, or the ligands. Further knowledge, along with controlling the placement of atoms at specific locations, will allow for precise alteration of many of the physical, electronic, and optical properties of these nanocrystals.

One advantage of the electronegativity effect is that it allows for the fine-tuning of the white-light emission. The current work may provide a new approach for modification of trap state emission in other systems, such as ZnO. Further exploration into this phenomenon with other branched chain, conjugated, and functionalized ligands would clarify the relationship between the ligand's electronic properties and nanocrystal emission. Additionally, further theoretical and modeling studies—in the same vein as those of Hill, *et al.*[120]—may illuminate the exact nature and location of the trap states responsible for the broad emission from these ultrasmall nanocrystals.

CHAPTER IV

ENCAPSULATION OF WHITE-LIGHT CDSE NANOCRYSTALS

4.1 Introduction

The overall goal of this project was to create a solid-state lighting device based on the photoluminescent white-light of ultrasmall, CdSe nanocrystals. In order for such device to be considered viable for widespread usage, it must fulfill three main requirements. The first constraint is that this device must provide good quality white-light illumination, which is really a two-fold requirement as such a light source would be required to have white 1931 chromaticity coordinates (1/3, 1/3) and a very high color rendering index (> 80, CRI) as defined by the Commission Internationale de L'Eclairage or International Commission on Illumination (CIE).[10, 135, 136]

The second requirement for the fabricated devices is that they be more efficient than current lighting sources. Incandescent light bulbs are commonly known to be less than 10% efficient, while fluorescent lighting is approximately 25% efficient.[4, 10, 136] A more efficient device could be created by combining high quantum yield nanocrystals (>85%)[137] with ultra-violet (UV) or blue LEDs at the 60% efficiency predicted by the Department of Energy (DOE), assuming >60% extraction efficiency.

The last requirement for a practical solid-state device is that it exhibit long lifetimes. Lifetimes for nanocrystal devices would need to be on the same order or longer than current light sources, which can only be accomplished if the nanocrystals are protected from photooxidation and heating damage. Temperatures inside UV LEDs junctions have

been determined to run as hot as 140 ºC at higher than normal input wattages.[138] Although the temperature on the dome of UV LEDs is much lower, future iterations of this work may require layering the composite films directly on the junctions to increase the absorbance and extraction efficiencies of devices.

These device requirements were the main driving force for researching encapsulants for the white-light nanocrystals. In addition to providing protection against excessive heating and photooxidation, the encapsulant should: a) have no intrinsic emission of its own, b) preserve the ultrasmall nanocrystals' natural white light, c) prevent nanocrystal aggregation (reducing quenching and scattering), d) allow ease of application, and d) have good adhesion to UV LED surfaces. An encapsulant possessing these properties should permit further research on nanocrystal phosphor based devices; mainly on the efficiency effects due to better extraction efficiency, higher nanocrystal quantum yields, higher LED efficiency, and the use of excitation LEDs of different wavelengths.

For these experiments thirteen different encapsulants (Table 2.1), all optically clear and having dissimilar chemical composition, were examined to determine which would best meet the above criteria. Additionally, several monomers of a thermoplastic polymer were also studied. Films of encapsulated nanocrystals were studied to determine the extent of nanocrystal aggregation, change in absorption or emission of the nanocrystals due to encapsulation, and the efficiency of devices fabricated by exciting said films with UV LEDs. The distinct polymer structures (Figure 4.1) proved to have a significant impact on the quality of the nanocrystal encapsulation.

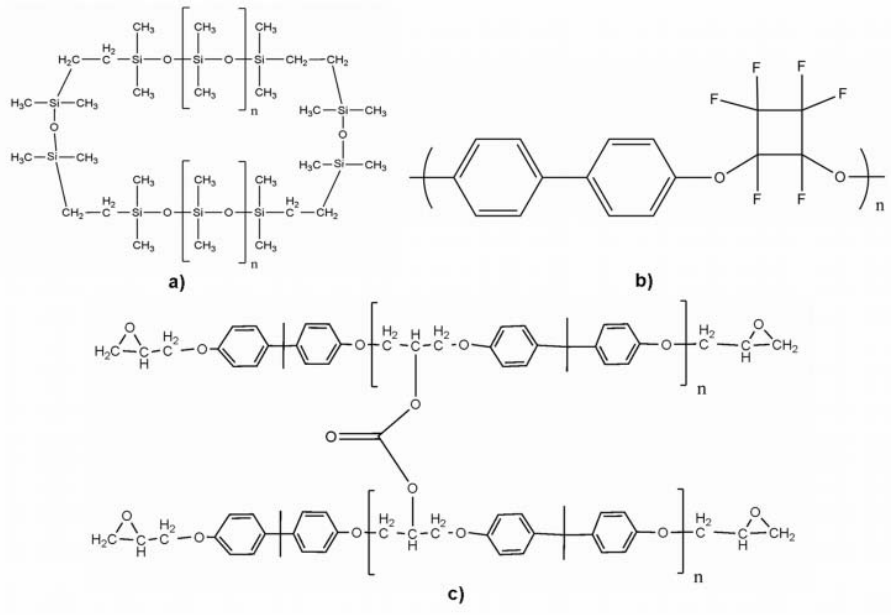

Figure 4.1 General structures of the polymers studied: a) silicones (also referred to as siloxanes), b) BP-PFCB, and c) epoxies.

4.2 Results and Discussion

4.2.1 Encapsulant Variance

As can be seen in Figure 4.2, only BP-PFCB and TSE 3033 did not significantly quench the emission from the white-light nanocrystals. Of these two encapsulants, only BP-PFCB maintained the unique absorption and emission spectra of ultrasmall nanocrystals (Figure 4.3). The best alternative, TSE 3033, provided less than half the overall emission intensity as BP-PFCB film with the same w/w nanocrystal loading and thickness. The remaining encapsulants shown in Figure 4.4 not only emitted at less than 25% of the BP-PFCB emission intensity, but also altered the emission spectrum of the nanocrystals. The spectral modifications can be noted most easily through the absence or

decreased intensity of the most blue emission peak. It should be noted that the trap state responsible for this peak is modulated by the surface ligands.

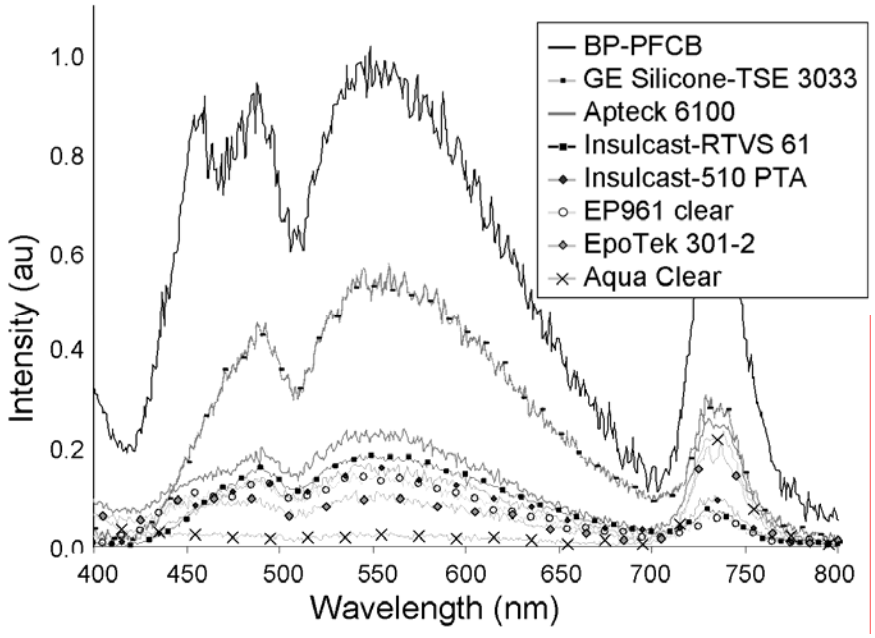

Figure 4.2 The emission from white-light ultrasmall nanocrystals in various encapsulants. The samples were all 50 ± 3 μm thick films with a 9% w/w nanocrystal to polymer loading. The feature at 400 nm is an artifact due to the tail of the excitation source's emission, and the emission feature at 730 nm is a 2nd order diffraction peak introduced by the detection setup

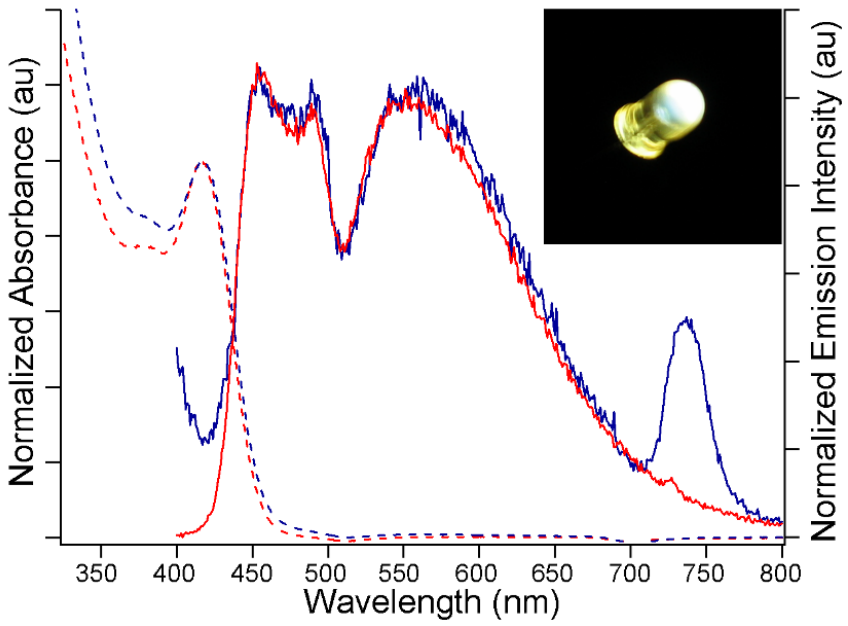

Figure 4.3 Absorbance and emission spectra of white-light ultrasmall nanocrystals. The dashed lines are the absorbance spectra, while the continuous lines represent the emission of the nanocrystals. The red spectra are the nanocrystals solvated in toluene; the blue spectra are 12% w/w nanocrystals in biphenyl-perfluorocyclobutyl polymer (BP-PFCB). The feature at 400 nm (blue solid line) is an artifact due to the tail of the excitation source's emission, and the emission feature at 730 nm is a 2nd order diffraction peak introduced by the detection setup. The inset is a true color photograph of a 365 nm LED coated with encapsulated nanocrystals.

In general, the epoxies quenched the nanocrystal emission more than the silicones, while both quenched the emission more than BP-PFCB. In addition, none of the encapsulants were as robust as the BP-PFCB films. When the encapsulated films were annealed at 190 °C for 48 hours, most became extremely discolored and the emission of the nanocrystals decreased to an almost unobservable level in all but the BP-PFCB, TSE 3033, and RTVS61 (Figure 4.4).

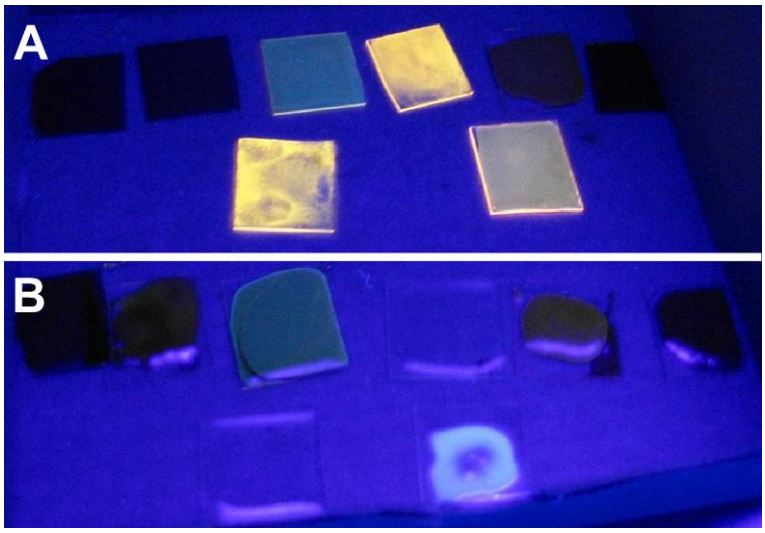

Figure 4.4 Image of A) nanocrystals encapsulated in 8 of the polymers and pure polymer films B) under ultraviolet excitation. The polymers are from left to right, row 1: EpoTek 301-2, Insulcast 510 PTA-B, Aptek Labs 6100-1AB, Insulcast RTVS61, Artmolds AquaClear, ResinLab/Ellsworth EP961 clear; row 2: GE silicone TSE3033 and BP-PFCB.

The disparity in emission intensity seen in the diverse encapsulants is due to the nanocrystals aggregating to varying degrees in each polymer. White-light fluorescence images clearly show the aggregation discrepancies (Figure 4.5). Silicone encapsulants caused the largest nanocrystal aggregates (~10 μm in diameter, Figure 4.5A), with a micelle-like structure. These large aggregates appeared to quench the nanocrystals less than the epoxy polymers. The epoxy encapsulants caused much smaller aggregates to form (~1 μm in diameter, Figure 4.5B), quenching a large part of the emission intensity. Monodisperse nanocrystal encapsulation was only achieved in BP-PFCB (Figure 4.5C). The fluorescence from these encapsulated nanocrystals was not only much more intense than in the other encapsulants, but also maintained its spectral purity (Figures 4.2 and 4.3).

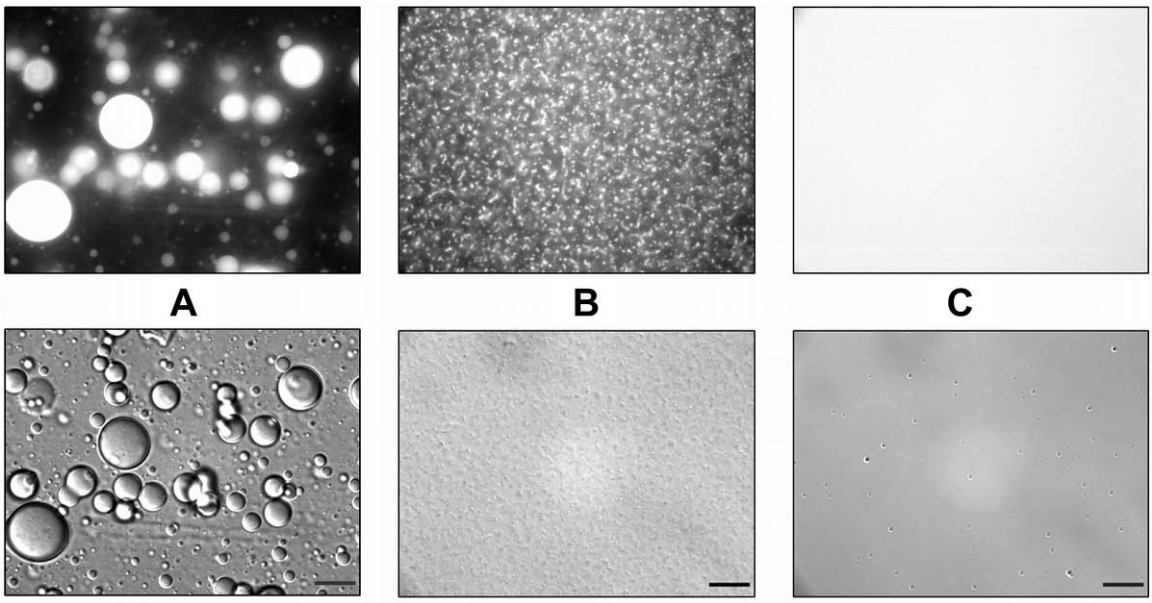

Figure 4.5 Representative white-light fluorescence (top) and bright field differential interference contrast (bottom) micrographs of encapsulated nanocrystals at 5% w/w loading in: A) siloxane B) epoxy C) BP-PFCB. All images were acquired with an exposure time of 5 ms, displayed with equivalent thresholds, and at the same thickness (~2 μm). The scale bars are 10 μm on all the images. The uniform fluorescence illustrated in c) is representative of disperse nanocrystal fluorescence in BP-PFCB and is not an artifact due to overexposure of the image.

The aggregation differences in each of the encapsulants can be traced back to the structure. The assorted structures provide a unique Hildebrand solubility parameter (δ). This Hildebrand solubility parameter can be separated into Hansen's solubility parameters (HSPs), as seen by equation 1. These three parameters relate the atomic/dispersive interactions (δ_D), dipole-dipole interactions (δ_P), and hydrogen bonding interactions (δ_H).[139, 140] These parameters are commonly used to determine the interactions between solutes and solvent systems. The more similar the Hansen solubility parameters between the solute and solvent, the more likely the two are to combine. This holds true for polymer-liquid and solute-polymer interactions as well. Table 4.1 shows

the solubility parameters for some common solvents and representative encapsulants examined. Toluene is used to provide representative values for the nanocrystals and mesitylene is considered representative for BP-PFCB.

$$\delta^2 = (\delta_D)^2 + (\delta_P)^2 + (\delta_H)^2 \qquad (4.1)$$

Three of the encapsulants tested were siloxane polymers: TSE3033, RTVS61, and 510PTA-B. The backbones of the siloxane polymers are more polar than toluene (a good solvent for the nanocrystals), however the methyl side-chains on the repeat unit (Figure 4.1a) give theses siloxane polymers an overall Hildebrand solubility parameter of 14.9-17.5 δ(SI), similar to toluene's Hildebrand value of 18.2 δ(SI).[139, 140] However, the differences between the HSPs for toluene and for the siloxanes indicate that these polymers are inappropriate for use with the nanocrystals, due to the extremely polar silicon-oxygen bonds.[141-143] The emission of the ultrasmall nanocrystals in the silicone polymers showed marked quenching of the first two emission peaks compared to the natural emission in solution (Figure 4.6).

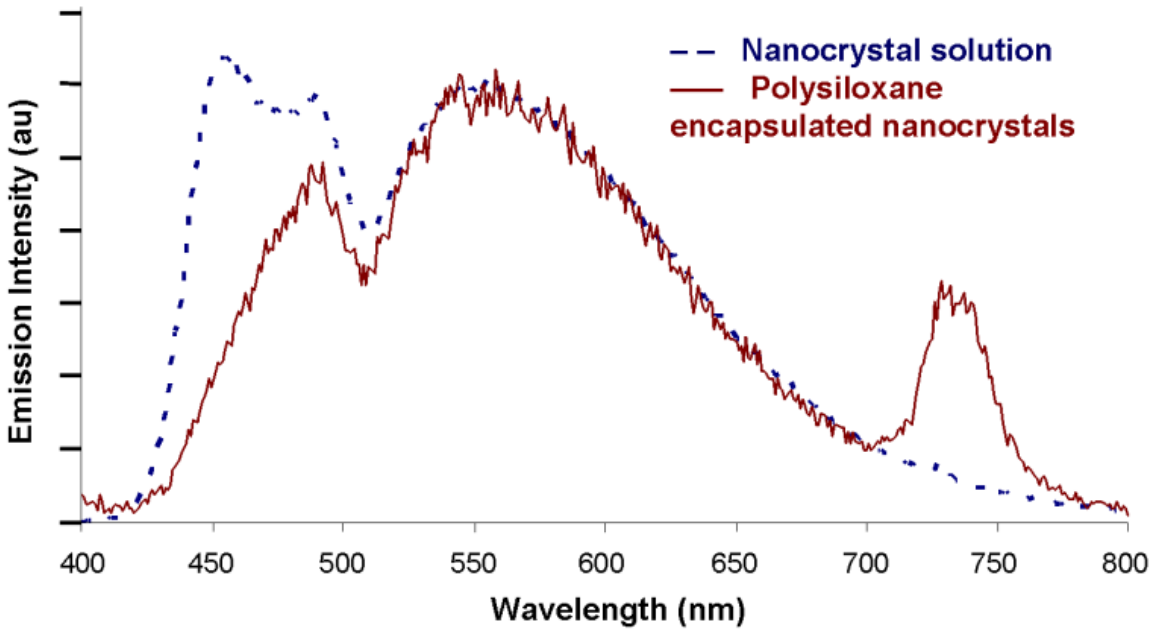

Figure 4.6 Normalized emission of ultrasmall nanocrystals in a silicone/siloxane polymer film (red) and in solution (blue). Note the almost complete quenching of the first emission peak and significant quenching of the second peak.

Table 4.1 Hildebrand solubility parameter for various polymers and solvents of interest. Representative Hansen values are shown for the various solvents and types of polymers. Toluene and mesitylene are included as good approximations for the values of the nanocrystals and BP-PFCB, respectively. Methanol is included as a contrast to toluene, since the nanocrystals are insoluble in it. All values were taken from references 6-11.

Encapsulant or Solvent	δ (SI)	δ_D (SI)	δ_P (SI)	δ_H (SI)
Methanol	29.6	15.1	12.3	22.3
Toluene	18.2	18.0	1.4	2.0
Mesitylene	18.0	18.0	0.0	0.6
Epoxies	18-26	18.3	12.3	9.7
Silicones	14.9-17.5	16.4	1.6	7.8

Six of the encapsulants typify bisphenol-A epoxies (EasyCast, EpoTek 301-2, 6100-1AB, EP965LVLX, EP961, and AquaClear). These polymer backbones are relatively less polar than siloxanes and should mix well with the nanocrystals in toluene.

However, as can be seen in Figure 4.2c, the endgroup on the polymer is an epoxide and the crosslinking group is an acrylate. This combination of polar and non-polar functional groups gives epoxies Hildebrand solubility parameters of 18-26 δ(SI).[139, 140] Additionally, the δ_P and δ_H for epoxies are significantly higher than the solvents generally used with these nanocrystals (Table 4.1).[141, 144] Therefore, it is not surprising that epoxies are not an appropriate choice of encapsulant for the nanocrystals. The emission of the ultrasmall nanocrystals in the epoxy polymers showed quenching of the first emission peak and overall decreased intensity compared to the natural emission in solution (Figure 4.7).

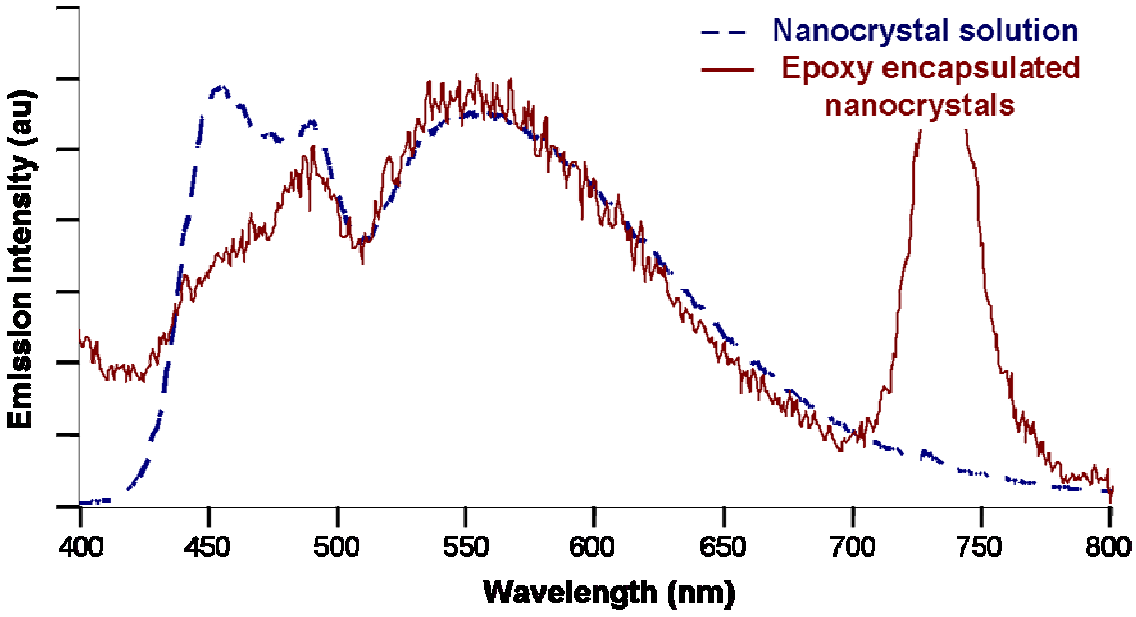

Figure 4.7 Normalized emission of ultrasmall nanocrystals in an epoxy polymer film (red) and in solution (blue). Note the almost complete quenching of the first emission peak and significant quenching of the second peak.

The BP-PFCB was the most effective encapsulant found due to its unique structure (Figure 4.2b). The Hildebrand value of mesitylene (18.0), a good approximation for BP-PFCB, is very similar to that of toluene. Additionally, the HSPs for mesitylene are notably more similar to those of toluene than those for silicones and epoxies (Table 4.1). This combination of solubility parameters explains why BP-PFCB causes less aggregation than the other polymers tested.

Encapsulants not shown in Figure 4.2 did not appropriately mix with the nanocrystals. This was seen in three ways: improper curing of the encapsulant, non-uniform nanocrystal dispersion in the films, or visible modification of the nanocrystals. These problems could all be traced back to structural differences in the polymers or the components used to cure them. The Castin' Craft polyester encapsulant contained a peroxide hardener which quickly oxidized the nanocrystals, eliminating any absorbance or fluorescence. The Series 40 and 2300 Halowaxes had melting points which prohibited nanocrystal encapsulation. The Series 40 wax is a liquid at room temperature, while the melting point of the Series 2300 (>132 ºC) is greater than the boiling point of toluene. The remaining encapsulants, EP965LVLX and EasyCast did not cure according to schedule, due to the acrylate hardener and excess DDPA, from the nanocrystal synthesis participating in a nucleophilic substitution (Figure 4.8). It is likely that these two epoxy encapsulants, if cured properly, would have exhibited similar nanocrystal aggregation as the other epoxy polymers.

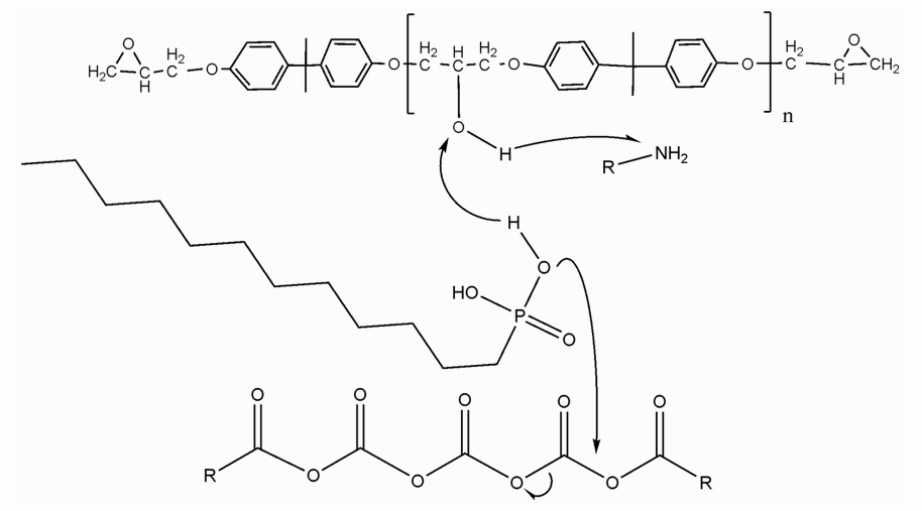

Figure 4.8 Nucleophilic substitution of dodecylphosphonic acid onto an epoxy's acrylate hardener. Note that although this is shown as a concerted reaction, this would occur in a number of steps.

4.2.2 Films and Device Characteristics of Nanocrystals in BP-PFCB

As seen in Figure 4.3, the nanocrystals encapsulated in BP-PFCB have almost identical absorption and emission spectra as prior to encapsulation, indicating that the size distribution of the nanocrystals is not changed and very little nanocrystal aggregation is occuring during the encapsulation process. CIE chromaticity coordinates for the sample shown in Figure 4.3 in solution (0.326, 0.342) were only slightly changed when encapsulated in BP-PFCB (0.328, 0.349), both falling well within the limits of white light as defined by the CIE.[135] The nanocrystals' quantum yield (6% to 10%) was not significantly affected by the encapsulation. The quantum yields of the films were determined in a manner similar to Greenham, *et al.*[145] Moreover, BP-PFCB encapsulated nanocrystals maintained at 190 ºC for 48 hours showed very little change in spectral characteristics, demonstrating the protection

afforded by BP-PFCB against heating at temperatures nearly double the standard operating termperature normally attained by LEDs.

BP-PFCB, clearly the best encapsulant, was used to study the effect of nanocrystal loading and sample thickness. Over the thickness range considered (10 to 100 μm), no noteworthy change in spectral shape was detected, while the absorbance and emission intensity was approximately proportional to the thickness (Figure 4.9). The absorbance curve followed the expected path (similar to a power function) with increasing thickness. Initially the relationship was linear; however, past ~40 μm a diminished return was noticed. Such a trend was expected from commonly seen absorbance vs. path length trends.

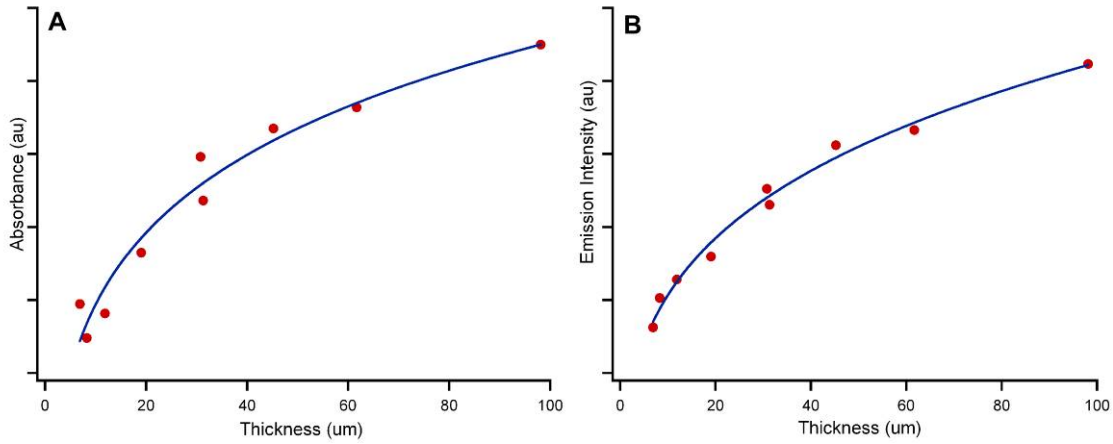

Figure 4.9 A) Absorbance at 420 nm vs. thickness in 10% w/w nanocrystals in BP-PFCB films. B) Integrated emission intensity (450-570 nm) vs. thickness of the same films. The emission detection was done using the setup shown in Figure 2.14. The blue lines on each graph are power function fits meant to guide the eye.

Changes to the nanocrystal loading in BP-PFCB also did not modify the quality emitted light; however, the emission intensity increases sharply as the nanocrystal

loading increases from 5% to 9 % w/w (Figure 4.10). Below 5% w/w loading, the emission intensity appears to be linear with a different slope; although, this could be due to the detection limits of our measurement system. Increased nanocrystal loading above 9% w/w does not have as significant an effect on the emission intensity and the intensity almost fully plateaued around 18% w/w. Chosen as representative siloxane and epoxy encapsulants, Insulcast-RTVS61 and EpoTek 301-2 exhibited a similar trend in changes to the emission intensity due to thickness and loading. However, their emission intensity plateaued at much lower nanocrystal concentrations (0.36% and 0.25%, respectively) due to the nanocrystals excessive aggregating. BP-PFCB film lifetimes and inert atmosphere encapsulation data will be described when the functionalized BP-PFCB films are discussed (Section 4.2.3).

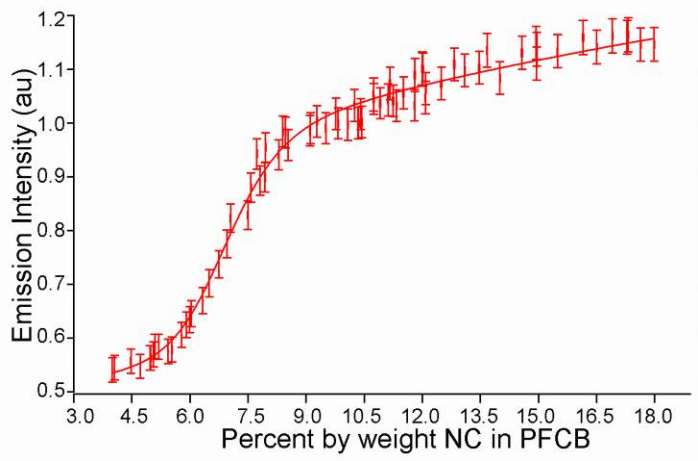

Figure 4.10 Emission intensity of ultrasmall nanocrystals in BP-PFCB vs. percent by weight loading in films with approximately the same thickness. The line drawn is meant only as a guide to the eye. The emission detection was done using the setup shown in Figure 2.14.

Devices fabricated using BP-PFCB encapsulated nanocrystals presented some impressive results. The CIE chromaticity coordinates for a 365 nm emitting LED coated with a nanophosphor layer were (0.324, 0.322), with a measured CRI of 93 (Figure 4.3 inset and Figure 4.11). These values are superior to those of several commercially available LEDS purchased from CoolerGuys.com: 3 mm, 5 mm, and 5 mm ultra-bright (Table 4.2). Unfortunately, the preliminary luminous efficiency results obtained for various coated LEDs ranged from 0.19 lm/watt to just below 1 lm/watt. These values are well below the projected goal of the DOE for SSL and still below the efficiencies for current incandescent and fluorescent lighting technologies.[4, 10, 136]

Table 4.2 Values for several commercially available "white" LEDs (obtained from CoolerGuys.com) and a 365 nm LED coated with a thin layer of ultrasmall nanocrystals in BP-PFCB.

LED type	CIE x	CIE y	CRI
3 mm	0.256	0.251	80.2
5 mm	0.243	0.234	75.7
5 mm ultra-bright	0.298	0.321	73.0
Fabricated	0.324	0.322	93.0

Figure 4.11 Images (from left to right) of three UV LEDs inside the SLMS integrating sphere alone, with a nanocrystals in BP-PFCB cap, and a commercially available "white" LED.

4.2.3 Monomers and Other Tetramer Technologies Polymers

Due to the success of the BP-PFCB as an encapsulant for the white-light CdSe nanocrystals, several monomers and functionalized BP-PFCB polymers were provided for testing (Figure 4.12). The monomers were expected to show whether any improved protection against photooxidation or improved efficiency could be obtained through encapsulating the nanocrystals, while simultaneously polymerizing the monomer. The functionalized BP-PFCB polymers were chosen detect any improved encapsulation with the functional groups similar (amine and C_{10} chain) and dissimilar (carboxylic acid) to the ligands on the surface.

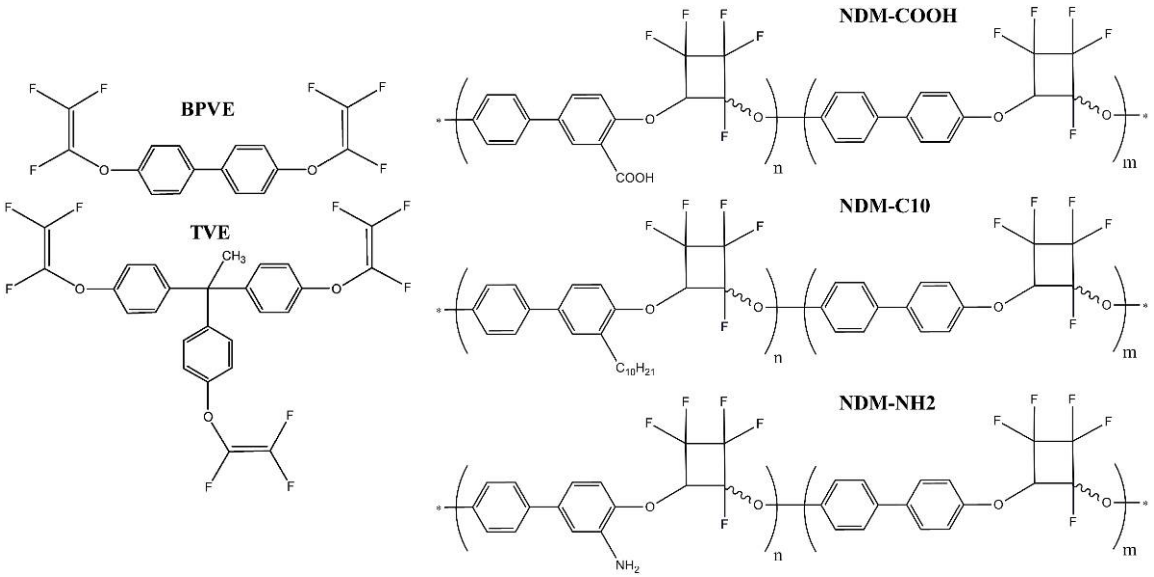

Figure 4.12 Monomer structures (TVE and BPVE) and functionalized BP-PFCB polymers used for these encapsulation studies.

The two monomers were ineffective at encapsulating the ultrasmall nanocrystals. Smooth films were formed; however, the visual cloudiness and lack of the slight yellow color noted for ultrasmall BP-PFCB films illustrated the poor encapsulation with these films. In addition to poor color quality, inhomogeneity with large nanocrystal aggregates could be seen when exciting the low w/w % films with UV light (Figure 4.13A). The TVE film was slightly more homogenous than the BPVE film, particularly apparent with the core-shell nanocrystal films. For the core-shell film of TVE, the emission quality was good: however, for the white-light nanocrystals in TVE film the first two peaks were quenched, yielding a pale orange color (Figure 4.13B). The pure BPVE film showed significant blue emission by itself; however, it seemed to have areas of proper ultrasmall nanocrystals encapsulation. Both monomers were discarded as candidates due to the higher loading achievable, better color quality, and ease of use with the BP-PFCB polymer.

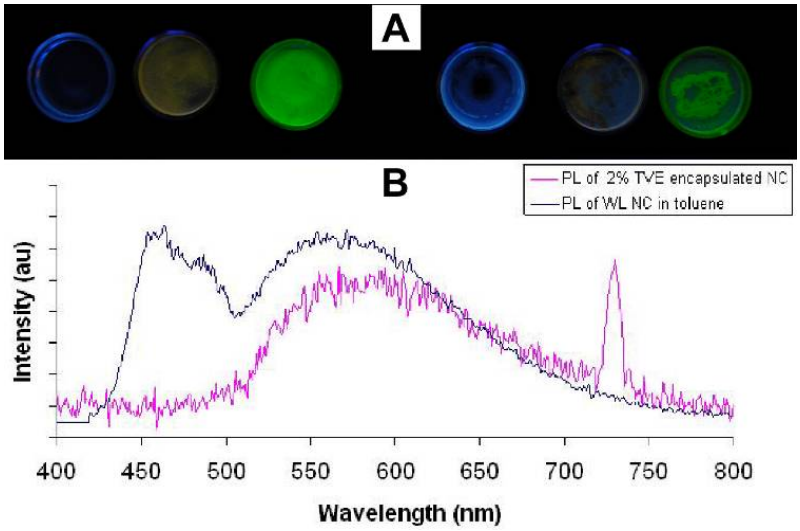

Figure 4.13 A) Image of monomer encapsulated nanocrystals excited by UV light. From left to right the films are: pure TVE, 2.5% w/w ultrasmall nanocrystals in TVE, 4.0% w/w CdSe/ZnS in TVE, pure BPVE, 3.7% w/w ultrasmall nanocrystals in BPVE, 5.2% w/w CdSe/ZnS in BPVE. B) Emission spectra of TVE film with emission of nanocrystals in solution.

Films of ultrasmall nanocrystals in functionalized BP-PFCB polymers were fabricated and characterized in the same way as the standard BP-PFCB polymer films. The worst of these polymer encapsulants was the NDM-NH2. The films fabricated demonstrated a complete loss of the standard absorbance and emission qualities (Figure 4.14). Aggregates of nanocrystals were not noted in films studied with fluorescence microscopy, but no emission was noted either. Most likely, either the amines on the polymer or excess amine from the polymer synthesis destroyed the nanocrystals when heated as amines are known to etch nanocrystals.[90]

Figure 4.14 Films of nanocrystals under room light (top) and under UV excitation (bottom). For both images the films from left to right are BP-PFCB, NDM-NH2, NDM-COOH, and NDM-C10. For the UV excited image, from top to bottom the films are polymer with no nanocrystals, 4% w/w loading, and 8% w/w loading. The room light image is 8% w/w loading to show the transparency of the films.

The films fabricated with NDM-COOH were surprisingly good, considering the addition of the carboxylic acid group. Films fabricated with this polymer were still transparent at 8% w/w loading and ~30-40% as bright compared to the normal polymer. The encapsulation significantly quenched the first emission feature; however, the emission was still very bright and retained a relatively white color (Figures 4.14 and 4.15B). Using fluorescence microscopy, no aggregation was noted in these films. The quenched peak is due to a trap state modulated by the ligand phosphonic acid; it may be possible, that some ligand exchange with the carboxylic acid occurred quenching some of this emission or due to small scale aggregation occurring not observed using optical microscopy.

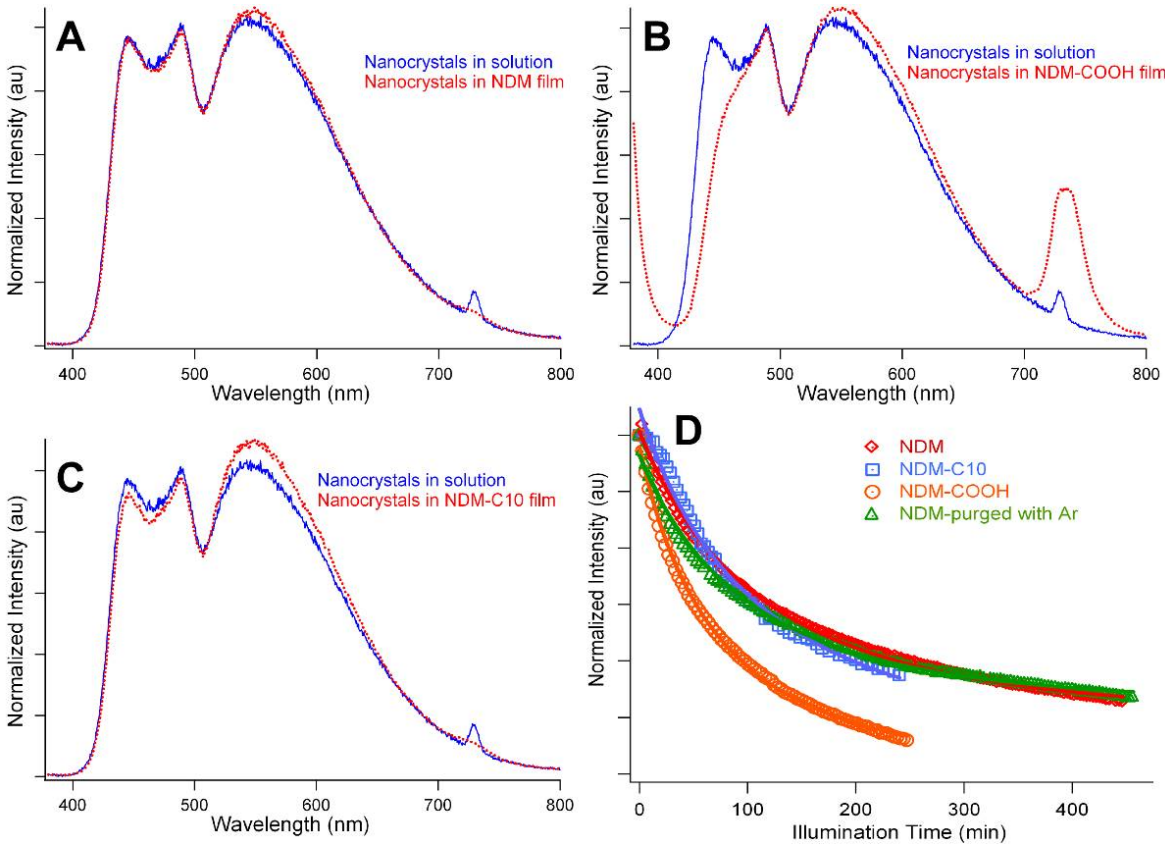

Figure 4.15 Emissions of encapsulated ultrasmall nanocrystals in A) BP-PFCB and toluene, B) NDM-COOH and toluene, C) NDM-C10 and toluene. D) Lifetime data for films of each of these polymers and a film of CdSe:BP-PFCB encapsulated under an Ar atmosphere. Lifetime data is normalized to all have the same starting intensity.

Films of NDM-C10 showed the best encapsulation of the functionalized polymers. The films were transparent and smooth (Figure 4.14). The emission of the nanocrystals showed very little change from toluene solution to film and the intensity was between 85% and 115% of the BP-PFCB films at the same concentrations (Figure 4.15C). No correlation was found between these intensity variations.

Films of BP-PFCB (in air and under Ar atmosphere) and the 2 successful functionalized polymers were fabricated in order to study the lifetimes of any devices built using these encapsulants. The films were constantly illuminated with a 365 nm

LED using the standard holder and PC1 detector, for several hours, while scanning the emission every few minutes. Of the films studied, NDM-COOH had the fastest decay, most likely due to extra oxygen available for photooxidation in this more polar polymer (Figure 4.15D). NDM-C10 actually had almost the same lifetime—defined as the time when the emission intensity reached 70%—as the BP-PFCB films; however, its overall decay showed that its steady-state intensity would probably be lower. Purging the BP-PFCB film with Ar and encapsulating the nanocrystal under an Ar atmosphere did not show a drastic change in the lifetime or steady-state intensity of this film compared to the normal encapsulation procedure. Both PB-PFCB and the NDM-C10 film appeared to approach steady-state intensity above 50%, while the NDM-COOH film would have been closer to 40%. Further NDM-COOH testing was not performed due to a hardware and software error with the PC1 spectrometer, which required several months to repair.

4.3 Conclusions

Ultrasmall white-light CdSe nanocrystals were encapsulated in various polymers. A correlation between the Hildebrand parameter and the HSPs of the various encapsulants and their effectiveness at encapsulating these nanocrystals was found. This correlation is true only for nanocrystals with these particular ligands; nanocrystals with different ligands may show a preference to other polymers. Experimentally, of the thirteen encapsulants studied, only BP-PFCB represents the only practical option for encapsulation, creating a rugged, color-stable environment for the white-light nanocrystals. Encapsulation in BP-PFCB allowed the nanocrystals to be combined with UV LEDs to create a potentially viable, solid-state white-light source.

Simultaneous polymerization and encapsulation through the use of monomers proved unsuccessful in maintaining the nanocrystals' white color quality. The TVE monomer could be used to create films of core-shells; however, BP-PFCB has the benefit of being easy to coat on LEDs. Functionalized BP-PFCB polymers did not show any improvement over the standard polymer backbone. NDM-NH2 decomposed the nanocrystals, NDM-COOH decreased the film life-time, and NDM-C10 showed a mild decrease in the steady-state intensity of nanocrystal:polymer films. Additionally, encapsulating the nanocrystals under an inert atmosphere did not appear to prevent the rate of photooxidation of the nanocrystals.

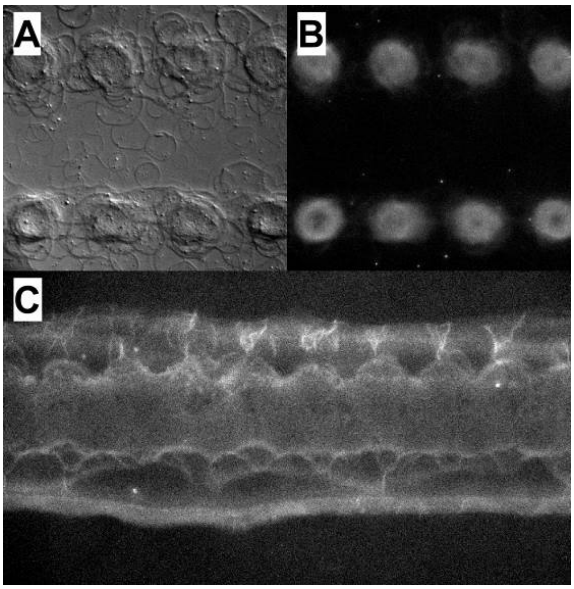

Figure 4.16 A) Bright field and B) and C) fluorescent images of printed white-light nanocrystals in BP-PFCB. These dot films were printed with a Dimatics piezoelectric inkjet printer onto a microscope slide.

Initial attempts at coating UV LEDs were successful in meeting two out of three DOE goals for general illumination by exhibiting CIE chromaticity coordinates (0.324, 0.322) and a CRI of 93. Having already surpassed several commercial devices in color quality,

future developments should be aimed at improving the luminous efficiency of white-light CdSe nanophosphor devices to a commercially realistic number and improved lifetimes. The overall luminous efficiency may be improved through the use of more efficient pump LEDs (currently 5-10%), higher wavelength LEDs to reduce the Stokes loss, and increasing the light extraction efficiency through improved device geometry. Table 4.3 demonstrates possible efficiency improvements due to various factors. Printing the nanocrystals directly onto an LED junction with a piezoelectric inkjet printer (Figure 4.16) may be an option for improved device structure. Regardless of any of the improvements mentioned above, the most important advance will have to be with the ultrasmall nanocrystal material. These materials are sensitive to changes in their environment, have a low efficiency (on average ~8%), and photobleach too quickly to be commercially viable at this time. Improvement studies, such as the one conducted with the phosphonic acid ligands in Chapter 3, may yield a more resilient and bright material. Once that material has been designed and synthesized, the work described here may prove valuable in fabricating devices.

Table 4.3 Measured and calculated values for current nanophosphor LED structures and predicted efficiency improvements. For reference the average luminous efficiencies for incandescent and fluorescent lighting are 13 and 58 lm/watt, with maximum reported values around 25 and 90 lm/watt, respectively. The black values are current values, the blue are reasonable predicted values, and the green values are the values required to fabricate commercially competitive devices.

Device description	LED η	Abs. η	CdSe QY	Stokes loss efficiency	Extraction efficiency	Luminous Efficiency (lm/watt)
365 nm LED	0.029	0.932	0.08	0.676	0.40	0.192
405 nm LED	0.119	0.875	0.08	0.750	0.40	0.831
423 nm LED	0.130	0.865	0.08	0.784	0.40	0.939
365 nm LED	0.40	0.950	0.25	0.676	0.50	10.6
405 nm LED	0.60	0.950	0.25	0.750	0.50	17.7
423 nm LED	0.60	0.950	0.25	0.784	0.50	18.5
365 nm LED	0.80	0.990	0.50	0.676	0.80	71.1
405 nm LED	0.80	0.990	0.50	0.750	0.80	78.9
423 nm LED	0.80	0.990	0.50	0.784	0.80	82.4

CHAPTER V

ELECTROLUMINESCENCE OF WHITE-LIGHT CDSE NANOCRYSTALS

5.1 Introduction

The object of this endeavor was to create a proof-of-concept, solid-state lighting device based on the electroluminescence of ultrasmall CdSe nanocrystals. When synthesized according to the methods described in Chapter 2, ultrasmall nanocrystals exhibit broad-band emission. Electrically exciting these nanocrystals directly was thought to be a possible way to harness their white color characteristics and avoid some of the efficiency losses of photoluminescent devices. Semiconductor nanocrystal-based monochromatic electroluminescent devices have been developed by taking advantage of conducting polymers.[47, 51, 84] White light-emitting diodes have been fabricated using a combination of nanocrystal sizes and polymers;[53, 54] however, these also have lower color quality than incandescent light bulbs (CRI = 100) due to their use of narrow emission bands.

Trap state emission from nanocrystals has been previously seen in both photoluminescence (PL) and electroluminescence (EL); however, trap state EL was only observed from deep trap emission.[48, 51, 53] Deep trap emission, due to dangling Se bonds on the nanocrystal surface, remains static at a broad range of orange/red wavelengths regardless of the nanocrystal size on which these dangling bonds are present.[124, 126, 146] In addition to deep trap emission, ultrasmall nanocrystals have demonstrated emission from

other ligand-modulated trap states, due to their uniquely small size and distinctive synthetic conditions.[56, 77, 115] These ligand-rooted trap states emit at specific blue and green wavelengths which effectively balance out the red deep trap emission, creating a pure white-spectra.[56, 77, 147]

Devices were fabricated which mimic the successful EL devices previously published in the literature.[47, 51, 53, 54] Briefly, PEDOT:PSS was spun cast onto an ITO-coated slide, followed spin casting a layer of nanocrystals in TPD. Onto this a silver cathode was thermally evaporated, completing the device structure (Figure 5.1). Each of the layers was individually characterized by AFM, SEM, and profilometry, before the devices were characterized to determine their electroptical properties.

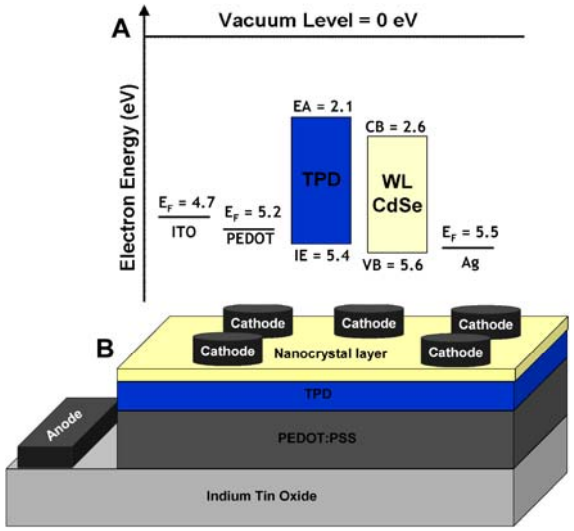

Figure 5.1 A) Energy level diagram of the various layers for the EL devices fabricated and B) illustration of the device structure.

5.2 Results and Discussion

5.2.1 Layer Characterization

At the outset, the thickness of the PEDOT:PSS on the ITO coated slides was examined as a function of spin parameters. A 50:50 solution of commercially available PEDOT:PSS in DI-water was spun cast onto clean ITO slides at varying either the spin rate or spin time. The samples were annealed and the thickness of the PEDOT:PSS films analyzed by profilometry (Figure 5.2A and 5.2B). Additionally, the effect of changing the TPD solution concentration on the final TPD layer thickness was determined (Figure 5.2C).

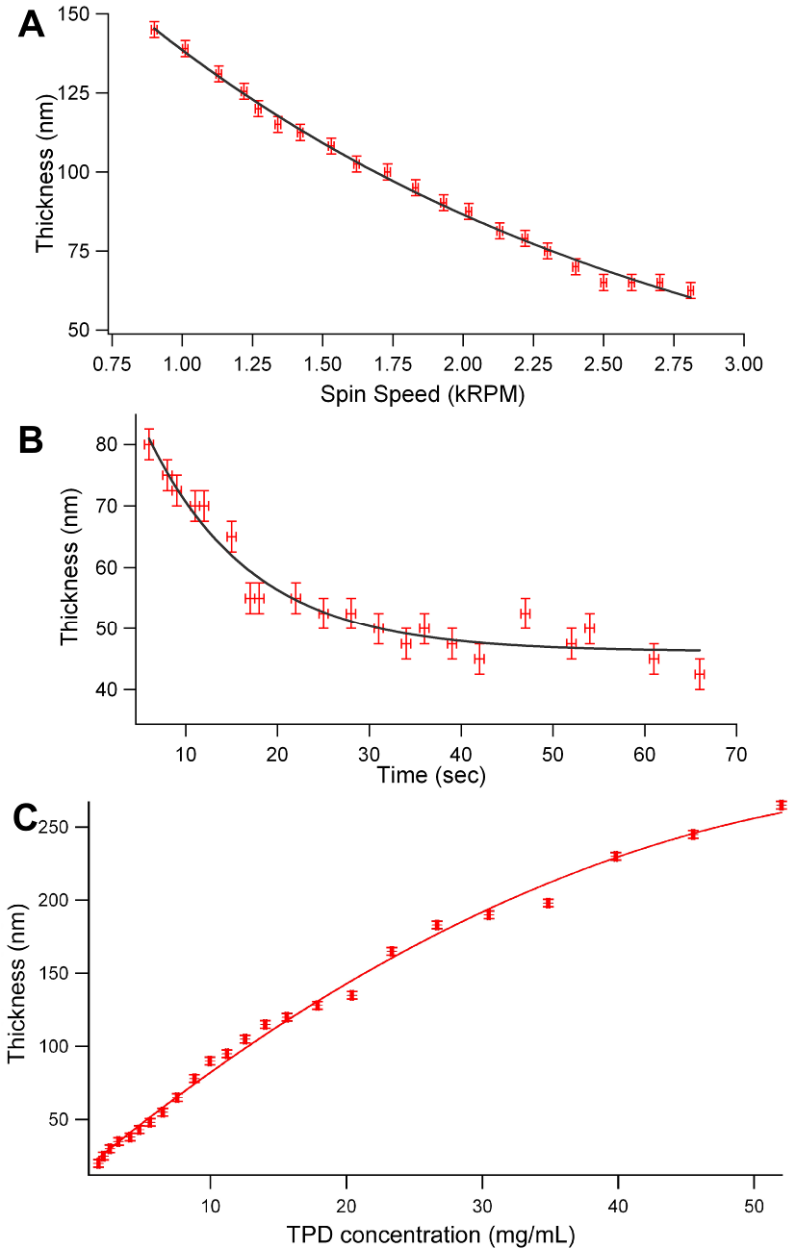

Figure 5.2 A) Thickness of PEDOT:PSS layer vs. spin rate and B) thickness of PEDOT:PSS layer vs. spin time. C) Thickness of TPD layer vs. concentration of TPD in chloroform.

The efficiency of EL devices depends on several factors, one of which is the surface roughness of the various layers. Large nanostructures of one layer pushing through the layer above create shorts in the devices. In such a scenario, a portion of the current may

bypass the nanocrystals, essentially eliminating any chance for those charge carriers to radiatively recombine. The surface roughness of the ITO, PEDOT:PSS, TPD, and nanocrystal layers over a micron square area were determined by AFM (Figure 5.3). The surface roughness for the cleaned ITO surface and the PEDOT:PSS layer shown in Figure 5.3 were nearly the same as the literature values. The ITO surface had the largest range of features and each of the polymer layers made the surface smoother. The nanocrystal layer showed definite signs of phase segregation between the nanocrystals and the TPD with which it was simultaneously spun cast (Figures 5.3C-F). Over this small area (1 x 1 μm for the height images and 500 x 500 nm for the phase images) it appeared that the nanocrystals formed an ordered coating with few defects, as expected based on the work of Bulovic, *et al.*[47, 85, 87, 148]

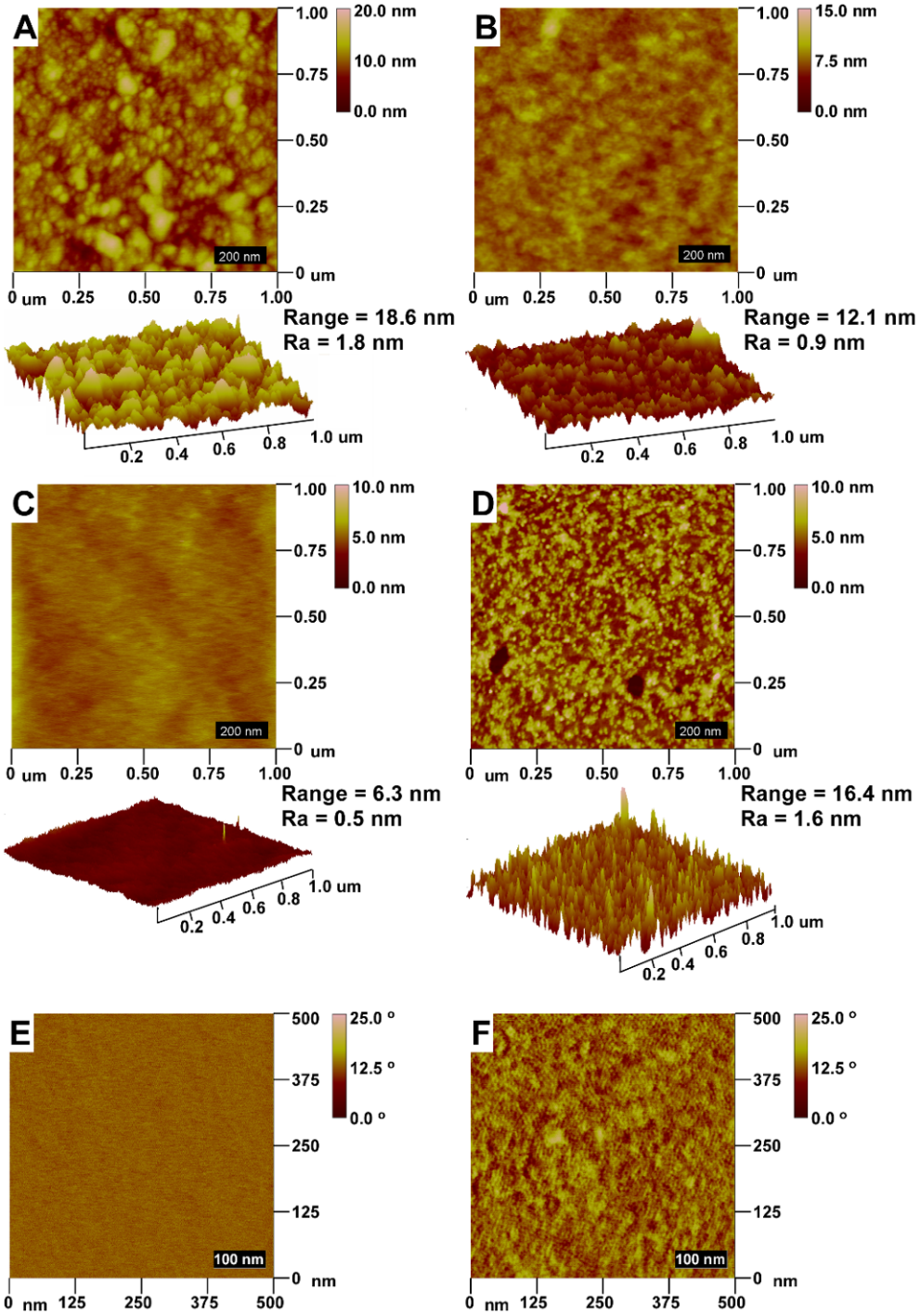

Figure 5.3 Bird's eye and angled view AFM height images of A) clean ITO, B) a ~30 nm thick PEDOT:PSS layer spun cast on ITO, C) a ~50nm TPD layer spun cast onto the PEDOT:PSS layer, D) a core-shell nanocrystal:TPD layer spun cast onto the PEDOT:PSS layer. The average surface roughness (R_a) and height range for several samples of each layer is listed below the images. AFM phase images of E) a TPD layer and F) an ordered core-shell nanocrystal layer on TPD. The phase images were used to confirm the small scale (500 x 500 nm) phase segregation of the nanocrystals and TPD layers.

Fluorescent and SEM images were used to characterize the larger scale surface features. The relatively large features of the ITO surface easily seen were presumed to be due to the sputtering technique used to coat the float-glass slides (Figure 5.4A). Due to the depth resolution with SEM through conducting polymers, it was difficult to discern any structural features of the PEDOT:PSS as opposed to those features due to the ITO (Figure 5.4C). However, a significant difference between the conducting properties of the ITO and the PEDOT:PSS on ITO layers were very apparent (Figure 5.4B). As expected from the low R_a determined by AFM, the SEM images collected of the TPD layer showed almost no features. The few features which were noted while imaging the TPD layer were either due to imaging the ITO features through the two polymer layers (Figure 5.4D) or possible surface debris (images not shown). Using SEM, the partial segregation of the nanocrystals onto the TPD was found to depend on the concentration of the nanocrystals in the solution more than the TPD concentration. At low concentrations (less than ~2.5 mg/mL) the nanocrystals would form small island groupings on the TPD (Figure 5.4E), while at increasingly higher concentrations partial monolayers formed and then multilayer coatings. Fluorescence microscopy demonstrated more clearly that a complete layer was not being formed (Figure 5.4F). Additionally, the optical images showed what appeared to be groups of nanocrystals imbedded within the TPD layer. It appeared to that these nanocrystals were still emissive and a review of the literature confirmed that complete phase segregation was not necessary to demonstrate nanocrystal emission; thus, the importance of a completely phase segregated and complete nanocrystal on TPD layer was diminished despite any decreased in efficiency

for devices fabricated using these parameters. These results were all in accordance with the previously published work of Bulovic, *et al*.[47, 85, 87, 148]

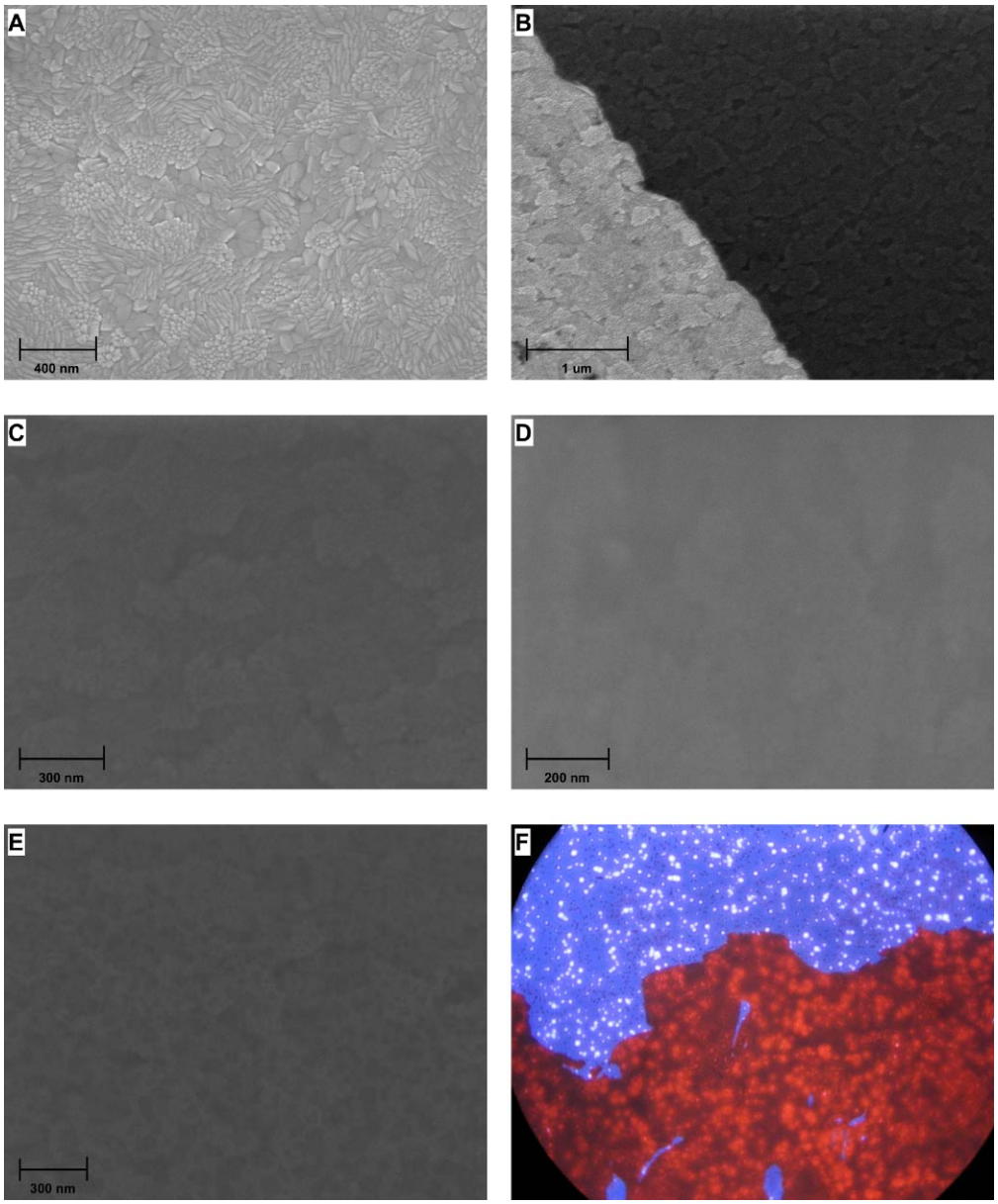

Figure 5.4 Representative SEM images collected of A) clean ITO, B) a ~30 nm thick PEDOT:PSS layer spun cast on ITO, C) an ITO and PEDOT:PSS layer boundary, D) a ~40nm TPD layer spun cast onto a PEDOT:PSS on ITO layer, E) a core-shell nanocrystal:TPD layer spun cast onto a PEDOT:PSS on ITO layer and a true-color fluorescence image of F) the partial phase segregation of red CdSe/ZnS nanocrystals from blue TPD. The concentration of the solution of nanocrystals used to prepare the sample in E was much lower than the concentration used in F, hence the islands which can be seen in E versus the large scale layer seen in F. The white spots in F are most likely due to the emission of nanocrystal within the TPD.

5.2.2 Device Analysis

Core-shell nanocrystal light-emitting devices were found to have nearly identical emission as the same nanocrystals in solution (Figure 5.5A). The TPD under-layer was found to emit a significant intensity light when higher concentrations of the TPD were used (Figure 5.5B). Although the increased TPD concentration should not effect the nanocrystal surface layer's properties,[87] the increased TPD thickness improved the likelihood that a portion of the nanocrystals did not reach the top surface during the phase segregation. Consequently, the opportunity for radiative recombinations both within this layer, as opposed to in the nanocrystal surface layer, and TPD recombination were increased. In addition, the peak emission intensity voltage and the turn-on voltage both increased with increasing TPD concentration. A device's turn-on voltage can be defined as the voltage at which the emission of light begins, generally noted by a slope change in the I-V curve. Devices showed a tendency to brighten with increased voltage, reach a peak, and then dim as the nanocrystals began to quench (Figure 5.5C and 5.5D). For devices where TPD emission was detected, its emission followed a similar trend, reaching a peak at lower voltages. The brightest nanocrystal electroluminescence for these core-shell devices was obtained using 1 mg/mL TPD in CH_3Cl and 8 mg/mL CdSe/ZnS in CH_3Cl. The core-shell LED device structure demonstrated standard electrical LED diode behavior prior to the dimming, with an average turn-on voltage around 2 V and peak brightness at 4.2 V (Figure 5.5D).

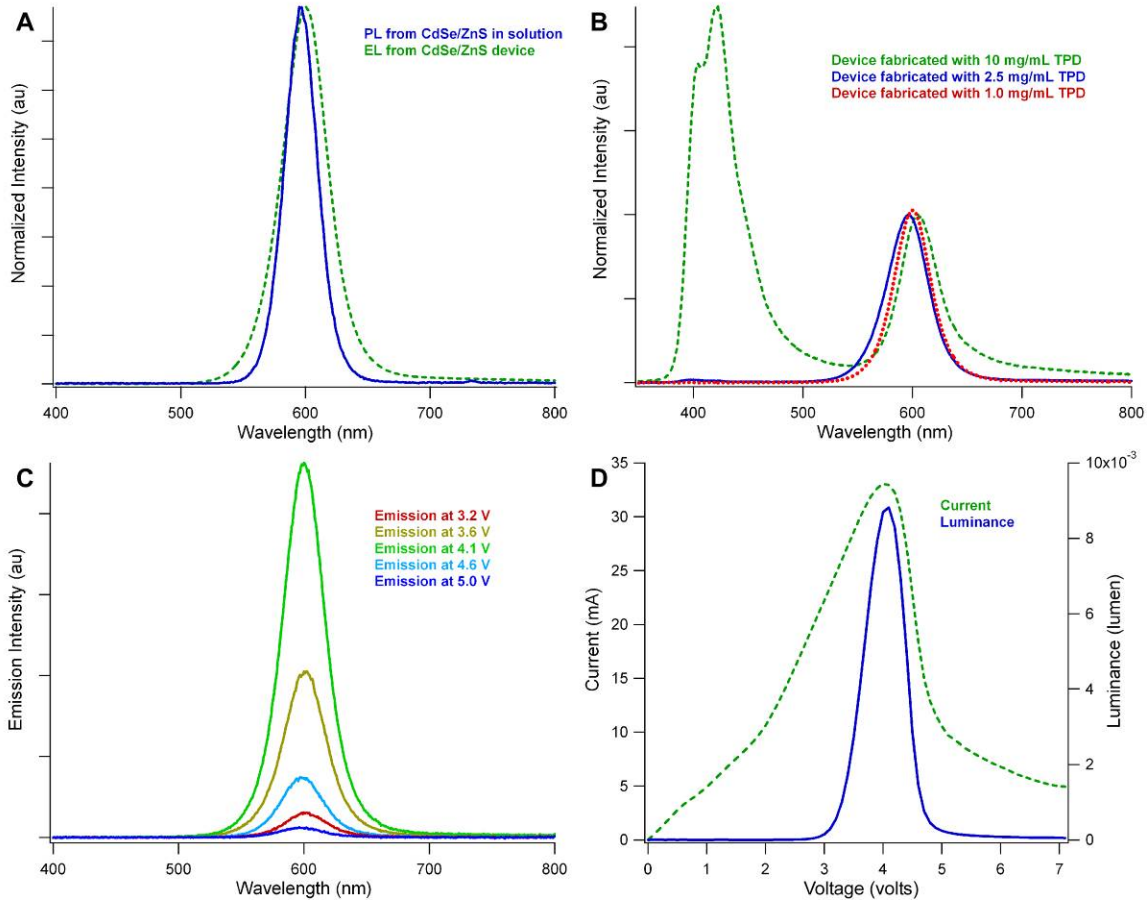

Figure 5.5 A) Electroluminescence spectra of CdSe/ZnS device and emission of the same nanocrystals in solution. B) Electroluminescence spectra of various CdSe/ZnS devices fabricated with different concentration of TPD. These spectra are normalized at the nanocrystal EL peak. C) Electroluminescence of a single CdSe/ZnS LED at various voltages. D) Representative current vs. voltage curve (green, dashed) and luminance (brightness) vs. voltage curve (blue, solid) for core-shell devices.

The EL from ultrasmall nanocrystal LEDs had a slightly broader emission than the PL of the same nanocrystals in a chloroform solution (Figure 5.6). However, the LEDs fabricated with these white nanocrystals still provided excellent CIE coordinates (0.333, 0.333), correlated color temperatures of 5461 to 6007 K, and color rendering indexes as high as 96.6 which mimic noon-day sunlight.[149]

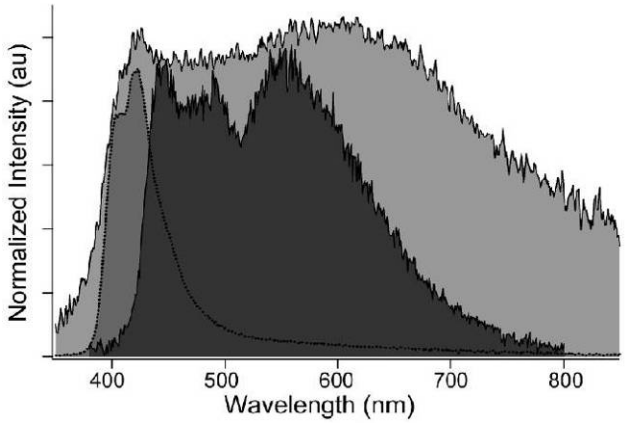

Figure 5.6 Comparison of nanocrystal EL (lightest shade) with the PL of TPD and nanocrystals in solution. The PL from ultrasmall nanocrystals is the darkest spectra; the TPD only emission is the middle shade (centered at 410 nm). The broad EL emission has CIE coordinates of (0.333, 0.333), a CRI of 96.6, a CCT of ~5500 K, and was white to the eye.

The emission changes in Figure 5.6 were attributed to the broadening and red-shifting of the deep trap emission, broadening of the ligand-modulated emission, and a blue contribution from the TPD layer. The red-shifting and broadening from PL to EL were primarily a consequence of the change in physical environment and the injection of the charge carriers as opposed to their generation directly on the nanocrystal due to light absorption. Monochromatic core-shell nanocrystal LEDs did not demonstrate this broadening as the band-edge state responsible for the emission is not dependent on the nanocrystal's environment. The trap-states responsible for the white emission are all located at the nanocrystal surface and any modification to these surface traps will change the energy of their emission, see Chapter 3.[77, 150] Although the surrounding polymer and Ag have not quenched the trap emission, it is likely this environment along with the simple liquid to solid-state change modified the wavelengths at which both the Se and ligand traps were emitting. Additionally, heating of the sample from current flow may

contribute to this broadening, particularly the tailing of the deep trap emission into the near-infrared.[83] It has been previously seen that with larger sizes (diameter > 2 nm) of nanocrystals the deep trap emission is more strongly pronounced in EL than in PL when compared to the band-edge emission.[82] As the ultrasmall nanocrystals' emission is due entirely to trap states, a comparative increase in the efficiency of deep trap emission compared to the ligand trap states was not expected or observed.

The EL described here is from the smallest nanocrystals size reported to date. Previous work by Mattoussi, *et al.* noted that emission from nanocrystals with these small dimensions was unattainable.[82] The use of the wider band-gap polymer, TPD relative to poly(phenylene vinylene) used by Mattoussi, provided access to the previously unseen ligand-mediated blue/green trap state EL from ultrasmall nanocrystals. It is possible that the TPD may be pumping these states as opposed to direct carrier injection, although this seems unlikely due to the quenching of the TPD prior to the quenching of the nanocrystal trap states described below.

The electrical characteristics of the ultrasmall nanocrystal devices exhibit standard diode behavior and are similar to core-shell nanocrystal LEDs, with the exception of higher turn-on voltages (~10 to 16V) for these devices and their "leaky diode" behavior (Figure 5.7).[47, 48, 51, 82] Due to their small size and molecular weight, ultrasmall nanocrystals have proven difficult to separate from excess ligands and synthetic precursors.[151] This surplus material may have formed a thin insulating layer between the nanocrystals and the polymer or Ag cathode, reducing the current through the nanocrystals. Furthermore, the environmental dependence of the trap state emission does not allow for this ultrasmall size to be shelled, without damage to the white emission. In

addition, most low turn-on devices have organic hole-transport and electron-transport layers, which are tuned to ease carrier injection in the nanocrystals. For these initial studies, these layers were not used due to the belief that they may inhibit the pure white nanocrystal emission or exhibit extraneous emission. Lastly, the small size may also contribute to the higher turn-on voltage compared to devices fabricated with larger CdSe nanocrystals. The current and luminance seen prior to the actual diode-like behavior, can be attributed what might be called a "leaky-diode." In this case, current has begun to flow and the nanocrystals have begun to emit, prior to the actual "turn-on" voltage of the device. Behavior of this sort can be attributed two factors: the excess precursor material, which may be preventing charge carriers from reaching some of the nanocrystals, and the small changes in the nanocrystal ligand-coverage and structure. At the ultrasmall size, even changes in the nanocrystal structure of a few atoms represent relatively significant alterations.

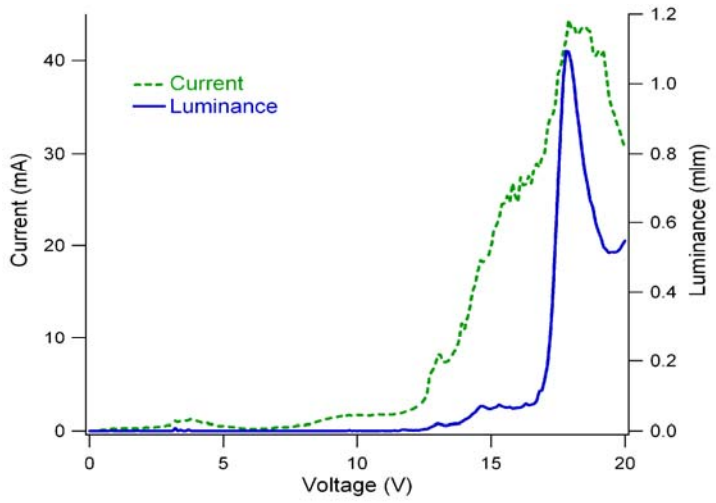

Figure 5.7 Current-voltage and luminance-voltage behavior of white CdSe nanocrystal devices.

Each of the various emission states demonstrated a unique longevity when powered at high voltages, affecting both the emission intensity and color quality. For devices where the voltage dwell time was several seconds at each increasing step, it was seen that the emission from both the TPD and nanocrystals' ligand trap states are quenched prior to the deep trap emission (Figure 5.8). In order to monitor quenching of the emission processes, devices were scanned with 1 second dwell times at each 0.1 volt step with a range of 0-18 volts. Comparing three regions of the white EL—deep trap, ligand traps, and TPD emission—showed that the emission intensity for each process is reached at different voltages (Figure 5.9). The TPD emission reached its maximum and began to decay first, most likely due to the sensitivity of organic conducting polymers to high current, heat, and exposure to oxygen. At high voltages the TPD emission had disappeared and the ligand-dependent nanocrystal emission had been significantly quenched. It is not surprising that the ligand-modulated emission also began to decay prior to the deep trap, since at these voltages the ligands are more susceptible to heat damage than the dangling Se bonds that are responsible for the deep trap emission. This may also have been an effect of the decreased polymer emission no longer aiding in the pumping of these states. Time was considered to be a factor in this non-uniform decay; however, as a significant disparity in the emission wavelengths was not noted when devices were monitored at a lower static voltage, the main culprit was suspected to be voltage and the associated heat damage.

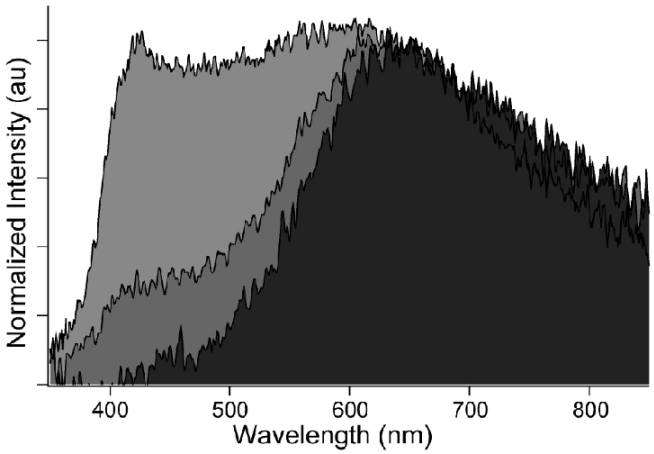

Figure 5.8 Normalized electroluminescence from an ultrasmall nanocrystal based device at 15.9 V (lightest shade), 16.8 V, and 17.2 V (darkest shade). At large applied voltages, the small contribution from the organic polymer is quenched and the blue/green emission features of the ultrasmall nanocrystals are reduced, despite the deep trap emission remaining quite strong.

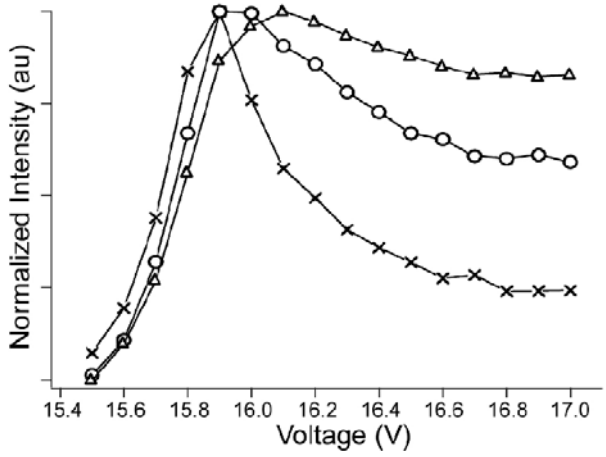

Figure 5.9 Integrated intensity of three wavelength regions of the EL emission spectra versus voltage. The TPD emission (x, integrated from 395 to 415 nm) is shown to decrease significantly above 15.9 V. The ligand-modulated emission (o, integrated from 460 to 480 nm) begins to decrease at 16 V; however, the decline is much less pronounced than that of TPD. Deep trap nanocrystal emission (Δ, integrated from 600 to 620 nm) is shown to be largely unquenched by the voltage increase. The integrated intensities were normalized to the peak emission intensity of each region. The disproportion between increasing intensities prior to 15.9 V should not be interpreted as unbalanced color emission; unbalanced color quality was noted only after the TPD and ligand-dependent emissions had diminished, while the deep-trap intensity continued to increase, in this case at ~16.1 V.

The external quantum efficiency of the ultrasmall nanocrystal devices (~0.00013 %) is significantly lower than the efficiency of core-shell nanocrystal EL devices with a similar device structure (~0.52 %).[82] LEDs with enhanced device structures have demonstrated much higher efficiency on the order of 1%. The existing efficiency can be explained partially by that fact that these white-light nanocrystals have lower quantum efficiencies in solution (~4 % in undistilled chloroform) compared to core-shell nanocrystals (>50 %).[47, 78] Not all of the low efficiency should be attributed to the quantum yield difference as this represents only a change of one order of magnitude and not the three orders of magnitude difference between these devices. The extra precursor material found in ultrasmall nanocrystal solutions compared to traditionally sized or core-shell solution has been incorporated into the EL devices. This organic material represents an insulating barrier layer that probably accounts for a significant portion of the decreased efficiency.

It is also possible that the addition of organic transport layers and the tuning their energetic bands would increase the efficiency. Any increase in efficiency due to these transport layers, would have to be balanced with any loss of color quality due to their quenching of any nanocrystal trap state emission. It should be noted that the luminous efficiency of these devices (currently, $4.83*10^{-5}$ lumen/watt) will always suffer when compared to monochromatic or narrow-band LEDs due to the broad emission covering the entire visible spectrum, which provides the high color rendering index of 96.6 and ~5500 K correlated color temperature. This trade-off between color quality and luminous efficiency has been previously noted, but accounts for only a small portion of the disparity between the efficiencies.[9, 136]

5.3 Conclusions

A proof of concept result demonstrated that pure white-light electroluminescence from a single size of ultrasmall CdSe nanocrystals is possible, opening the door to simple and high quality nanocrystal-based light sources which approximate natural sunlight. The white LEDs replicated noon-day sunlight with CIE coordinates of (0.333, 0.333), a CRI as high as 96.6, and correlated color temperatures from 5500 to 6000 K. Now that electroluminescence from these new trap states has been demonstrated, further control over these states should be pursued. It may be possible to voltage-tune not only the emission wavelength of the various states, but the intensity of each state as well, allowing for a single light source to obtain a significant degree of color tenability. Furthermore, this trap state EL research may prove transferable to other trap state emissive materials, such as ZnO.[152, 153]

Additionally, work must be continued on improving the efficiency of the devices. Improved nanocrystal and TPD deposition should be considered, as well as improved device configuration through the addition of other electron and hole-transport layers. Ultimately, improving the efficiency of ultrasmall nanocrystals is the limiting step in producing a bright and high-quality white LED.

CHAPTER VI

CONCLUSIONS AND FUTURE OUTLOOK

6.1 Overall Conclusions

The pinned emission wavelength of ultrasmall nanocrystals is dependent on the phosphonic acid surface ligand. For straight alkyl chain phosphonic acids, longer chains (more carbon atoms) pinned the bluest emission feature at longer wavelengths than shorter chains. For these, as well as branched or conjugated ligands, the energy of the pinned emission was shown to correlate with the electronegativity the phosphonic acid. Additionally, these ligands were shown to modulate quantum yield in both the traditional and ultrasmall size regimes. The phosphonic acid chosen to form the Cd-phosphonate precursor was also shown to influence the nanocrystal growth kinetics. The electronegativity of the phosphonic acid controls the speed at which Cd atoms become available for growth; butyl phosphonic slowed the reaction the most, while docosyl phosphonic acid represented the fastest growth rate.

A variety of polymers were tested to determine which would best encapsulate the ultrasmall, white-light emitting nanocrystals for use in a photoluminescent LED. A correlation between the Hildebrand and Hansen solubility parameters of the polymers and their effectiveness at encapsulating the nanocrystals was found. Experimentally, of the thirteen encapsulants studied, only BP-PFCB was a practical option. No improvements in color quality or nanocrystal device lifetime were noted when using a modified BBP-PFCB polymer backbone. Nanocrystals encapsulated in BP-PFCB were combined with

ultraviolet LEDs to create a white-light solid-state LED. These LEDs exhibited white CIE chromaticity coordinates (0.324, 0.322) and a high color rendering index of 93. The luminous efficiency of these devices was on the order of 1 lumen/watt, well below the efficiency of even an incandescent light bulb.

White-light electroluminescence from ultrasmall CdSe nanocrystals was shown to be feasible. A solid-state device was fabricated by placing these nanocrystals into a device structure similar to that used for monochromatic nanocrystal-based and organic dye-based LEDs. This electroluminescence is from the smallest CdSe size known to date. Emission from the devices mimicked the photoluminescent devices, having CIE coordinates of (0.333, 0.333), a color rendering index as high as 96.6, and correlated color temperatures from 5500 to 6000 K.

6.2 Future Directions

Studies into controlling the middle emission feature of the ultrasmall nanocrystals, through changes to the synthesis should be pursued. It may be that using different amines or Se-solvents will provide the desired control. Using a different high boiling solvent other than hexadecylamine may allow the functionalized phosphonic acids described in Chapter 3 to synthesize and isolate nanocrystals. The synthesis and use of new phosphonic acid structures will elucidate the exact nature of the ligand modulation of emitting trap states. Particularly, phosphonic acids containing a phenyl group with electron-donating or withdrawing groups attached may advance the inductive electronegativity theory proposed here. An attempt should be made to replicate the studies of the phosphonic acid ligand with carboxylic acids other than oleic acid. These

ligands may demonstrate new trap states or more sensitive control of the same trap states. Novel cleanup procedures should also be attempted to remove the excess precursor and ligand material from the ultrasmall nanocrystal solutions. The use of alumina powder or gel electrophoresis could be attempted easily.

In addition to the synthetic proposals above, new materials should be explored. Cadmium-based devices have been or are under consideration for being banned in Europe by the European Union. At this point, with this large market closed to lighting based on CdSe white-light emitting nanocrystals, it is unlikely that any progress made in fabricating these LEDs will translate to a commercially available device. The discovery of white trap-state emission in CdSe was unexpected; it may be that another such trap-based material can be found. The exact toxicity of CdSe in nanocrystal form should also be studied to confirm or refute the belief that technologies based on nanocrystals are impractical for general use.

Efficiency and stability improvements in both the photoluminescent and electroluminescent devices should be considered. Printing the nanocrystals directly onto a UV LED die is currently the most promising option for more efficient PL devices. New or modified hole- and electron-transport layers should be studied in the EL devices. Replacing TPD with PVK and the addition of Bathocuprione and/or tris(8-quinoline) aluminum are probably the first experiments which should be carried out. Modifications to the way the nanocrystals and TPD are deposited should also be explored. Lastly, a switch from ITO to carbon nanotubes as the conducting substrate may prove helpful, if not economical. Any improvement in efficiency will need to be balanced with color quality losses.

The most important efficiency exertions lie with the ultrasmall nanocrystals themselves. Any efficiency enhancement due to factors other than the nanocrystal quantum yield will pale in comparison to what is possible with improved nanocrystals. Reliably, the quantum yield for purified, toluene-solvated nanocrystals is around 6%. With a predicted maximum luminous efficiency for the white emission around 330, even with all the other efficiency factors at unity, devices based on this quantum yield will fall below 20 lumen/watt. At least a 40% quantum yield for the ultrasmall nanocrystals must be achieved to compensate for any other deficiencies in the device.

APPENDIX A

CIE, CRI, AND CCT CALCULATIONS AND EFFICIENCY TERMS

A.1 Color Calculations

Generally, the CIE color coordinates, CRI, and CCT calculations are done by the programs used to collect emission spectra *via* an integrating sphere or other LED testing setup. However, these programs are not always available, in which case, the calculations are most easily done using an excel spreadsheet. For the 1931 color coordinates the following procedure should be used. 1) Collect an emission spectra from 390 to 800. 2) Multiply wavelength intensity values times each of the x, y, and z color matching functions provided to obtain xbar, ybar, and zbar values for each wavelength (http://cvrl.ioo.ucl.ac.uk/database/data/cmfs/ciexyz31_1.txt). 3) Sum all of the values for xbar, ybar, and zbar to obtain Xbar, Ybar, Zbar. 4) Normalize to the tri-stimulus values using the following equations to obtain Xstim, Ystim, and Zstim.

$$\text{Xstim} = \frac{\text{Xbar}}{(\text{Xbar} + \text{Ybar} + \text{Zbar})} \qquad \text{(A.1)}$$

$$\text{Ystim} = \frac{\text{Ybar}}{(\text{Xbar} + \text{Ybar} + \text{Zbar})} \qquad \text{(A.2)}$$

$$\text{Zstim} = \frac{\text{Zbar}}{(\text{Xbar} + \text{Ybar} + \text{Zbar})} \qquad \text{(A.3)}$$

5) The 1960 color coordinates u and v can be obtained via the following equations:

$$u = \frac{4 * Xstim}{(Xstim + 15 * Ystim + 3 * Zstim)} \qquad (A.4)$$

$$v = \frac{6 * Ystim}{(Xstim + 15 * Ystim + 3 * Zstim)} \qquad (A.5)$$

6) The 1931 color coordinates x and y can be obtained via the following equations:

$$x = \frac{3 * u}{(2 * u - 8 * v + 4)} \qquad (A.6)$$

$$y = \frac{2 * v}{(2 * u - 8 * v + 4)} \qquad (A.7)$$

The procedure for calculating color rendering indexes and correlated color temperatures are too complicated to be included here. An excel spreadsheet was obtained from David Gross via Jon D. Gosnell which had the equations correctly entered.

A.2 Efficiency Terms Comment

In all my work, I have referred to luminous efficiency as the optical output in lumens divided by the input electrical power. In other writings, efficiency and efficacy are interchanged and wall-plug efficiency is also mixed in with these two terms. A significant portion of the scientific community, as well as the general population, confuse

these terms. Some researchers will disagree with this nomenclature, but I had chosen this course since the beginning and will continue to do so. The main reason for this choice is that the US Department of Energy roadmaps to solid-state lighting, several nanocrystal LED papers used as references in my manuscripts, and commonly cited efficiencies for current light sources follow this arrangement.

APPENDIX B

CHARCTERIZATION OF PHOSPHONIC ACIDS

Although only the data for dodecylphosphonic acid was presented in this dissertation and a paper published in the Journal of Physical Chemistry C, a significant amount of work went into characterizing each phosphonic acid. Due to the time spent on the following spectra, I have chosen to include them here. They may prove useful to anyone characterizing phosphonic acids on their own. These spectra do not represent pure phosphonic acids, but they are the best that I obtained for each ligand.

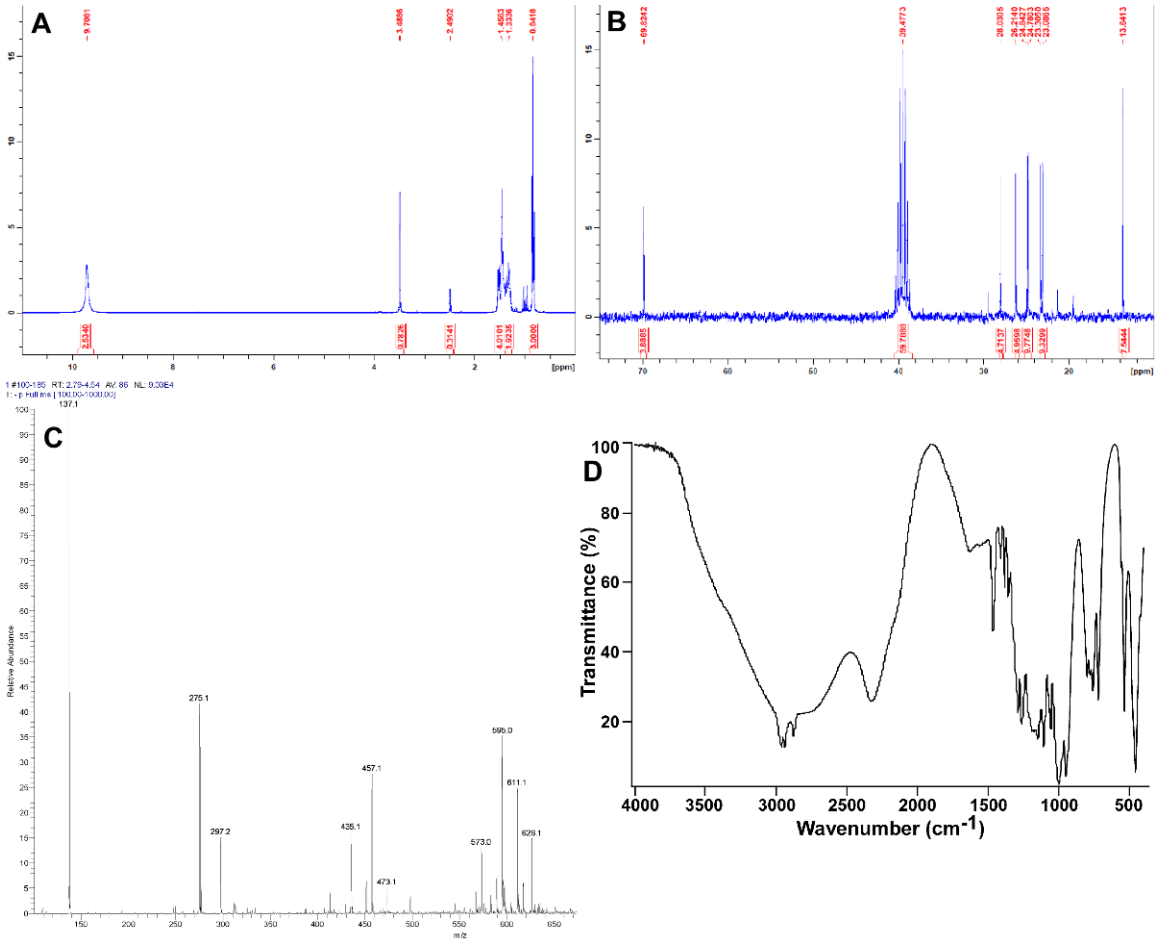

Figure B.1 Spectra for butylphosphonic acid: A) Proton NMR, B) Carbon NMR, C) ESI-mass spectrum, and D) IR-transmittance spectra

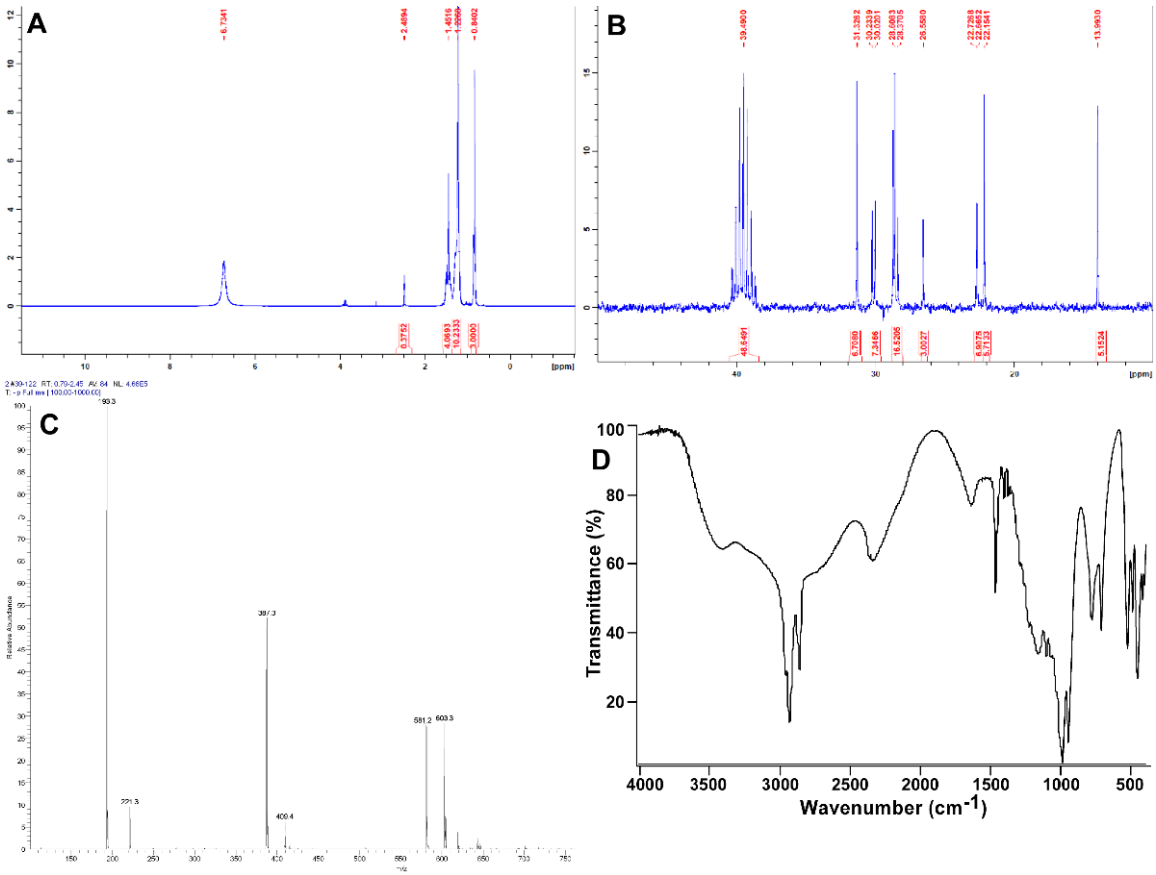

Figure B.2 Spectra for octylphosphonic acid: A) Proton NMR, B) Carbon NMR, C) ESI-mass spectrum, and D) IR-transmittance spectra

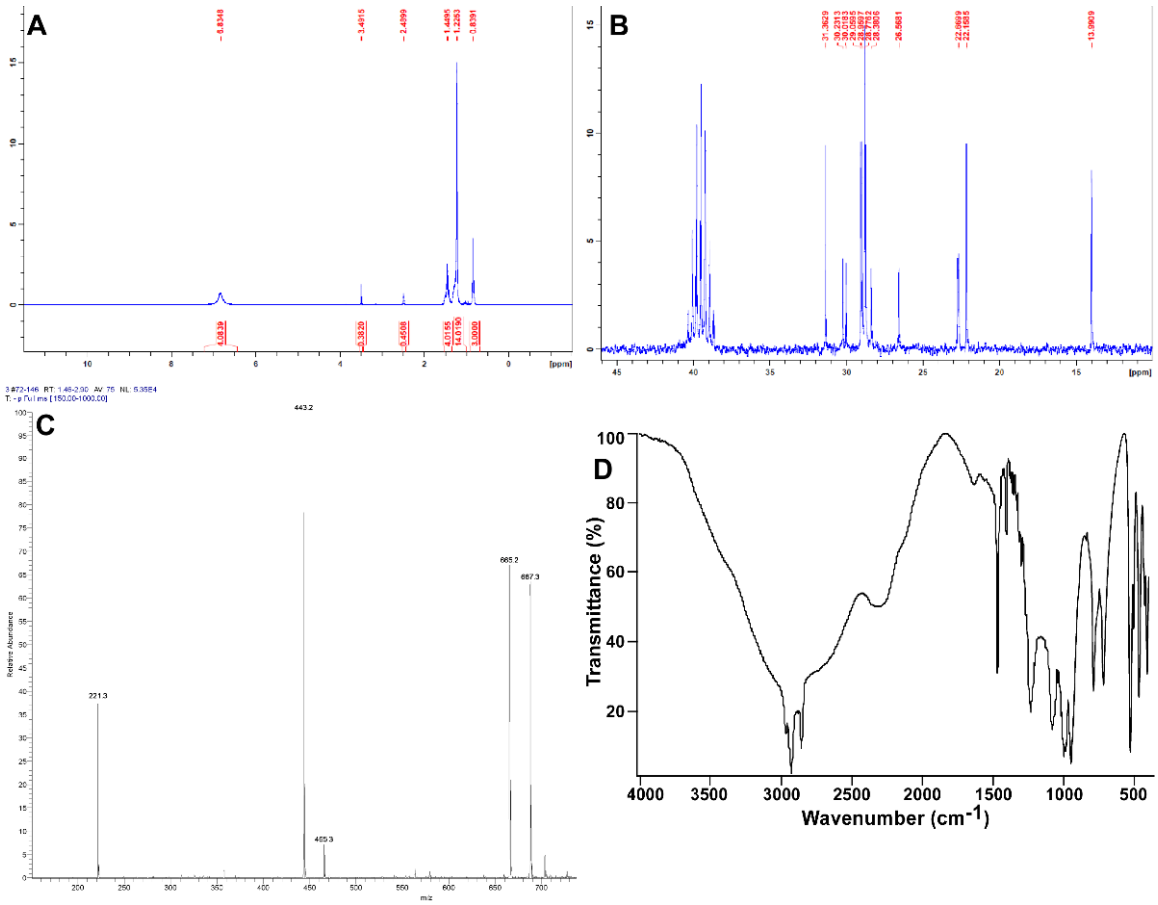

Figure B.3 Spectra for decylphosphonic acid: A) Proton NMR, B) Carbon NMR, C) ESI-mass spectrum, and D) IR-transmittance spectra

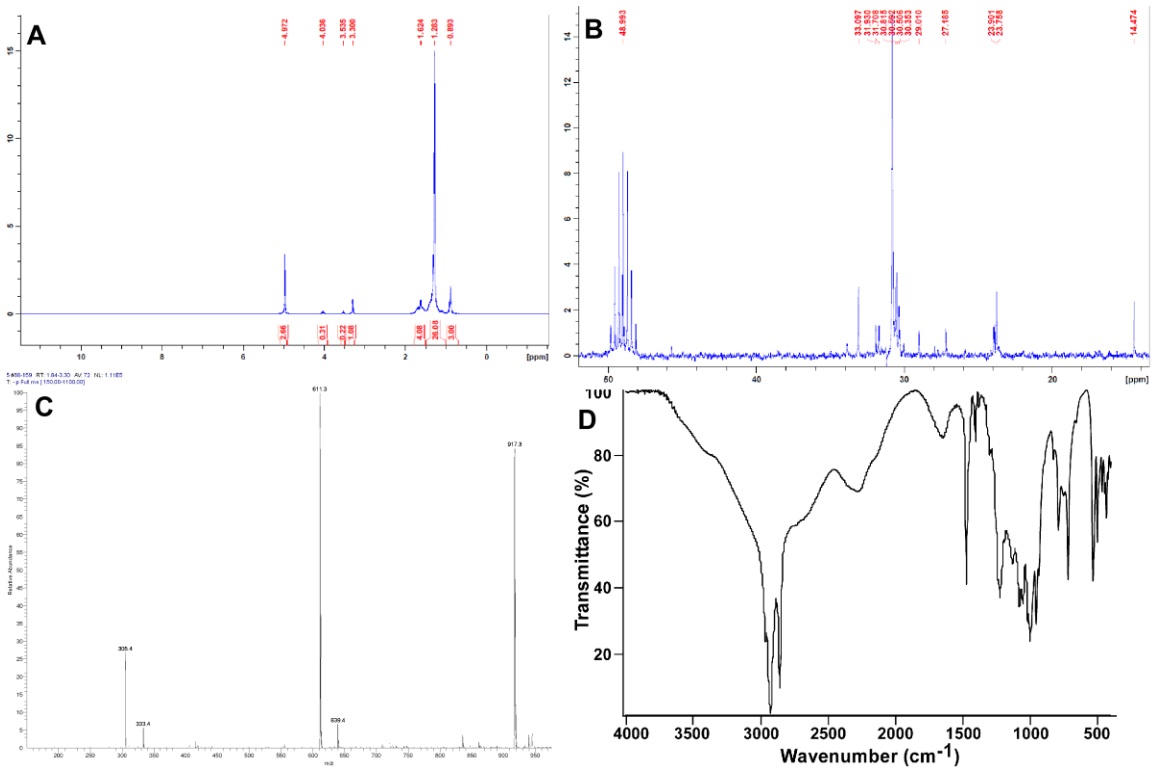

Figure B.4 Spectra for hexadecylphosphonic acid: A) Proton NMR, B) Carbon NMR, C) ESI-mass spectrum, and D) IR-transmittance spectra

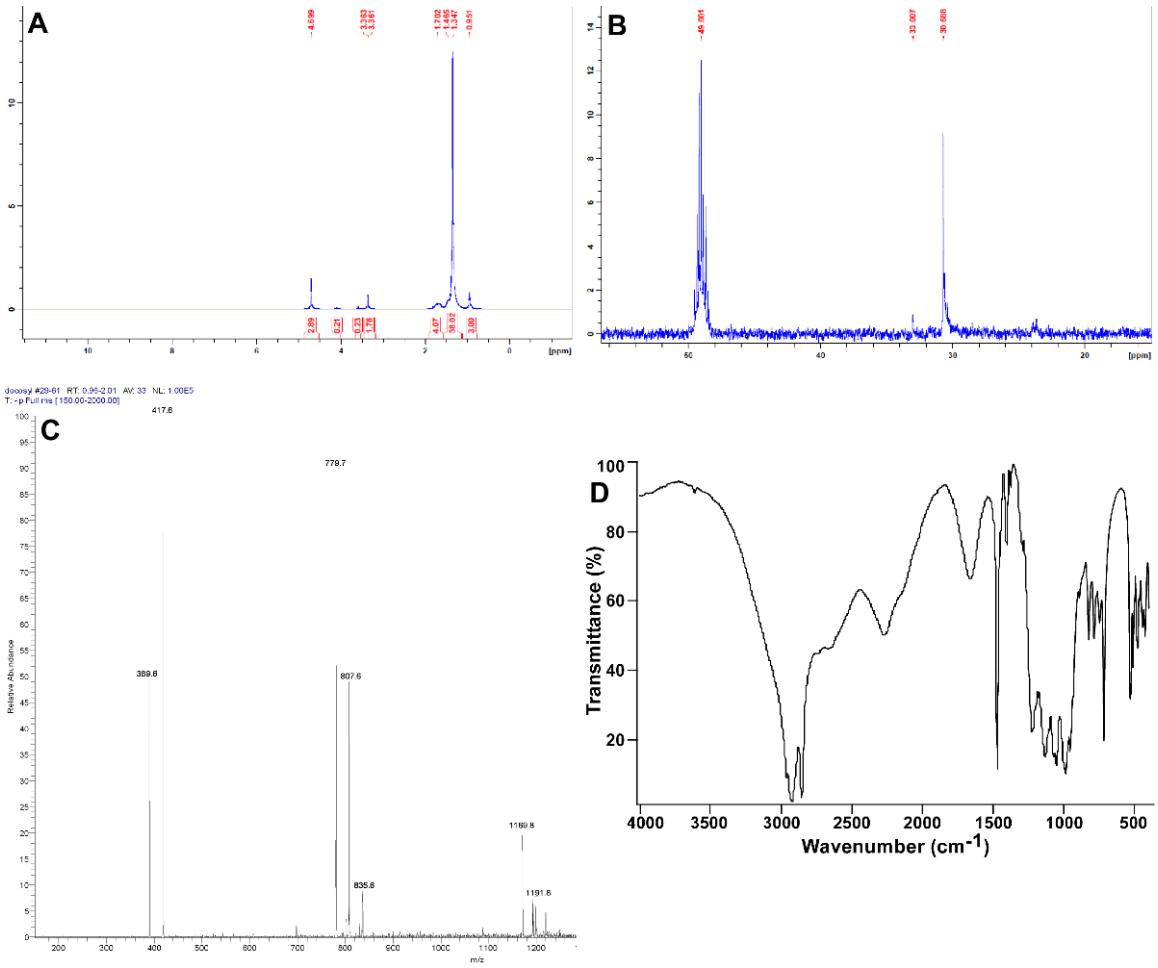

Figure B.5 Spectra for docosylphosphonic acid: A) Proton NMR, B) Carbon NMR, C) ESI-mass spectrum, and D) IR-transmittance spectra

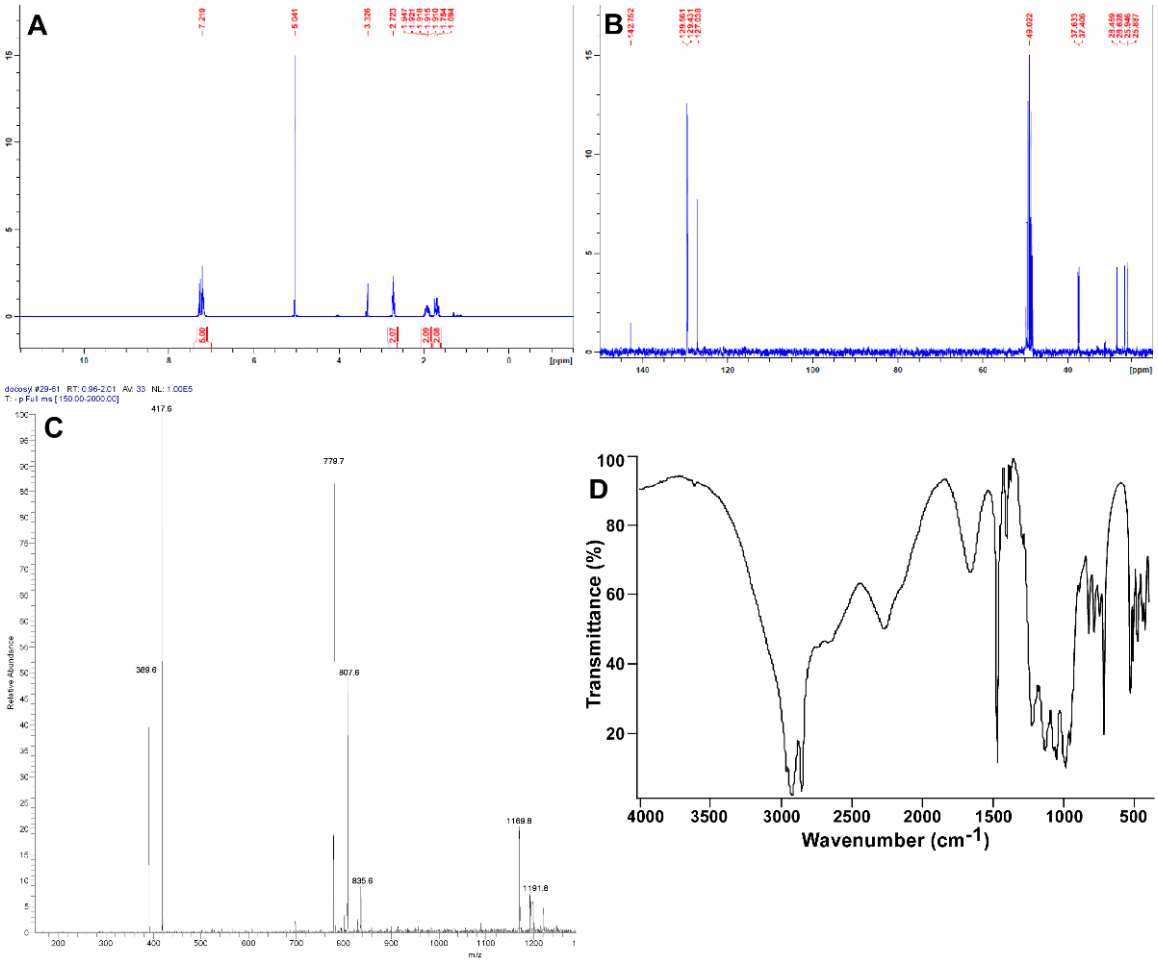

Figure B.6 Spectra for 3-phenyl,propylphosphonic acid: A) Proton NMR, B) Carbon NMR, C) ESI-mass spectrum, and D) IR-transmittance spectra

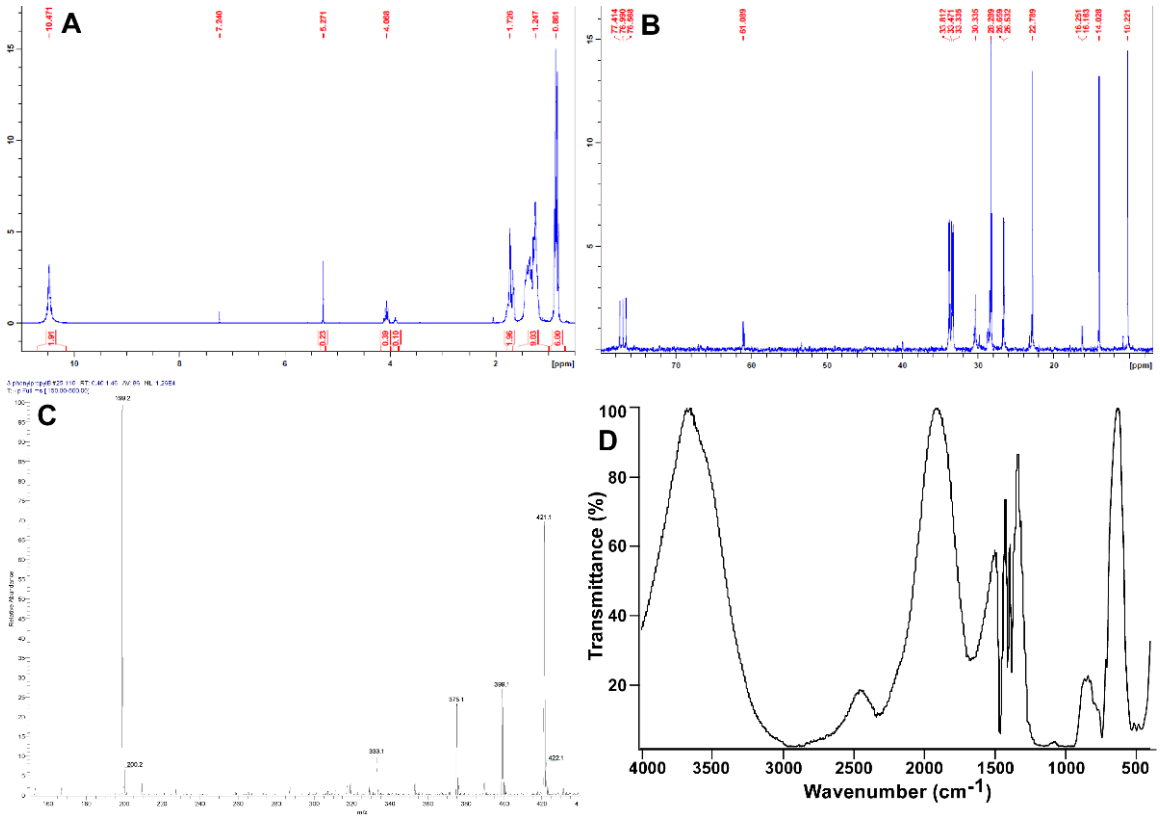

Figure B.7 Spectra for 2-ethyl,hexylphosphonic acid: A) Proton NMR, B) Carbon NMR, C) ESI-mass spectrum, and D) IR-transmittance spectra

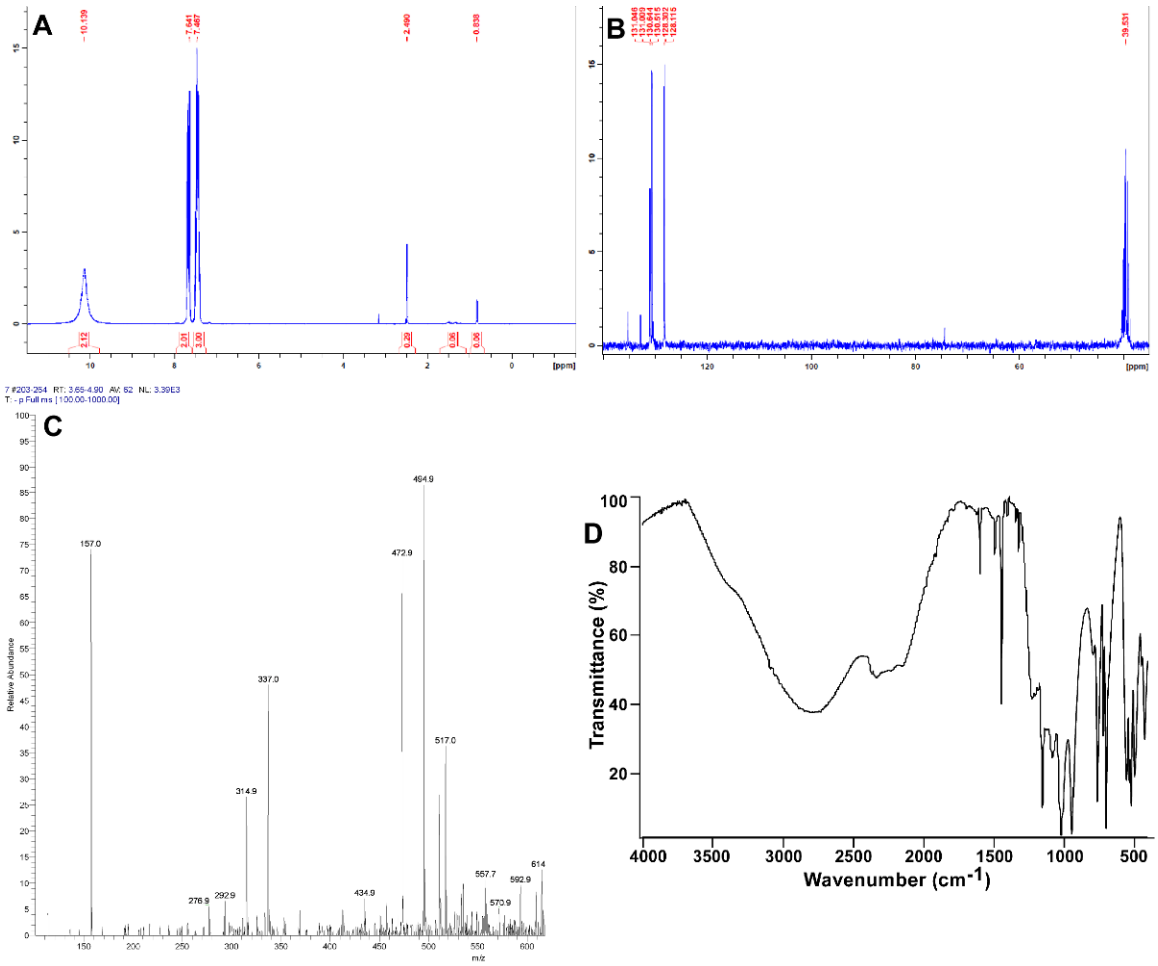

Figure B.8 Spectra for phenylphosphonic acid: A) Proton NMR, B) Carbon NMR, C) ESI-mass spectrum, and D) IR-transmittance spectra

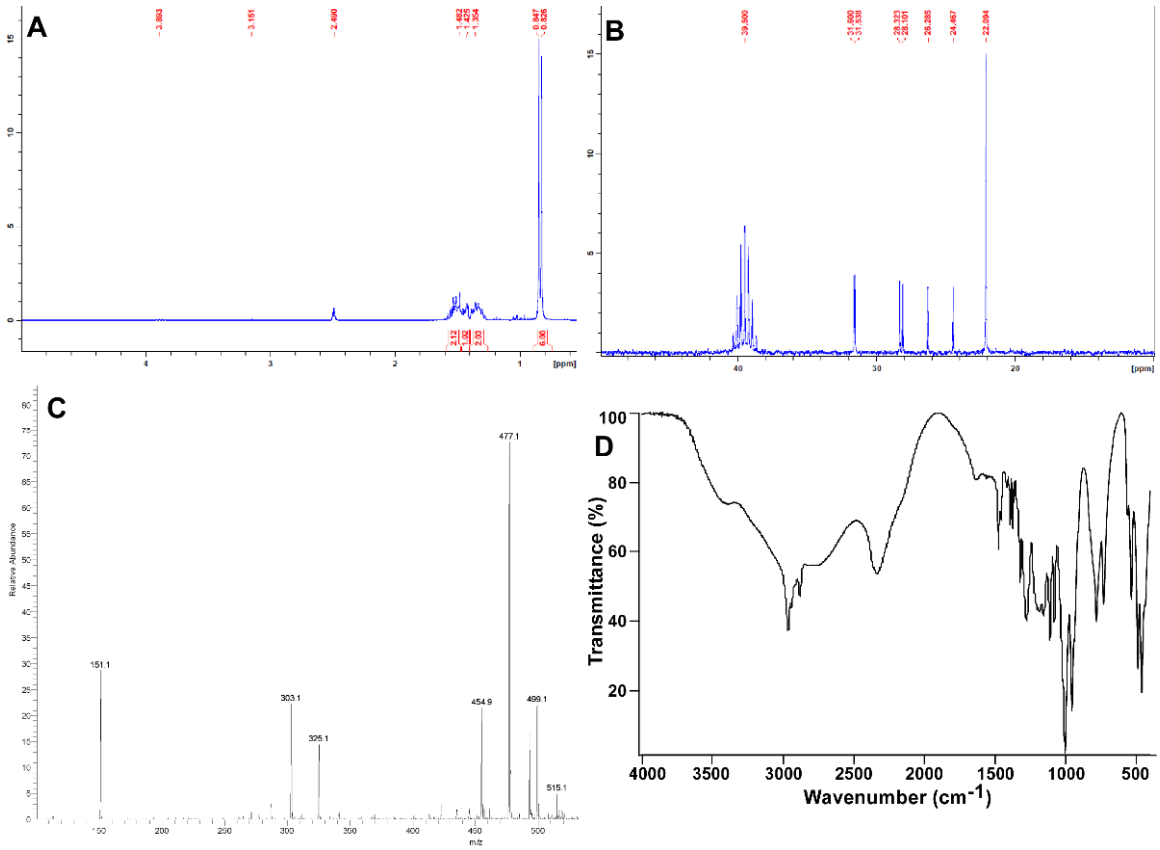

Figure B.9 Spectra for 3-methyl,butylphosphonic acid: A) Proton NMR, B) Carbon NMR, C) ESI-mass spectrum, and D) IR-transmittance spectra

REFERENCES

(1) G. Holland and J. Provenzano, *The Hydrogen Age: Empowering a Clean-Energy Future*. Gibbs Smith 2007.

(2) J. Hemminger, G. Crabtree and M. Kastner, *New Science for a Secure and Sustainable Energy Future for the Basic Energy Sciences Advisory Committee*. US Department of Energy. 2008

(3) *Light's Labour's Lost: Policies for Energy-Efficient Lighting*. OECD/IEA Paris, 2006.

(4) P. Alivisatos, P. Cummings, J. De Yorco, K. Fichthorn, B. Gates, R. Hwang, D. Lowndes, A. Majumdar, L. Makowski, T. Michaelske, J. Misewich, C. Murray, S. Sibener, C. Teague and E. Williams, *Nanoscience Research for Energy Needs*. US Department of Energy. 2004

(5) J. M. Phillips and P. E. Burrows, *Basic Research Needs for Solid-state Lighting*. US Department of Energy. 2006

(6) C. Mandil, *World Energy Outlook*. International Energy Agency. 2006

(7) World Health Organization (WHO) Health impact of climate change needs attention. http://www.who.int/mediacentre/news/notes/2009/climate_change_20090311/en/ (accessed on October 22, 2009),

(8) E. F. Schubert, *Light-Emitting Diodes*. Second ed.; Cambridge University Press New York, 2006.

(9) *Building Energy Data Book 2006. US Department of Energy*. 2006

(10) J. R. Brodrick *Energy Savings Potential of SSL in General Illumination Applications*; US Department of Energy, Navigant Consulting Inc: Washington, DC, 2003.

(11) E. D. Jones, *The Promise of Solid State Lighting for General Illumination*. Optoelectronics Industry Development Association for the Department of Energy. 2001

(12) N. Zheludev. The life and times of the LED--a 100-year history *Nature Photonics* **2007,** 1, 189-192.

(13) H. J. Rounds. A Note on Carborundum *Electrical World* **1907,** 49, 308.

(14) K. Lehovec, C. A. Accardo and E. Jamgochian. Injected Light Emission of Silicon Carbide Crystals *Physical Review* **1951,** 83, (3), 603-607.

(15) R. N. Hall, G. E. Fenner, J. D. Kingsley, T. J. Soltys and R. O. Carlson. Coherent Light Emission from GaAs Junctions *Physical Review Letters* **1962,** 9, 366-368.

(16) T. M. Quist, R. H. Rediker, R. J. Keyes, W. E. Krag, B. Lax, A. L. McWhorter and H. J. Zeigler. Semiconductor Maser of GaAs *Applied Physics Letters* **1962,** 1, (4), 91-92.

(17) M. I. Nathan, W. P. Dumke, G. Burns, F. H. Dill and G. Lasher. Stimulated Emission of Radiation from GaAs p-n Junctions *Applied Physics Letters* **1962,** 1, (3), 62-63.

(18) N. Holonyak and S. F. Bevacqua. Coherent (Visible) Light Emission from Ga(As1-xPx) Junction *Applied Physics Letters* **1962,** 1, (4), 82-83.

(19) E. Hecht, *Physics: Calculus*. Brooks/Cole of Thomson Learning Pacific Grove, 2000.

(20) R. Black, *Lighting the Key to Energy Savings*. UK, 2006.

(21) A. P. Alivisatos. Perspectives on the Physical Chemistry of Semiconductor Nanocrystals *Journal of Physical Chemistry* **1996,** 100, (31), 13226-13239.

(22) U. Banin, Y. W. Cao, D. Katz and O. Millo. Identification of atomic-like electronic states in indium arsenide nanocrystal quantum dots *Nature* **1999,** 400, (6744), 542-544.

(23) D. J. Norris, Electronic Structure in Semiconductor Nanocrystals. In *Semiconductor and Metal Nanocrystals*, V. I. Klimov, Ed. Marecel Dekker, Inc.: 2004.

(24) B. D. Bartolo, *Spectroscopy of Systems with Spatially Confined Structures*. Kluwer Academic Publishers Norwell, MA, 2001.

(25) C. R. Ronda and T. Justel, Quantum Dots and Nanophosphors. In *Luminescence: from theory to applications*, C. R. Ronda, Ed. Wiley-VCH: 2008.

(26) R. Rossetti, J. L. Ellison, J. M. Gibson and L. E. Brus. Size Effects in the Excited Electronic States of Small Colloidal Cds Crystallites *Journal of Chemical Physics* **1984,** 80, (9), 4464-4469.

(27) N. Chestnoy, T. D. Harris, R. Hull and L. E. Brus. Luminescence and Photophysics of Cds Semiconductor Clusters - the Nature of the Emitting Electronic State *Journal of Physical Chemistry* **1986,** 90, (15), 3393-3399.

(28) L. E. Brus. A simple model for the ionization potential, electron affinity, and aqeous redox potentials of small semiconductor crystallites *Journal of Chemical Physics* **1983,** 79, 5566-5572.

(29) L. E. Brus. Electron-electron and electron-hole interactions in small semiconductor crystallites: The size dependence of the lowest excited electronic state *Journal of Chemical Physics* **1984,** 80, 4403-4410.

(30) A. P. Alivisatos. Semiconductor clusters, nanocrystals, and quantum dots *Science* **1996,** 271, 933-937.

(31) J. A. Hollingsworth and V. I. Klimov, "Soft" Chemical Synthesis and Manipulation of Semiconductor Nanocrystals. In *Semiconductor and Metal Nanocrystals*, V. I. Klimov, Ed. Marcel Dekker, Inc: New York, 2004.

(32) T. Kippeny, L. Swafford and S. J. Rosenthal. Semiconductor Nanocrystals: A Powerful Visual Aid for Introducing the Partile in a Box *Journal of Chemical Education* **2002,** 79, 1094.

(33) A. I. Ekimov, F. Hache, M. C. Schanneklein, D. Ricard, C. Flytzanis, I. A. Kudryavtsev, T. V. Yazeva, A. V. Rodina and A. L. Efros. Absorption and

Intensity-dependent Photoluminescence Measurements on CdSe Quantum Dots-Assignment of the 1st Electronic-transitions *Journal of the Optical Society of America B-Optical Physics* **1993,** 10, 100-107.

(34) D. J. Norris and M. G. Bawendi. Measurement and assignment of the size-dependent optical spectrum in CdSe quantum dots *Physical Review B* **1996,** 53, (24), 16338-16346.

(35) H. Landolt, *Landolt-Bornstein: Numerical Data and Functional Relationships in Science and Technology*. Springer New York, 1982; Vol. III-17B.

(36) V. N. Soloviev, A. Eichhofer, D. Fenske and U. Banin. Molecular Limit of a Bulk Semiconductor: Size Dependence of the "Band Gap" in CdSe Cluster Molecule *Journal of the American Chemical Society* **2000,** 122, (11), 2673-2674.

(37) M. R. Warnement, I. D. Tomlinson and S. J. Rosenthal. Fluorescent imaging applications of Quantum Dot probes *Current Nanoscience* **2007,** 3, (4), 273-284.

(38) S. J. Rosenthal, A. Tomlinson, E. M. Adkins, S. Schroeter, S. Adams, L. Swafford, J. McBride, Y. Q. Wang, L. J. DeFelice and R. D. Blakely. Targeting cell surface receptors with ligand-conjugated nanocrystals *Journal of the American Chemical Society* **2002,** 124, (17), 4586-4594.

(39) M. M. Erwin, A. V. Kadavanich, J. McBride, T. Kippeny, S. Pennycook and S. J. Rosenthal. Material characterization of a nanocrystal based photovoltaic device *European Physical Journal D* **2001,** 16, (1-3), 275-277.

(40) N. Tessler, V. Medvedev, M. Kazes, S. Kan and U. Banin. Efficient Near-Infrared Polymer Nanocrystal Light-emitting Diodes *Science* **2002,** 295, 1506-1508.

(41) M. Bruchez, M. Moronne, P. Gin, S. Weiss and A. P. Alivisatos. Semiconductor Nanocrystals as Fluorescent Biological Labels *Science* **1998,** 281, 2013-2016.

(42) W. C. W. Chan and S. M. Nie. Quantum Dot Bioconjugates for Ultrasensative Nonisotopic Detection *Science* **1998,** 281, 2016.

(43) A. J. Nozik. Multiple exciton generation in semiconductor quantum dots *Chemical Physics Letters* **2008,** 457, (1-3), 3-11.

(44) R. D. Schaller and V. I. Klimov. High efficiency carrier multiplication in PbSe nanocrystals: Implications for solar energy conversion *Physical Review Letters* **2004,** 92, (18).

(45) S. Kim, Y. T. Lim, E. G. Soltesz, A. M. De Grand, J. Lee, A. Nakayama, J. A. Parker, T. Mihaljevic, R. G. Laurence, D. M. Dor, L. H. Cohn, M. G. Bawendi and J. V. Frangioni. Near-infrared fluorescent type II quantum dots for sentinel lymph node mapping *Nature Biotechnology* **2004,** 22, (1), 93-97.

(46) J. K. Jaiswal, H. Mattoussi, J. M. Mauro and S. M. Simon. Long-term multiple color imaging of live cells using quantum dot bioconjugates *Nature Biotechnology* **2003,** 21, (1), 47-51.

(47) S. Coe, W. K. Woo, M. Bawendi and V. Bulovic. Electroluminescence from single monolayers of nanocrystals in molecular organic devices *Nature* **2002,** 420, (6917), 800-803.

(48) M. Gao, B. Richter and S. Kirstein. Electroluminescence and photoluminescence in CdSe/poly (p-phenylene vinylene) composite films *Synthetic Metals* **1999,** 102, (1-3), 1213-1214.

(49) A. V. Firth, D. J. Cole-Hamilton and J. W. Allen. Optical properties of CdSe nanocrystals in a polymer matrix *Applied Physics Letters* **1999,** 75, (20), 3120-3122.

(50) N. C. Greenham, J. Shinar, J. Partee, P. A. Lane, O. Amir, F. Lu and R. H. Friend. Optically detected magnetic resonance study of efficient two-layer conjugated polymer light-emitting diodes *Physical Review B* **1996,** 53, (20), 13528-13533.

(51) V. L. Colvin, M. C. Schlamp and A. P. Alivisatos. Light-Emitting-Diodes Made from Cadmium Selenide Nanocrystals and a Semiconducting Polymer *Nature* **1994,** 370, (6488), 354-357.

(52) Y. Li, A. Rizzo, M. Mazzeo, L. Carbone, L. Manna, R. Cingolani and G. Gigli. White organic light-emitting devices with CdSe/ZnS quantum dots as a red emitter *Journal of Applied Physics* **2005,** 97, (11), 113501.

(53) B. O. Dabbousi, M. G. Bawendi, O. Onitsuka and M. F. Rubner. Electroluminescence from Cdse Quantum-Dot Polymer Composites *Applied Physics Letters* **1995,** 66, (11), 1316-1318.

(54) P. O. Anikeeva, J. E. Halpert, M. G. Bawendi and V. Bulovic. Electroluminescence from a mixed red-green-blue colloidal quantum dot monolayer *Nano Letters* **2007,** 7, (8), 2196-2200.

(55) M. Achermann, M. A. Petruska, S. Kos, D. L. Smith, D. D. Koleske and V. I. Klimov. Energy-transfer pumping of semiconductor nanocrystals using an epitaxial quantum well *Nature* **2004,** 429, (6992), 642-646.

(56) M. J. Bowers, J. R. McBride and S. J. Rosenthal. White-light emission from magic-sized cadmium selenide nanocrystals *Journal of the American Chemical Society* **2005,** 127, (44), 15378-15379.

(57) G. M. Kosolapoff, *Organophosphorus compounds*. Wiley New York, NY, 1950; p 376.

(58) A. Michaelis and R. Kaehne. Ueber das Verhalten der Jodalkyle gegen die sogen. Phosphorigsaureester oder O-Phosphine *Berichte* **1898,** 31, 1048.

(59) A. E. Arbuzov. *Journal of the Russian Physical Chemistry Society* **1906,** 38, 687.

(60) R. Engel, *Synthesis of Carbon-Phosphorus Bonds*. CRC Press, Inc. Boca Raton, FL, 1988; p 229.

(61) S. R. Landauer and H. N. Rydon. The organic chemistry of phosphorus. Part I. Some new methods for the preparation of alkyl halides *Journal of the Chemical Society (Resumed)* **1953**, 2224-2234.

(62) E. Cherbuliez, Organic Derivaties of Phosphoric Acid. In *Organic Phosphorus Compounds*, G. M. Kosolapoff and L. Maier, Eds. John Wiley and Sons, Inc.: New York, 1973; Vol. 6.

(63) R. F. Hudson, Structure and Mechanism in Organo-phosphorus Chemistry. In *Organic Chemistry*, A. T. Blomquis, Ed. Academic Press: New York, 1965.

(64) H. Gunzler and H. U. Gremlich, *IR Spectroscopy*. Wiley, VCH Weinheim, Germany, 2002; p 361.

(65) K. Nakamoto, *Infrared and Raman Spectra of Inorganic and Coordination Compounds*. John Wiley and Sons New York, NY, 1978; p 448.

(66) K. Nakanishi and P. H. Solomon, *Infrared Absorption Spectroscopy*. 2nd ed.; Holden-Day, Inc. San Fancisco, CA, 1977; p 287.

(67) L. Daasch and D. Smith. Infrared Spectra of Phosphorus Compounds *Analytical Chemistry* **1951,** 23, (6), 853-868.

(68) C. B. Murray, S. H. Sun, W. Gaschler, H. Doyle, T. A. Betley and C. R. Kagan. Colloidal Synthesis of Nanocrystals and Nanocrystal Superlattices *IBM Journal of Research and Development* **2001,** 45, (1), 47-56.

(69) B. L. Wehrenberg, C. Wang and P. Guyot-Sionnest. Interband and Intraband Optical Studies of PbSe Colloidal Quantum Dots *Journal of Physical Chemistry B* **2002,** 106, 10634-10640.

(70) K. S. Cho, D. V. Talapin, W. Gaschler and C. B. Murray. Designing PbSe nanowires and nanorings through oriented attachement of nanoparticles *Journal of the American Chemical Society* **2005,** 127, (19), 7140-7147.

(71) C. B. Murray, D. J. Norris and M. G. Bawendi. Synthesis and Characterization of Nearly Monodisperse Cde (E = S, Se, Te) Semiconductor Nanocrystallites *Journal of the American Chemical Society* **1993,** 115, (19), 8706-8715.

(72) A. Nag, S. Sapra, S. Chakraborty, S. Basu and D. D. Sarma. Synthesis of CdSe Nanocrystals in a Noncoordinating Solvent: Effect of Reaction Temperature on Size and Optical Properties *Journal of Nanoscience and Nanotechnology* **2007,** 7, (6), 1965-1968.

(73) X. G. Peng, L. Manna, W. D. Yang, J. Wickham, E. Scher, A. Kadavanich and A. P. Alivisatos. Shape control of CdSe nanocrystals *Nature* **2000,** 404, (6773), 59-61.

(74) S. J. Rosenthal, J. McBride, S. J. Pennycook and L. C. Feldman. Synthesis, surface studies, composition and structural characterization of CdSe, core/shell and biologically active nanocrystals *Surface Science Reports* **2007,** 62, 111-157.

(75) Z. A. Peng and X. G. Peng. Formation of high-quality CdTe, CdSe, and CdS nanocrystals using CdO as precursor *Journal of the American Chemical Society* **2001,** 123, (1), 183-184.

(76) Z. A. Peng and X. G. Peng. Nearly monodisperse and shape-controlled CdSe nanocrystals via alternative routes: Nucleation and growth *Journal of the American Chemical Society* **2002,** 124, (13), 3343-3353.

(77) M. A. Schreuder, J. R. McBride, A. D. Dukes III, J. A. Sammons and S. J. Rosenthal. Control of Surface State Emission via Phosphonic Acid Modulation in Ultrasmall CdSe Nanocrystals: The Role of Ligand Electronegativity *The Journal of Physical Chemistry C* **2009,** 113, (19), 8169-8176.

(78) M. A. Hines and P. Guyot-Sionnest. Synthesis and characterization of strongly luminescing ZnS-Capped CdSe nanocrystals *Journal of Physical Chemistry* **1996,** 100, (2), 468-471.

(79) X. Peng, M. C. Schlamp, A. Kadavanich and A. P. Alivisatos. Epitaxial Growth of Highly Luminescent CdSe/CdS Core/Shell Nanocrystals with Photostability and Electronic Accesibilty *Journal of the American Chemical Society* **1997,** 119, (30), 7019-7029.

(80) J. R. McBride, J. Treadway, L. C. Feldman, S. J. Pennycook and S. J. Rosenthal. Structural Basis for Near Unity Quantum Yield Core/Shell Nanostructures *Nano Letters* **2006,** 6, (7), 1496-1501.

(81) J. van Embden and P. Mulvaney. Nucleation and Growth of CdSe Nanocrystals in a Binary Ligand System *Langmuir* **2005,** 21, (22), 10226-10233.

(82) H. Mattoussi, L. H. Radzilowski, B. O. Dabbousi, E. L. Thomas, M. G. Bawendi and M. F. Rubner. Electroluminescence from heterostructures of poly(phenylene vinylene) and inorganic CdSe nanocrystals *Journal of Applied Physics* **1998,** 83, (12), 7965-7974.

(83) M. C. Schlamp, X. Peng and A. P. Alivisatos. Improved efficiencies in light emitting diodes made with CdSe(CdS) core/shell type nanocrystals and a semiconducting polymer *Journal of Applied Physics* **1997,** 82, (11), 5837-5842.

(84) A. L. Rogach, N. Gaponik, J. M. Lupton, C. Bertoni, D. E. Gallardo, S. Dunn, N. L. Pira, M. Paderi, P. Repetto, S. G. Romanov, C. O'Dwyer, C. M. Sotomayor

Torres and A. Eychmuller. Light-Emitting Diodes with Semiconductor Nanocrystals *Angewandte Chemie-International Edition* **2008,** 47, (35), 6538-6549.

(85) J. S. Steckel, P. Snee, S. Coe-sullivan, J. P. Zimmer, J. E. Halpert, P. O. Anikeeva, L.-A. Kim, V. Bulovic and M. G. Bawendi. Color-Saturated Green-Emitting QD-LEDs *Angewandte Chemie-International Edition* **2006,** 118, (5928-5931).

(86) C. D. Williams, R. O. Robles, M. Zhang, S. Li, R. H. Baughman and A. A. Zakhidov. Multiwalled carbon nanotube sheets as transparent electrodes in high brightess organic light-emitting diodes *Applied Physics Letters* **2008,** 93, (18), 183506.

(87) S. Coe-Sullivan, J. S. Steckel, W. K. Woo, M. G. Bawendi and V. Bulovic. Large-area ordered quantum-dot monolayers via phase separation during spin-casting *Advanced Functional Materials* **2005,** 15, (7), 1117-1124.

(88) M. Kuno, J. K. Lee, B. O. Dabbousi, F. V. Mikulec and M. G. Bawendi. The band edge luminescence of surface modified CdSe nanocrystallites: Probing the luminescing state *Journal of Chemical Physics* **1997,** 106, (23), 9869-9882.

(89) Y. Yin and A. P. Alivisatos. Colloidal nanocrystal synthesis and the organic-inorganic interface *Nature* **2005,** 437, (7059), 664-670.

(90) C. Landes, M. Braun, C. Burda and M. A. El-Sayed. Observation of large changes in the band gap absorption energy of small CdSe nanoparticles induced by the adsorption of a strong hole acceptor *Nano Letters* **2001,** 1, (11), 667-670.

(91) X. B. Chen, A. C. S. Samia, Y. B. Lou and C. Burda. Investigation of the crystallization process in 2 nm CdSe quantum dots *Journal of the American Chemical Society* **2005,** 127, 4372-4375.

(92) C. Bullen and P. Mulvaney. The effects of chemisorption on the luminescence of CdSe quantum dots *Langmuir* **2006,** 22, (7), 3007-3013.

(93) N. Pradhan, D. Reifsnyder, R. G. Xie, J. Aldana and X. G. Peng. Surface ligand dynamics in growth of nanocrystals *Journal of the American Chemical Society* **2007,** 129, (30), 9500-9509.

(94) A. M. Munro, I. J. L. Plante, M. S. Ng and D. S. Ginger. Quantitative study of the effects of surface ligand concentration on CdSe nanocrystal photoluminescence *Journal of Physical Chemistry C* **2007,** 111, (17), 6220-6227.

(95) I. S. Liu, H. H. Lo, C. T. Chien, Y. Y. Lin, C. W. Chen, Y. F. Chen, W. F. Su and S. C. Liou. Enhancing photoluminescence quenching and photoelectric properties of CdSe quantum dots with hole accepting ligands *Journal of Materials Chemistry* **2008,** 18, (6), 675-682.

(96) A. M. Munro and D. S. Ginger. Photoluminescence quenching of single CdSe nanocrystals by ligand adsorption *Nano Letters* **2008,** 8, (8), 2585-2590.

(97) A. M. Munro, J. A. Bardecker, M. S. Liu, Y. J. Cheng, Y. H. Niu, I. J. L. Plante, A. K. Y. Jen and D. S. Ginger. Colloidal CdSe quantum dot electroluminescence: ligands and light-emitting diodes *Microchimica Acta* **2008,** 160, (3), 345-350.

(98) X. H. Ji, D. Copenhaver, C. Sichmeller and X. G. Peng. Ligand bonding and dynamics on colloidal nanocrystals at room temperature: The case of alkylamines on CdSe nanocrystals *Journal of the American Chemical Society* **2008,** 130, (17), 5726-5735.

(99) S. M. Kim, K. Kyhm, H. S. Yang and K. S. Hong. Optical properties and surface conditions of CdSe quantum dots *Journal of the Korean Physical Society* **2006,** 49, S688-S691.

(100) A. M. Smith, H. W. Duan, M. N. Rhyner, G. Ruan and S. M. Nie. A systematic examination of surface coatings on the optical and chemical properties of semiconductor quantum dots *Physical Chemistry Chemical Physics* **2006,** 8, (33), 3895-3903.

(101) T. Ozel, I. M. Soganci, S. Nizamoglu, I. O. Huyal, E. Mutlugun, S. Sapra, N. Gaponik, A. Eychmuller and H. V. Demir. Selective enhancement of surface-state emission and simultaneous quenching of interband transition in white-luminophor CdS nanocrystals using localized plasmon coupling *New Journal of Physics* **2008,** 10, (8), 083035.

(102) A. L. Washington and G. F. Strouse. Microwave synthesis of CdSe and CdTe nanocrystals in nonabsorbing alkanes *Journal of the American Chemical Society* **2008,** 130, (28), 8916-8922.

(103) W. Wang, S. Banerjee, S. G. Jia, M. L. Steigerwald and I. P. Herman. Ligand control of growth, morphology, and capping structure of colloidal CdSe nanorods *Chemistry of Materials* **2007,** 19, (10), 2573-2580.

(104) J. Park, J. Joo, S. G. Kwon, Y. Jang and T. Hyeon. Synthesis of monodisperse spherical nanocrystals *Angewandte Chemie-International Edition* **2007,** 46, 4630-4660.

(105) J. Hambrock, A. Birkner and R. A. Fischer. Synthesis of CdSe nanoparticles using various organometallic cadmium precursors *Journal of Materials Chemistry* **2001,** 11, (12), 3197-3201.

(106) L. H. Qu, Z. A. Peng and X. G. Peng. Alternative routes toward high quality CdSe nanocrystals *Nano Letters* **2001,** 1, (6), 333-337.

(107) P. S. Nair, K. P. Fritz and G. D. Scholes. A multiple injection method for exerting kinetic control in the synthesis of CdSe nanorods *Chemical Communications* **2004**, 2084-2085.

(108) H. T. Liu, J. S. Owen and A. P. Alivisatos. Mechanistic study of precursor evolution in colloidal group II-VI semiconductor nanocrystal synthesis *Journal of the American Chemical Society* **2007,** 129, (2), 305-312.

(109) A. G. Kanaras, C. Sonnichsen, H. T. Liu and A. P. Alivisatos. Controlled synthesis of hyperbranched inorganic nanocrystals with rich three-dimensional structures *Nano Letters* **2005,** 5, (11), 2164-2167.

(110) K. T. Yong, Y. Sahoo, M. T. Swihart and P. N. Prasad. Growth of CdSe quantum rods and multipods seeded by noble-metal nanoparticles *Advanced Materials* **2006,** 18, (15), 1978-+.

(111) P. S. Nair, K. P. Fritz and G. D. Scholes. Evolutionary shape control during colloidal quantum-dot growth *Small* **2007,** 3, (3), 481-487.

(112) L. Manna, L. W. Wang, R. Cingolani and A. P. Alivisatos. First-principles modeling of unpassivated and surfactant-passivated bulk facets of wurtzite CdSe: A model system for studying the anisotropic growth of CdSe nanocrystals *Journal of Physical Chemistry B* **2005,** 109, (13), 6183-6192.

(113) A. Puzder, A. J. Williamson, N. Zaitseva, G. Galli, L. Manna and A. P. Alivisatos. The effect of organic ligand binding on the growth of CdSe nanoparticles probed by Ab initio calculations *Nano Letters* **2004,** 4, (12), 2361-2365.

(114) J. T. Kopping and T. E. Patten. Identification of acidic phosphorus-containing ligands involved in the surface chemistry of CdSe nanoparticles prepared in tri-n-octylphosphine oxide solvents *Journal of the American Chemical Society* **2008,** 130, (17), 5689-5698.

(115) A. D. Dukes, M. A. Schreuder, J. A. Sammons, J. R. McBride, N. J. Smith and S. J. Rosenthal. Pinned emission from ultrasmall cadmium selenide nanocrystals *Journal of Chemical Physics* **2008,** 129, (12), 121102-1 -121102-4.

(116) A. Nag and D. D. Sarma. White light from Mn2+-doped Cds nanocrystals: A new approach *Journal of Physical Chemistry C* **2007,** 111, 13641-13644.

(117) S. Singh, P. Thiyagarajan, K. M. Kant, D. Anita, S. Thirupathiah, N. Rama, B. Tiwari, M. Kottaisamy and M. S. R. Rao. Structure, microstructure and physical properties of ZnO based materials in various forms: bulk, thin film and nano *Journal of Physics D-Applied Physics* **2007,** 40, 6312-6327.

(118) W. W. Yu, L. H. Qu, W. Z. Guo and X. G. Peng. Experimental determination of the extinction coefficient of CdTe, CdSe, and CdS nanocrystals *Chemistry of Materials* **2003,** 15, (14), 2854-2860.

(119) L. H. Qu, W. W. Yu and X. P. Peng. In situ observation of the nucleation and growth of CdSe nanocrystals *Nano Letters* **2004,** 4, (3), 465-469.

(120) N. A. Hill and K. B. Whaley. A Theoretical-Study of the Influence of the Surface on the Electronic-Structure of Cdse Nanoclusters *Journal of Chemical Physics* **1994,** 100, (4), 2831-2837.

(121) N. E. Jacobsen, *NMR Spectroscopy explained: simplified theory, applications, and examples for organic chemistry and structural biology*. Wiley-Interscience Hoboken, NJ, 2007; p 668.

(122) W. Kemp, *Organic Spectroscopy*. 2nd ed.; Macmillan 1987; p 299.

(123) S. G. Bratsch. A Group Electronegativity Method with Pauling Units *Journal of Chemical Education* **1985,** 62, (2), 101-103.

(124) E. Lifshitz, I. Dag, I. D. Litvitn and G. Hodes. Optically detected magnetic resonance study of electron/hole traps on CdSe quantum dot surfaces *Journal of Physical Chemistry B* **1998,** 102, (46), 9245-9250.

(125) E. Lifshitz, I. Dag, I. Litvin, G. Hodes, S. Gorer, R. Reisfeld, M. Zelner and H. Minti. Properties of CdSe nanoparticle films prepared by chemical deposition and sol-gel methods *Chemical Physics Letters* **1998,** 288, (2-4), 188-196.

(126) D. F. Underwood, T. Kippeny and S. J. Rosenthal. Ultrafast carrier dynamics in CdSe nanocrystals determined by femtosecond fluorescence upconversion spectroscopy *Journal of Physical Chemistry B* **2001,** 105, (2), 436-443.

(127) N. A. Hill and B. Whaley. Electronic-Structure of Semiconductor Nanoclusters - a Time-Dependent Theoretical Approach *Journal of Chemical Physics* **1993,** 99, (5), 3707-3715.

(128) V. I. Klimov, D. W. McBranch, C. A. Leatherdale and M. G. Bawendi. Electron and hole relaxation pathways in semiconductor quantum dots *Physical Review B* **1999,** 60, (19), 13740-13749.

(129) D. E. Gomez, J. van Embden, J. Jasieniak, T. A. Smith and P. Mulvaney. Blinking and surface chemistry of single CdSe nanocrystals *Small* **2006,** 2, 204-208.

(130) J. E. B. Katari, V. L. Colvin and A. P. Alivisatos. X-ray Photoelectron Spectroscopy of CdSe Nanocrystals with Applications to Studies of the Nanocrystal Surface *Journal of Physical Chemistry* **1994,** 98, (15), 4109-4117.

(131) J. Taylor, T. Kippeny and S. J. Rosenthal. Surface Stoichiometry of CdSe Nanocrystals Determined by Rutherford Backscattering Spectroscopy *Journal of Cluster Science* **2001,** 12, (4), 571-582.

(132) M. G. Berrettini, G. Braun, J. G. Hu and G. F. Strouse. NMR analysis of surfaces and interfaces in 2-nm CdSe *Journal of the American Chemical Society* **2004,** 126, (22), 7063-7070.

(133) M. D. Garrett, A. D. Dukes, J. R. McBride, N. J. Smith, S. J. Pennycook and S. J. Rosenthal. Band edge recombination in CdSe, CdS and CdSxSe1-x alloy nanocrystals observed by ultrafast fluorescence upconversion: The effect of surface trap states *Journal of Physical Chemistry C* **2008,** 112, (33), 12736-12746.

(134) N. Stock, N. Guillou, J. Senker, G. Ferey and T. Bein. Synthesis and characterization of the tetraphosphonic acid ester (Et2O3PCH2)(4)C6H2 and the open-framework cadmium tetraphosphonate, Cd-2[(Ho3PCH2)(4)C6H2] *Zeithschrift fur Anorganische und Allgemeine Chemie* **2005,** 631, (2-3), 575-581.

(135) CIE, In *Commission Internationale de l'Eclairage Proceedings, 1931*, Cambridge University Press, Cambridge: 1932.

(136) J. Y. Tsao, *Light Emitting Diodes (LEDs) for General Illumination*. Optoelectronics Industry Development Association for the US Department of Energy. 2002

(137) C. d. M. Donega, S. G. Hickey, S. F. Wuister, D. Vanmaekelbergh and A. Meijerink. Single-Step Synthesis to Control the Photoluminescence Quantum Yield and Size Dispersion of CdSe Nanocrystals *Journal of Physical Chemistry B* **2003,** 107, (2), 489-496.

(138) Y. Xi, T. Gessmann, J. Xi, J. K. Kim, J. M. Shah, E. F. Schubert, A. J. Fisher, M. H. Crawford, K. H. A. Bogart and A. A. Allerman. Junction Temperature in Ultraviolet Light-Emittind Diodes *Japanese Journal of Applied Physics* **2005,** 55, 7260-7266.

(139) A. F. M. Barton, *CRC Handbook of Solubility Parameters and Other Cohesion Parameters*. CRC Press Boca Raton, 2000.

(140) C. M. Hansen, *Hansen Solubility Parameters (A Users's Handbook)*. CRC Press Boca Raton, 2000.

(141) R. H. Baney, C. E. Voigt and J. W. Mentele, In *Structure-Solubility Relationship in Polymers*, F. W. Harris and R. B. Seymour, Eds. Academic Press: New York, 1977; pp 228-231.

(142) A. F. M. Barton, *CRC Handbook of Solubility Parameters and Other Cohesion Parameters*. CRC Press Boca Raton, 1991.

(143) L. N. Lewis, In *Silicones and Silicone-modified Materials*, S. J. Clarson, J. J. Fitzgerald, M. J. Owen and S. D. Smith, Eds. Oxford University Press: Oxford, 2000; pp 11-19.

(144) S. H. Goodman, *Handbook of Thermoset Plastics*. Noyes Publication Park Ridge, 1986.

(145) N. C. Greenham, I. D. W. Samuel, G. R. Hayes, R. T. Phillips, Y. A. R. R. Kessener, S. C. Moratti, A. B. Holmes and R. H. Friend. Measurement of absolute photoluminescence quantum efficiencies in conjugated polymers *Chemical Physics Letters* **1995,** 241, (1-2), 89-96.

(146) K. Leung and K. B. Whaley. Surface relaxation in CdSe nanocrystals *The Journal of Chemical Physics* **1999,** 110, (22), 11012-11022.

(147) M. A. Schreuder, J. D. Gosnell, N. J. Smith, M. R. Warnement, S. M. Weiss and S. J. Rosenthal. Encapsulated white-light CdSe nanocrystals as nanophosphors for solid-state lighting *Journal of Materials Chemistry* **2008,** 18, (9), 970-975.

(148) S. Coe-Sullivan, W. K. Woo, J. S. Steckel, M. Bawendi and V. Bulovic. Tuning the performance of hybrid organic/inorganic quantum dot light-emitting devices *Organic Electronics* **2003,** 4, (2-3), 123-130.

(149) White light has the CIE coordinates of (1/3, 1/3) on the 1931 CIE scale, and noonday sunlight has a CCT of about 5500-6000K and a CRI of 100.

(150) M. D. Garrett, M. J. Bowers II, J. R. McBride, R. L. Orndorff, S. J. Pennycook and S. J. Rosenthal. Band Edge Dynamics in CdSe Nanocrystals Observed by Ultrafast Fluorescence Upconversion *Journal of Physical Chemistry C* **2008,** 112, (2), 436-442.

(151) M. J. Bowers II, J. R. McBride, M. D. Garrett, J. A. Sammons, A. D. Dukes III, M. A. Schreuder, T. L. Watt, A. R. Lupini, S. J. Pennycook and S. J. Rosenthal. Structure and Ultrafast Dynamics of White-Light-Emitting CdSe Nanocrystals *Journal of the American Chemical Society* **2009,** 131, (16), 5730-5731.

(152) A. Z. Mariano, V. Tobias, R. Carsten and C. Federico. Exciton-related electroluminescence from ZnO nanowire light-emitting diodes *Applied Physics Letters* **2009,** 94, (24), 241120.

(153) R. Konenkamp, C. W. Robert and C. Schlegel. Vertical nanowire light-emitting diode *Applied Physics Letters* **2004,** 85, (24), 6004-6006.